

EUROPEAN ORGANISATION FOR NUCLEAR RESEARCH (CERN)



Phys. Rev. D 94, 092003 (2016)
DOI: [10.1103/PhysRevD.94.092003](https://doi.org/10.1103/PhysRevD.94.092003)



CERN-EP-2016-144
November 15, 2016

Measurement of top quark pair differential cross-sections in the dilepton channel in pp collisions at $\sqrt{s} = 7$ and 8 TeV with ATLAS

The ATLAS Collaboration

Abstract

Measurements of normalized differential cross-sections of top quark pair ($t\bar{t}$) production are presented as a function of the mass, the transverse momentum and the rapidity of the $t\bar{t}$ system in proton-proton collisions at center-of-mass energies of $\sqrt{s} = 7$ TeV and 8 TeV. The dataset corresponds to an integrated luminosity of 4.6 fb^{-1} at 7 TeV and 20.2 fb^{-1} at 8 TeV, recorded with the ATLAS detector at the Large Hadron Collider. Events with top quark pair signatures are selected in the dilepton final state, requiring exactly two charged leptons and at least two jets with at least one of the jets identified as likely to contain a b -hadron. The measured distributions are corrected for detector effects and selection efficiency to cross-sections at the parton level. The differential cross-sections are compared with different Monte Carlo generators and theoretical calculations of $t\bar{t}$ production. The results are consistent with the majority of predictions in a wide kinematic range.

Contents

1	Introduction	2
2	ATLAS detector	3
3	Data and simulation samples	3
4	Object and event selection	6
4.1	Object definition	6
4.2	Event selection	7
5	Reconstruction	7
6	Differential cross-section determination	9
7	Uncertainties	12
7.1	Signal modeling uncertainties	12
7.2	Background modeling uncertainties	13
7.3	Detector modeling uncertainties	14
7.4	Summary of the main sources of systematic uncertainty	15
8	Results	15
9	Conclusions	27

1 Introduction

The top quark is the most massive elementary particle in the Standard Model (SM). Its mass is close to the scale of electroweak symmetry breaking, implying a unique sensitivity to interactions beyond the SM. The production of top quarks at the Large Hadron Collider (LHC) is dominated by pair production of top and antitop quarks ($t\bar{t}$) via the strong interaction. Possible new phenomena beyond the SM can modify the kinematic properties of the $t\bar{t}$ system. Thus measurements of these distributions provide a means of testing the SM prediction at the TeV scale. In addition, more accurate and detailed knowledge of top quark pair production is an essential component of the wide-ranging LHC physics program, since $t\bar{t}$ events are the dominant background to many searches for new physics as well as Higgs boson measurements.

The large $t\bar{t}$ production cross-section at the LHC leads to a large number of $t\bar{t}$ pairs, allowing precise inclusive and differential measurements in a wide kinematic range. The inclusive $t\bar{t}$ production cross-section ($\sigma_{t\bar{t}}$) has been measured in proton-proton (pp) collisions at $\sqrt{s} = 7$ TeV, 8 TeV and 13 TeV by the ATLAS and CMS experiments [1–6], with a best reported precision of 3.6% (3.7%) at 7 (8) TeV [4]. Measurements of the $t\bar{t}$ differential cross-section as a function of the kinematic properties of the top quark or the $t\bar{t}$ pair have also been performed by ATLAS [7–11] and CMS [12–15].

This paper presents measurements of the normalized differential $t\bar{t}$ cross-sections as a function of the invariant mass ($m_{t\bar{t}}$), the transverse momentum ($p_{T,t\bar{t}}$), and the rapidity ($|y_{t\bar{t}}|$) of the $t\bar{t}$ system in pp collisions at $\sqrt{s} = 7$ TeV and 8 TeV recorded by the ATLAS detector [16]. The dilepton $t\bar{t}$ decay mode used in this measurement yields a clean signal and thus provides an accurate test for the modeling of $t\bar{t}$ production.

This paper complements other ATLAS measurements that use the lepton+jets (ℓ +jets) $t\bar{t}$ decay mode [7–11].

A top quark pair is assumed to decay into two W bosons and two b -quarks with a branching ratio of 100%. The dilepton decay mode of $t\bar{t}$ used in this analysis refers to the mode where both W bosons decay into a charged lepton (electron or muon) and a neutrino. Events in which the W boson decays into an electron or a muon through a τ lepton decay are also included.

Dileptonic $t\bar{t}$ events are selected by requiring two leptons (electron or muon) and at least two jets, where at least one of the jets is identified as containing a b -hadron. The specific decay modes refer to the ee , $\mu\mu$, and $e\mu$ channels. In the 8 TeV measurement, one lepton must be an electron and the other must be a muon (the $e\mu$ channel). This channel provides a data sample large enough for the measurement to be limited by systematic uncertainties at 8 TeV. In the 7 TeV analysis, where the integrated luminosity is smaller, events containing same-flavor electron or muon pairs (the ee and $\mu\mu$ channels) are also selected in order to maximize the size of the available dataset.

2 ATLAS detector

The ATLAS detector¹ is a general-purpose, cylindrically symmetric detector with a barrel and two endcap components. The inner detector (ID) is closest to the interaction point and provides precise reconstruction of charged-particle tracks. It is a combination of high-resolution silicon pixel and strip detectors, and a straw-tube tracking detector. The ID covers a range of $|\eta| < 2.5$ and is surrounded by a superconducting solenoid that produces a 2 T axial field within the ID. Surrounding the ID are electromagnetic and hadronic sampling calorimeters. The liquid argon (LAr) sampling electromagnetic calorimeter covers the pseudorapidity range of $|\eta| < 3.2$ with high granularity. The hadronic sampling calorimeters use steel/scintillator-tiles in $|\eta| < 1.7$ and LAr technology for $1.5 < |\eta| < 4.9$. The muon spectrometer is the outermost subdetector and is composed of three layers of chambers. It is designed for precision measurement and detection of muons exploiting the track curvature in the toroidal magnetic field. The trigger system involves a combination of hardware- and software-based triggers at three levels to reduce the raw trigger rate of 20 MHz to 400 Hz.

3 Data and simulation samples

The datasets used in this analysis were collected from LHC pp collisions at $\sqrt{s} = 7$ and 8 TeV in 2011 and 2012. The total integrated luminosities are 4.6 fb^{-1} with an uncertainty of 1.8% at $\sqrt{s} = 7$ TeV and 20.2 fb^{-1} with an uncertainty of 1.9% at $\sqrt{s} = 8$ TeV. The luminosity was measured using techniques described in Refs. [17, 18]. The average number of pp interactions per bunch crossing (pileup) is about 9 for the 7 TeV dataset and increases to about 21 for the 8 TeV dataset. The data sample was collected using single-lepton triggers. The $\sqrt{s} = 7$ TeV dataset uses a single-muon trigger requiring at least one muon with transverse momentum p_T above 18 GeV and a single-electron trigger requiring at least one electron

¹ ATLAS uses a right-handed coordinate system with its origin at the nominal interaction point (IP) in the center of the detector and the z -axis along the beam pipe. The x -axis points from the IP to the center of the LHC ring, and the y -axis points upward. Cylindrical coordinates (r, ϕ) are used in the transverse plane, ϕ being the azimuthal angle around the beam pipe. The pseudorapidity is defined in terms of the polar angle θ as $\eta = -\ln \tan(\theta/2)$, and transverse momentum and energy are defined as $p_T = p \sin \theta$ and $E_T = E \sin \theta$. Distances in (η, ϕ) space are denoted by $\Delta R = \sqrt{(\Delta\eta)^2 + (\Delta\phi)^2}$.

with a p_T threshold of either 20 or 22 GeV, with the p_T threshold being increased during data-taking to cope with increased luminosity. In the $\sqrt{s} = 8$ TeV dataset, the logical OR of two triggers is used in order to increase the efficiency for isolated leptons at low transverse momentum, for each lepton type. For electrons the two p_T thresholds are 24 GeV and 60 GeV, and for muons the thresholds are 24 GeV and 36 GeV, where only the lower- p_T triggers impose lepton isolation requirements.

Samples of Monte Carlo (MC) simulated events are used to characterize the detector response and efficiency for reconstructing $t\bar{t}$ events, to estimate systematic uncertainties, and to predict the background contributions from various physics processes. The samples were processed through the GEANT4 [19] simulation of the ATLAS detector [20] and the ATLAS reconstruction software. For the evaluation of some systematic uncertainties, generated samples are passed through a fast simulation using a parameterization of the performance of the ATLAS electromagnetic and hadronic calorimeters [21]. The simulated events include pileup interactions to emulate the multiple pp interactions in each event present in the data.

The nominal signal $t\bar{t}$ sample, PowHEG+PYTHIA, is generated using the PowHEG (PowHEG-hvq patch4, revision 2330, version 3.0) [22–25] generator, which is based on next-to-leading-order (NLO) QCD matrix element calculations. The CT10 [26] parton distribution functions (PDF) are employed and the top quark mass (m_t) is set to 172.5 GeV. The h_{damp} parameter in PowHEG, which controls the p_T of the first additional emission beyond the Born configuration, is set to infinity for the 7 TeV sample and set to m_t for the 8 TeV sample. The main effect of this parameter is to regulate the high- p_T emission against which the top quark pair system recoils. In studies [27, 28] using data from $\sqrt{s} = 7$ TeV ATLAS $t\bar{t}$ differential cross-section measurements in the $\ell+\text{jets}$ channel [8], $h_{\text{damp}} = m_t$ was shown to give a better description of data than $h_{\text{damp}} = \infty$, especially in the $p_{T,t\bar{t}}$ spectrum [27, 28]. Thus, the PowHEG $h_{\text{damp}} = m_t$ sample was generated at 8 TeV as the nominal sample. At 7 TeV, while only the PowHEG $h_{\text{damp}} = \infty$ full MC sample is available, the generated parton-level distributions with $h_{\text{damp}} = m_t$ can be accessed and are used for comparison to the results. Parton showering and hadronization are simulated with PYTHIA [29] (version 6.427) using the Perugia 2011C (P2011C) set of tuned parameters (tune) [30] and the corresponding leading-order (LO) CTEQ6L1 PDF set [31].

The effect of the choice of generators and parton showering models are studied with predictions from MC@NLO [32, 33] (version 4.01) interfaced to HERWIG [34] (version 6.520) for parton showering and hadronization, and to JIMMY [35] (version 4.31) for modeling multiple parton scattering in the underlying event using the ATLAS AUET2 tune [36] and the CT10 PDFs, and predictions from PowHEG interfaced to HERWIG. The uncertainties in the modeling of extra QCD radiation in $t\bar{t}$ events are estimated with samples generated using ALPGEN (version 2.14) [37] with CTEQ5L [38] PDFs interfaced to PYTHIA with varied radiation settings and MC@NLO interfaced to HERWIG with varied renormalization and factorization scales ($\sqrt{s} = 7$ TeV), or PowHEG interfaced to PYTHIA ($\sqrt{s} = 8$ TeV) in which the parton shower parameters are varied to span the ranges compatible with the results of measurements of $t\bar{t}$ production in association with jets [27, 39, 40]. All $t\bar{t}$ samples are normalized to the NNLO+NNLL cross-sections [41–46]: $\sigma_{t\bar{t}} = 177.3^{+10}_{-11}$ pb at $\sqrt{s} = 7$ TeV and $\sigma_{t\bar{t}} = 253^{+13}_{-15}$ pb at $\sqrt{s} = 8$ TeV.

Backgrounds with two real prompt leptons from decays of W or Z bosons (including those produced via leptonic τ decays) include Wt single-top production, $Z+\text{jets}$ production, and diboson (WW , WZ , and ZZ)+jets production. The largest background in this analysis, Wt production, is modeled using PowHEG (PowHEG-st_wtch) [47] with the CT10 PDF set and showered with PYTHIA using the Perugia 2011C tune and the corresponding CTEQ6L1 PDF set. The baseline Wt sample uses the “diagram removal” scheme to remove interference terms involving $t\bar{t}$ production, and an alternative method using the “diagram subtraction” scheme [48] is used to cross-check the validity of the prediction from the diagram removal

Physics process	7 TeV analysis	8 TeV analysis
$t\bar{t}$	POWHEG+PYTHIA ($h_{\text{damp}} = \infty$)	POWHEG+PYTHIA ($h_{\text{damp}} = m_t$)
Wt	POWHEG+PYTHIA	POWHEG+PYTHIA
$Z(\rightarrow \tau\tau)+\text{jets}$	ALPGEN+HERWIG	ALPGEN+PYTHIA
$Z(\rightarrow ee/\mu\mu)+\text{jets}$	ALPGEN+HERWIG and data	-
Diboson+jets	ALPGEN+HERWIG	ALPGEN+HERWIG
Fake leptons	Data	Various MC samples and data

Table 1: List of baseline MC samples used in the 7 TeV and 8 TeV analyses. The $Z(\rightarrow ee/\mu\mu)+\text{jets}$ process is not included in the 8 TeV analysis as the analysis uses only the $e\mu$ channel.

scheme and to assess systematic uncertainties. The cross-section employed for Wt single-top event generation is 15.7 ± 1.2 pb ($\sqrt{s} = 7$ TeV) and 22.4 ± 1.5 pb ($\sqrt{s} = 8$ TeV), as obtained from NLO+NNLL calculations [49]. The $Z(\rightarrow \ell\ell)+\text{jets}$ background is modeled using ALPGEN with the CTEQ6L1 PDFs, interfaced either to HERWIG and JIMMY with the ATLAS AUET2 tune and the CT10 PDFs ($\sqrt{s} = 7$ TeV) or to PYTHIA6 with the Perugia P2011C tune and the CTEQ6L1 PDFs, including LO matrix elements for $Zb\bar{b}$ and $Zc\bar{c}$ production ($\sqrt{s} = 8$ TeV). Inclusive Z boson cross-sections are set to the NNLO predictions from FEWZ [50], but the normalizations of $Z(\rightarrow ee/\mu\mu)+\text{jets}$ in the $\sqrt{s} = 7$ TeV analysis are determined from data using the same procedure used in Refs. [51, 52]. The diboson background is modeled using ALPGEN with the CTEQ6L1 PDFs interfaced to HERWIG and JIMMY with the AUET2 tune and the CT10 PDFs, and the cross-sections are normalized to NLO QCD calculations [53].

Background processes where one or more of the reconstructed lepton candidates are nonprompt or misidentified (referred to as “fake leptons”) arise from $t\bar{t}$ production, $W+\text{jets}$ production, and single-top production in the t -channel or s -channel. The $\sqrt{s} = 7$ TeV analysis uses a matrix method [51] to estimate the fake-lepton background directly from data, while the $\sqrt{s} = 8$ TeV analysis uses event samples of same-sign leptons in both data and simulations to estimate the fake-lepton contributions in these processes [1]. The fake-lepton contributions from $t\bar{t}$ production are simulated from the same baseline $t\bar{t}$ signal sample, which includes the $\ell+\text{jets}$ decay channel, and $t\bar{t}+V$ samples where $V = W$ or Z , modeled by MADGRAPH [54] interfaced to PYTHIA with the Perugia P2011C tune and the CTEQ6L1 PDFs. The $W+\text{jets}$ production is simulated using ALPGEN with the CTEQ6L1 PDFs interfaced to PYTHIA6 with the Perugia P2011C tune and the CTEQ6L1 PDFs, including LO matrix elements for $Wb\bar{b}$, $Wc\bar{c}$, and Wc processes. The t -channel single-top production is modeled using the ACERMC [55] generator, while POWHEG is used for the production in the s -channel, and both generators are interfaced to PYTHIA6 using the Perugia P2011C tune and the CTEQ6L1 PDFs. Different methods are used in the two datasets due to the different trigger conditions and because the 7 TeV analysis uses all 3 dilepton channels. Other backgrounds are negligible after the event selections used in this analysis.

Table 1 summarizes the baseline signal and background MC simulated samples used in the 7 TeV and 8 TeV analyses.

4 Object and event selection

4.1 Object definition

Electron candidates are reconstructed as charged-particle tracks in the inner detector associated with energy deposits in the electromagnetic calorimeter, and must satisfy tight identification criteria [56]. Electron candidates are required to have transverse energy $E_T > 25\text{GeV}$ and pseudorapidity $|\eta| < 2.47$, while excluding the transition region between the barrel and the endcap calorimeters ($1.37 < |\eta| < 1.52$). Isolation requirements on calorimeter and tracking variables are used to reduce the background from nonprompt electrons. The calorimeter isolation variable is based on the energy sum of cells within a cone of size $\Delta R = 0.2$ around the direction of each electron candidate. This energy sum excludes cells associated with the electron cluster and is corrected for leakage from the electron cluster itself and for energy deposits from pileup. The tracking isolation variable is based on the track p_T sum around the electron in a cone of size $\Delta R = 0.3$, excluding the electron track. In every p_T bin, both requirements are chosen to result separately in a 90% (98%) electron selection efficiency for prompt electrons from $Z \rightarrow ee$ decays in the 7 TeV (8 TeV) analysis.

Muon candidates are identified by matching track segments in the muon spectrometer with tracks in the inner detector, and are required to be in the region $|\eta| < 2.5$ and have $p_T > 20(25)\text{GeV}$ in the 7 TeV (8 TeV) analysis. To reduce the background from muons originating from heavy-flavor decays inside jets, muons are required to be separated by $\Delta R = 0.4$ from the nearest jet, and to be isolated. In the 7 TeV analysis, the isolation of muons requires the calorimeter transverse energy within a cone of fixed size $\Delta R = 0.2$ and the sum of track p_T within a cone of fixed size $\Delta R = 0.3$ around the muon, except the contribution from the muon itself, to be less than 4GeV and 2.5GeV, respectively. In the 8 TeV analysis, muons are required to satisfy $I^\ell < 0.05$ where the isolation variable is the ratio of the sum of p_T of tracks, excluding the muon, in a cone of variable size $\Delta R = 10\text{GeV}/p_T(\mu)$ to the p_T of the muon [57]. Both isolation requirements result in an efficiency of about 97% for prompt muons from $Z \rightarrow \mu\mu$ decays.

Jets are reconstructed by the anti- k_t algorithm [58] with a radius parameter $R = 0.4$ using calorimeter energy clusters [59], which are calibrated at the electromagnetic energy scale for the $\sqrt{s} = 7\text{TeV}$ dataset, or using the local cluster weighting method for $\sqrt{s} = 8\text{TeV}$ [60]. The energies of jets are then calibrated using an energy- and η -dependent simulation-based calibration scheme with *in situ* corrections based on data. Different calibration procedures were used for the 7 TeV and 8 TeV datasets due to the different pileup conditions. The effects of pileup on the jet energy calibration at 8 TeV are further reduced using the jet area method as described in Ref. [61]. Jets with $p_T > 25\text{ GeV}$ and $|\eta| < 2.5$ are accepted. To suppress jets from pileup, a requirement on the jet vertex fraction (JVF), the ratio of the sum of the p_T of tracks associated with both the jet and the primary vertex to the sum of the p_T of all tracks associated with the jet, is imposed based on the different pileup conditions in the $\sqrt{s} = 7\text{TeV}$ and $\sqrt{s} = 8\text{TeV}$ [1]. At 7 TeV, jets are required to satisfy $|\text{JVF}| > 0.75$ while at 8 TeV, jets with $p_T < 50\text{ GeV}$ and $|\eta| < 2.4$ are required to satisfy $|\text{JVF}| > 0.5$. To prevent double-counting of electron energy deposits as jets, the closest jet lying $\Delta R < 0.2$ from a reconstructed electron is removed; and finally, a lepton lying $\Delta R < 0.4$ from a selected jet is discarded to reject leptons from heavy-flavor decays.

The purity of $t\bar{t}$ events in the selected sample is improved by tagging jets containing b -hadrons (“ b -tagging”). Information from the track impact parameters, secondary vertex position, and decay topology is combined in a multivariate discriminant (MV1) [62, 63]. Jets are defined to be b -tagged if the MV1

discriminant value is larger than a threshold (operating point) corresponding to an average 70% efficiency for tagging b -quark jets from top quark decays in $t\bar{t}$ events, with about 1% and 20% probability of misidentifying light-flavor jets and charm-jets, respectively.

The missing transverse momentum E_T^{miss} is derived from the vector sum of calorimeter cell energies within $|\eta| < 4.9$ associated with physics objects (electrons, muons, and jets) and corrected with their dedicated calibrations, as well as the transverse energy deposited in the calorimeter cells not associated with these objects [64].

4.2 Event selection

Events in the 7 TeV and 8 TeV analyses are selected based on the above definitions of reconstructed objects and the event quality. All events are required to have at least one primary vertex² reconstructed from at least five tracks with $p_T > 0.4$ GeV, and events compatible with cosmic-ray interactions are rejected. All jets are required to pass jet quality and timing requirements and at least one lepton is required to match in (η, ϕ) space with particle(s) that triggered the event. The dilepton event sample is selected by requiring exactly two charged leptons (electrons or muons) with opposite-sign charge and at least two jets, including at least one that is b -tagged.

To suppress backgrounds from Drell-Yan and multijet processes in the ee and $\mu\mu$ channels in the 7 TeV analysis, the missing transverse momentum E_T^{miss} is required to be greater than 60 GeV, and the dilepton invariant mass $m_{\ell\ell}$ is required to be outside the Z boson mass window $|m_{\ell\ell} - 91\text{GeV}| > 10\text{ GeV}$. The dilepton invariant mass is also required to be above 15 GeV in the ee and $\mu\mu$ channels to reject backgrounds from bottom-quark pair and vector-meson decays. No E_T^{miss} nor $m_{\ell\ell}$ requirements are applied in the $e\mu$ channel, but a reconstructed variable, H_T , defined to be the scalar sum of the p_T of all selected leptons and jets in an event, is required to be greater than 130 GeV to suppress remaining background from $Z/\gamma^* + \text{jets}$ processes at 7 TeV. In the 8 TeV analysis the H_T requirement is not applied, since the improvement is negligible due to a higher muon p_T requirement than the 7 TeV analysis.

In the 7 TeV analysis, an additional requirement using the invariant mass of a jet and a lepton is also applied to reject events where the reconstructed jet does not originate from the $t\bar{t}$ decay (wrong-jet events). Exploiting the kinematics of top quark decay with the constraint from the top quark mass m_t , the invariant mass of the jet with the second highest value of the b -tagging discriminant j_2 and either of the leptons ℓ^+/ℓ^- is required to be less than 0.8 of m_t ($m_{j_2\ell^+}/m_t < 0.8$ OR $m_{j_2\ell^-}/m_t < 0.8$). This cut value was optimized to provide about 94% selection efficiency while rejecting about 16% of the wrong-jet events in the simulated $t\bar{t}$ dilepton event sample.

Table 2 shows a summary of the event selections for the 7 TeV and 8 TeV analyses. The numbers of events that fulfill all selection requirements are shown in Table 3.

5 Reconstruction

To reconstruct the $t\bar{t}$ system the two jets identified as most likely to contain b -hadrons are used. This choice improves the resolution of the $t\bar{t}$ -system observables as the jets are more likely to have originated from top quark decay. In both the 7 TeV and 8 TeV analyses, the fractional resolution for $m_{t\bar{t}}$ is typically

² The primary vertex is defined to be the reconstructed vertex with the highest $\sum p_T^2$ of the associated tracks in the event.

	7TeV			8TeV
Selection	ee	$\mu\mu$	$e\mu$	$e\mu$
Leptons	Exactly 2 leptons, opposite-sign charge, isolated Electrons: $E_T > 25\text{GeV}$, $ \eta < 2.47$, excluding $1.37 < \eta < 1.52$ Muons: $p_T > 20\text{GeV}$, $ \eta < 2.5$			
Jets		≥ 2 jets, $p_T > 25\text{GeV}$, $ \eta < 2.5$ ≥ 1 b -tagged jet at $\epsilon_b = 70\%$		$p_T > 25\text{GeV}$, $ \eta < 2.5$
$m_{\ell\ell}$	$ m_{\ell\ell} - 91\text{GeV} > 10\text{GeV}$, $m_{\ell\ell} > 15\text{GeV}$		None	None
E_T^{miss} or H_T	$E_T^{\text{miss}} > 60\text{GeV}$		$H_T > 130\text{GeV}$	None
$m_{j\ell}$	$m_{j_2\ell^+}/m_t < 0.8$ OR $m_{j_2\ell^-}/m_t < 0.8$			None

Table 2: Summary of the event selections for the 7 TeV and 8 TeV analyses.

Channel	7TeV			8TeV
	ee	$\mu\mu$	$e\mu$	$e\mu$
$t\bar{t}$	480 ± 40	1420 ± 60	3740 ± 170	26700 ± 800
Wt	20 ± 4	58 ± 15	155 ± 23	1280 ± 110
Fake leptons	12 ± 6	11.4 ± 3.4	50 ± 20	230 ± 110
$Z(\rightarrow \tau\tau) + \text{jets}$	0.43 ± 0.33	2.6 ± 1.2	5.8 ± 1.2	80 ± 34
$Z(\rightarrow ee/\mu\mu) + \text{jets}$	2.2 ± 1.0	6 ± 4	-	-
Diboson+jets	1.03 ± 0.31	3.2 ± 1.0	9.0 ± 2.4	77 ± 31
Predicted	520 ± 40	1500 ± 60	3960 ± 180	28400 ± 800
Observed	532	1509	4038	28772

Table 3: Predicted event yields and uncertainties for $t\bar{t}$ signal and backgrounds compared to observed event yields in the 7 TeV and 8 TeV analyses. The uncertainties include all systematic uncertainties discussed in Section 7 except $t\bar{t}$ modeling.

below 20%, while for $p_{T,t\bar{t}}$ the fractional resolution is 35% at 100 GeV and improves as a function of $p_{T,t\bar{t}}$. The resolution for $|y_{t\bar{t}}|$ is on average 17%.

An approximate four-momentum of the $t\bar{t}$ system is reconstructed from two leptons, two jets, and missing transverse momentum E_T^{miss} as:

$$\begin{aligned}
 E_{\text{total}} &= E(\ell_1) + E(\ell_2) + E(j_1) + E(j_2) + E_T^{\text{miss}} \\
 p_x &= p_x(\ell_1) + p_x(\ell_2) + p_x(j_1) + p_x(j_2) + E_x^{\text{miss}} \\
 p_y &= p_y(\ell_1) + p_y(\ell_2) + p_y(j_1) + p_y(j_2) + E_y^{\text{miss}} \\
 p_z &= p_z(\ell_1) + p_z(\ell_2) + p_z(j_1) + p_z(j_2)
 \end{aligned}$$

where E indicates the energy of the corresponding objects, the $p_{x,y,z}$ is the momentum along to x -, y -, or z -axis, and the indices ℓ_1 , ℓ_2 , j_1 , and j_2 indicate the two leptons and two jets, respectively. The $t\bar{t}$ -system observables in consideration (invariant mass, transverse momentum, and rapidity) are obtained from this four-momentum.

Figures 1 and 2 show the distributions of the reconstructed $m_{t\bar{t}}$, $p_{T,t\bar{t}}$, and $|y_{t\bar{t}}|$ together with the MC

predictions at 7 TeV and 8 TeV, respectively. The bottom panel shows the ratio of the data to the total prediction. Overall there is satisfactory agreement between data and prediction.

6 Differential cross-section determination

The normalized differential cross-sections with respect to the $t\bar{t}$ -system observables, denoted as X , are obtained as follows. The estimated background contributions are subtracted from the observed number of events for each bin in the distribution of the reconstructed observable. The background-subtracted distributions are then corrected for detector acceptance and resolution effects (unfolded) and the efficiency to pass the event selection, thus extrapolated to the full phase space of $t\bar{t}$ production at parton level. The differential cross-sections are finally normalized by the total $t\bar{t}$ cross-section, obtained by integrating over all bins for each observable.

The differential cross-section is obtained from

$$\frac{d\sigma_{t\bar{t}}}{dX_i} = \frac{1}{\Delta X_i \cdot \mathcal{L} \cdot \sum_\alpha (\mathcal{B}^\alpha \cdot \epsilon_i^\alpha)} \sum_\alpha \sum_j (\mathcal{M}_{ij}^{-1})^\alpha (N_j^{\text{obs},\alpha} - N_j^{\text{bkg},\alpha}), \quad (1)$$

where i (j) indicates the bin for the observable X at parton (detector) level, N_j^{obs} is the number of observed events in data, N_j^{bkg} is the estimated number of background events, \mathcal{M}_{ij}^{-1} is the inverse of the migration matrix representing the correction for detector resolution effects, ϵ_i is the event selection efficiency with respect to the channel, \mathcal{B} is the branching ratio of the $t\bar{t}$ decays in the dilepton channel, \mathcal{L} is the integrated luminosity, ΔX_i is the bin width, and α is the dilepton channel being considered, where $\alpha = ee, \mu\mu$ or $e\mu$ for 7TeV and $\alpha = e\mu$ for 8TeV. The measured cross-section at each bin i represents the bin-averaged value at the bin. The normalized differential cross-section is obtained as $1/\sigma_{t\bar{t}} \cdot d\sigma_{t\bar{t}}/dX_i$, where $\sigma_{t\bar{t}}$ is the inclusive $t\bar{t}$ cross-section.

The unfolding from reconstruction level to parton level is carried out using the `RooUnfold` package [65] with an iterative method inspired by Bayes' theorem [66]. The number of iterations used in the unfolding procedure balances the goodness of fit and statistical uncertainties. The smallest number of iterations with χ^2/NDF (χ^2 between the unfolded and parton-level spectra over number of degrees of freedom) less than one is chosen for the distribution. In the 7 TeV analysis, two to four iterations are used depending on the observable; in the 8 TeV analysis, four iterations are used for all observables. The effect of varying the number of iterations by one was tested and confirmed to be negligible.

The detector response is described using a migration matrix that relates the generated parton-level distributions to the measured distributions. The migration matrix \mathcal{M} is determined using $t\bar{t}$ Monte Carlo samples, where the parton-level top quark is defined as the top quark after radiation and before decay.³ Figure 3 presents the migration matrices of $p_{T,t\bar{t}}$ for both 7 TeV and 8 TeV in the $e\mu$ channel. The matrix \mathcal{M}_{ij} represents the probability for an event generated at parton level with X in bin i to have a reconstructed X in bin j , so the elements of each row add up to unity (within rounding uncertainties). The probability for the parton-level events to remain in the same bin in the measured distribution is shown in the diagonal, and the off-diagonal elements represent the fraction of parton-level events that migrate into other bins. The fraction of events in the diagonal bins are the highest for $p_{T,t\bar{t}}$, while for other observables more significant migrations are present due to the effect of p_z of the undetected neutrinos in the reconstruction.

³ The generator status code for the top or antitop quark is required to be 3 in PYTHIA and 155 in HERWIG.

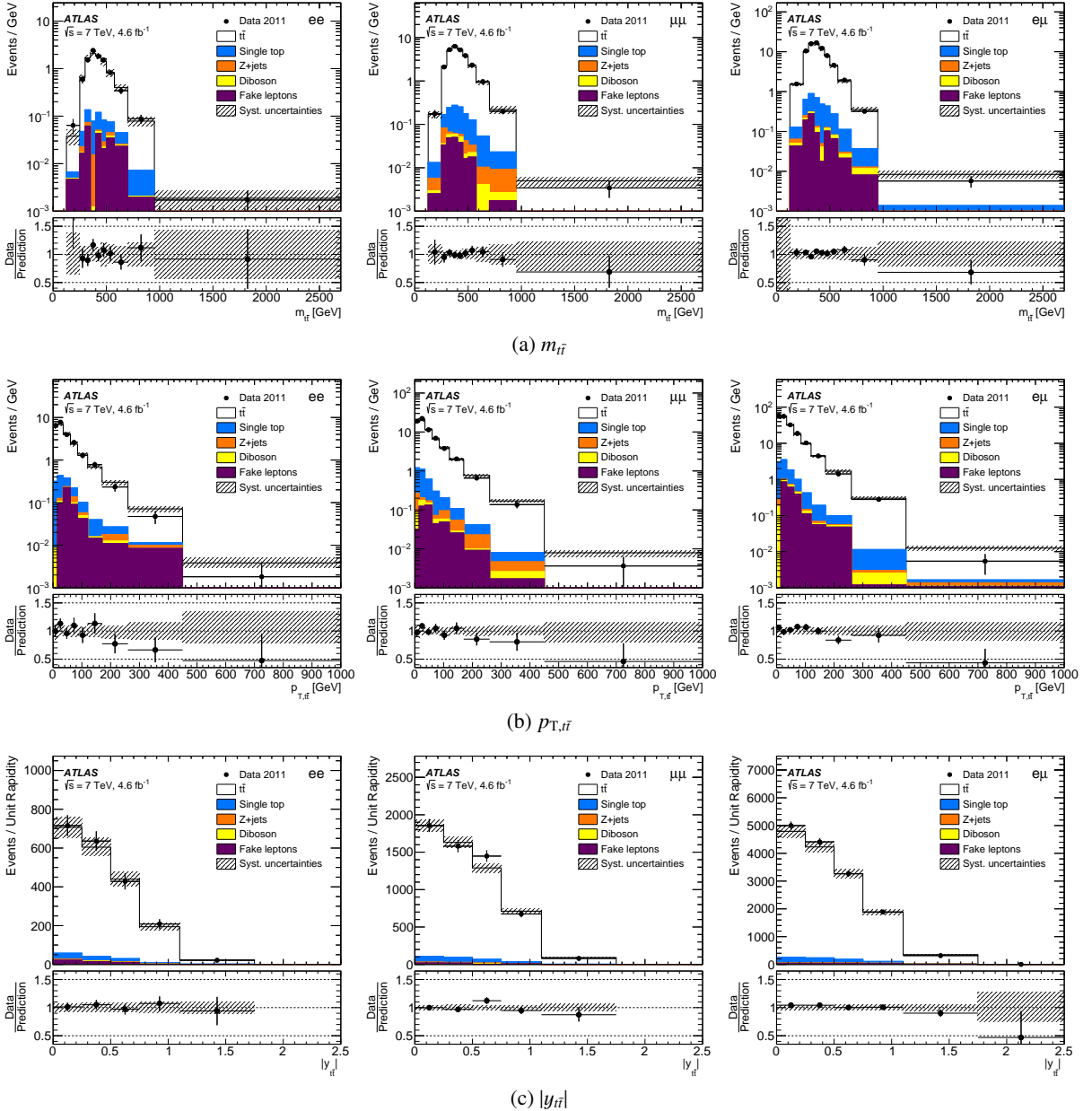


Figure 1: Distributions of (a) the invariant mass, (b) the transverse momentum, and (c) the rapidity of the $t\bar{t}$ system at the reconstruction level obtained from the $\sqrt{s} = 7$ TeV data compared with the total signal and background predictions, in the ee (left), $\mu\mu$ (center) and $e\mu$ (right) channels. The bottom panel shows the ratio of data to prediction. The error band includes all systematic uncertainties except $t\bar{t}$ modeling uncertainties. The Powheg+Pythia with $h_{\text{damp}} = \infty$ sample is used for the signal $t\bar{t}$ and is normalized to NNLO+NNLL calculations.

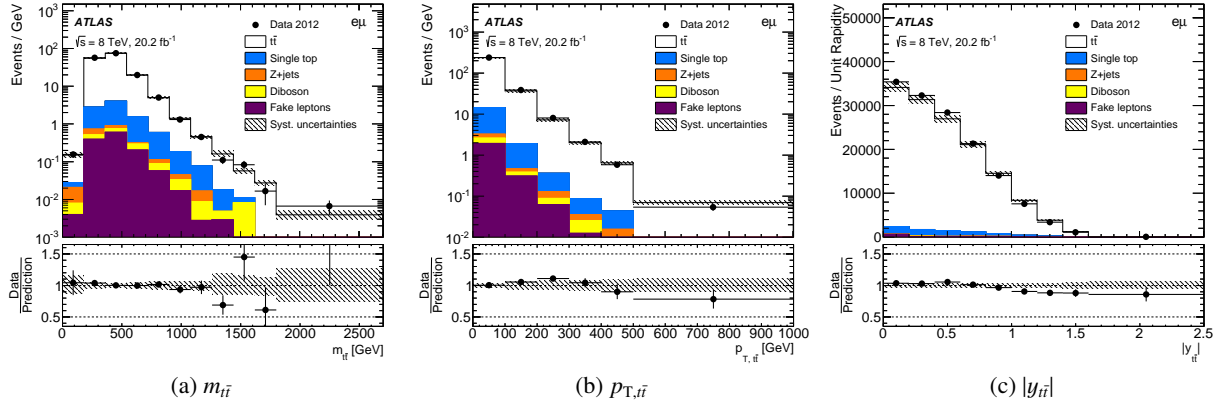


Figure 2: Distributions of (a) the invariant mass, (b) the transverse momentum, and (c) the rapidity of the $t\bar{t}$ system at the reconstruction level obtained from the $\sqrt{s} = 8$ TeV data compared with the total signal and background predictions. The bottom panel shows the ratio of data to prediction. The error band includes all systematic uncertainties except $t\bar{t}$ modeling uncertainties. The PowHEG+PYTHIA with $h_{\text{damp}} = m_t$ sample is used for the signal $t\bar{t}$ and is normalized to NNLO+NNLL calculations.

In the 7 TeV analysis, the effect of bin migrations in the ee and $\mu\mu$ channels are similar to those in the $e\mu$ channel. In the 8 TeV analysis, the bin boundaries for $m_{t\bar{t}}$ and $|y_{t\bar{t}}|$ are determined separately for the parton-level and reconstruction-level observables, based on the migrations between them.

The event selection efficiency ϵ_i for each bin i is evaluated as the ratio of the parton-level spectra before and after implementing the event selection at the reconstruction level. In both the 7 TeV and 8 TeV analyses, the efficiencies generally increase towards higher $m_{t\bar{t}}$ and $p_{T,t\bar{t}}$, while at high values of $|y_{t\bar{t}}|$ the efficiency decreases due to leptons and jets falling outside the required pseudorapidity range for reconstructed leptons and jets. The efficiencies are typically in the range of 15–20% for the $e\mu$ channel at both 7 and 8 TeV, and 3–5% and 8–13% for the ee and $\mu\mu$ channels, respectively, in the 7 TeV analysis. The lower values in the same-flavor channels are due to the rejection cuts for Drell-Yan and $Z \rightarrow \ell\ell$ events in these channels, while isolation requirements that are more restrictive for electrons than for muons in 7 TeV analyses result in further lowered efficiencies in the ee channel.

The bin width for each observable is determined by considering the resolution of the observable and the statistical precision in each bin. In the 7 TeV analysis, the bin widths are set to be the same as the ones used in the previous 7TeV ATLAS measurement in the $\ell+\text{jets}$ channel [8] due to comparable resolutions for each observable, and to enable a direct comparison of the results between the two channels. For the 8 TeV analysis, the determined bin widths are generally finer than the bin widths for the 7 TeV analysis due to the larger dataset available.

Possible biases due to the use of the MC generator in the unfolding procedure are assessed by altering the shape of the parton-level spectra in simulation using continuous functions. The altered shapes studied cover the difference observed between the default MC and data for each observable. These studies verify that the altered shapes are recovered by the unfolding based on the nominal migration matrices within statistical uncertainties.

A multichannel combination is performed in the 7TeV analysis by summing the background-subtracted observed events corrected by the migration matrix and the event selection efficiency over channels. The

results obtained from the combined dilepton channel are consistent with those from the individual channels.

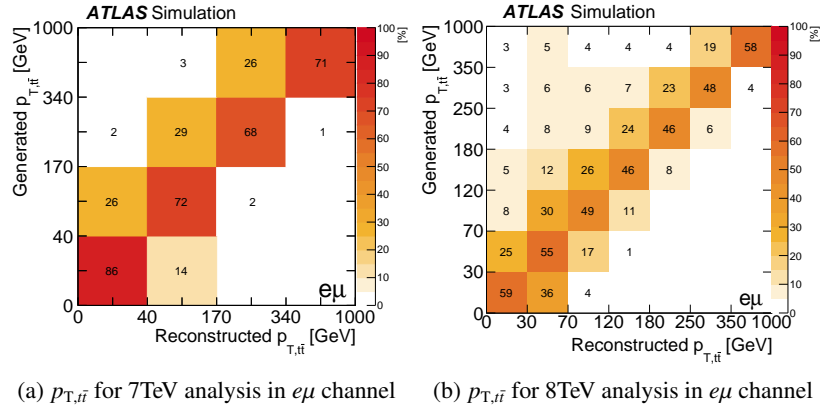


Figure 3: The migration matrix of $p_{T,tt}$ represented in probability for (a) 7TeV and (b) 8TeV in the $e\mu$ channel, obtained from $t\bar{t}$ simulation with the Powheg+Pythia generator. Different h_{damp} parameters are used at 7 TeV ($h_{\text{damp}} = \infty$) and 8 TeV ($h_{\text{damp}} = m_t$) in the Powheg+Pythia sample, where the effect of the different h_{damp} in the migration matrix is negligible. Elements in each row add up to unity. Empty elements indicate either a probability of lower than 0.5% or no events are present.

7 Uncertainties

Various sources of systematic uncertainty affect the measurement and are discussed below. The systematic uncertainties due to signal modeling and detector modeling affect the estimation of the detector response and the signal reconstruction efficiency. The systematic uncertainties due to the background estimation and the detector modeling affect the background subtraction.

The covariance matrix due to the statistical and systematic uncertainties for each normalized unfolded spectrum is obtained by evaluating the correlations between the bins for each uncertainty contribution. In particular, the correlations due to statistical fluctuations are evaluated from an ensemble of pseudoexperiments, each by varying the data event counts independently in each bin and propagating the variations through the unfolding procedure.

7.1 Signal modeling uncertainties

The signal modeling uncertainties are estimated by repeating the full analysis procedure, using an alternative MC sample to derive the migration matrix and the corrections for selection efficiency. The differences between the results obtained using the alternative and nominal MC samples are taken as systematic uncertainties.

At $\sqrt{s} = 7$ TeV, the uncertainties due to the choice of generator are estimated by comparing Powheg+Pythia and MC@NLO+HERWIG signal MC samples. The uncertainty is found to be up to 2% in $m_{t\bar{t}}$ and $|y_{t\bar{t}}|$, and in the range of 2–19% in $p_{T,tt}$ with larger values with increasing $p_{T,tt}$, due to the difference at the parton

level between the two MC $t\bar{t}$ samples in the high $p_{T,t\bar{t}}$ region. At $\sqrt{s} = 8$ TeV, the uncertainties related to the generator are estimated using PowHEG+HERWIG and MC@NLO+HERWIG signal MC samples, and the uncertainties due to parton shower and hadronization are estimated using PowHEG+PYTHIA and PowHEG+HERWIG signal MC samples. These uncertainties are typically less than 10% (3%) in $m_{t\bar{t}}$ and $p_{T,t\bar{t}}$ ($|y_{t\bar{t}}|$), and increase to 20% at large $m_{t\bar{t}}$ in the case of generator uncertainty.

The effects due to modeling of extra radiation in $t\bar{t}$ events are assessed at both the matrix element and parton shower levels. At $\sqrt{s} = 7$ TeV, the uncertainty due to matrix element renormalization and factorization scales is evaluated using MC@NLO+HERWIG samples with varied renormalization/factorization scales, and the uncertainty due to parton showering in different initial-state and final-state radiation (ISR/FSR) conditions is estimated using two different ALPGEN+PYTHIA samples with varied radiation settings. The overall effects in both cases are less than 1% in $|y_{t\bar{t}}|$ and up to 6% for $m_{t\bar{t}}$ and $p_{T,t\bar{t}}$ with the larger values towards higher values of $m_{t\bar{t}}$ and $p_{T,t\bar{t}}$. At $\sqrt{s} = 8$ TeV, the treatment of these uncertainties was improved by using PowHEG+PYTHIA samples with tuned parameters to span the variations in radiation compatible with the ATLAS $t\bar{t}$ gap fraction measurements at $\sqrt{s} = 7$ TeV [39] as discussed in detail in Ref. [67]. The samples have varied renormalization/factorization scales and h_{damp} parameter values, resulting in either more or less radiation than the nominal signal sample. The overall impact is typically less than 2% for all observables, and up to 4% towards higher values of $p_{T,t\bar{t}}$.

The uncertainties due to the choice of PDFs, which affect most significantly the signal selection efficiency, are estimated based on the PDF4LHC recommendations [68] using the MC@NLO+HERWIG sample with three different NLO PDF sets: CT10 [26], MSTW2008nlo68cl [69], and NNPDF2.3 [70]. An intra-PDF uncertainty is obtained for each PDF set by following its respective prescription while an inter-PDF uncertainty is computed as the envelope of the three intra-PDF uncertainties. The overall effect is less than 2% for all observables in both the 7 TeV and 8 TeV measurements (except for the highest $|y_{t\bar{t}}|$ bin at 8 TeV where the effect is up to 8%).

The dependence of the $t\bar{t}$ -system observables on the top quark mass m_t is evaluated at $\sqrt{s} = 7$ TeV using $t\bar{t}$ samples with different mass points at 170 GeV and 175 GeV to unfold the data, then the difference of the results at the two mass points is taken and divided by the difference Δm_t to extract the difference of the differential cross-section per GeV change of Δm_t . These studies show that the dependence of the differential cross-sections on the m_t is no more than 1% per GeV for all kinematic observables. These variations are not included in the total uncertainty.

7.2 Background modeling uncertainties

Uncertainties arising from the background estimates are evaluated by repeating the full analysis procedure, varying the background contributions by $\pm 1\sigma$ from the nominal values. The differences between the results obtained using the nominal and the varied background estimations are taken as systematic uncertainties.

The uncertainties due to the Wt background modeling are estimated by comparing the inclusive “diagram removal” and inclusive “diagram subtraction” samples. The uncertainty is typically below 1%, except for high $m_{t\bar{t}}$ and $p_{T,t\bar{t}}$ bins where the uncertainty is up to about 5% and 2%, respectively.

The relative uncertainties of 7.7% (7 TeV) and 6.8% (8 TeV) in the predicted cross-section of Wt production are applied in all bins of the differential cross-sections. An uncertainty of 5% is assigned to the predicted diboson cross-section, with an additional uncertainty of 24% per additional selected jet added

in quadrature to account for the assumption that the $(W + n + 1 \text{ jets})/(W + n \text{ jets})$ ratio is constant [51, 71]. The overall impact of these uncertainties is less than 1%.

For the $Z + \text{jets}$ background, in the $e\mu$ channel only the $Z(\rightarrow \tau\tau) + \text{jets}$ process contributes, while the $Z(\rightarrow ee) + \text{jets}$ ($Z(\rightarrow \mu\mu) + \text{jets}$) process contributes only to the ee ($\mu\mu$) channel. An inclusive uncertainty of 4% is assigned to the predicted cross-section of $Z(\rightarrow \tau\tau) + \text{jets}$, with an additional uncertainty of 24% per additional selected jet added in quadrature. The $Z(\rightarrow ee/\mu\mu) + \text{jets}$ background is estimated by a data-driven method [51, 52] that uses a control region populated with Z events. The uncertainty is evaluated by varying the control region (defined by $|m_{\ell\ell} - m_Z| < 10\text{GeV}$ and $E_T^{\text{miss}} > 30\text{GeV}$) by $\pm 5\text{ GeV}$ in E_T^{miss} . The overall impact of these uncertainties is less than 1% in both the 7 TeV and 8 TeV measurements.

The fake-lepton contribution is estimated directly from data, using a matrix method [51] in 7 TeV data and the same-sign dilepton events in the 8 TeV data sample [1]. In the 7 TeV analysis, the uncertainty of the fake-lepton background is evaluated by considering the uncertainties in the real- and fake-lepton efficiency measurements and by comparing results obtained from different matrix methods. In the 8 TeV analysis a conservative uncertainty of 50% is assigned to the fake-lepton background [1]. The impact of the uncertainty is typically less than 1% in all observables, except in high- $m_{t\bar{t}}$ and high- $p_{T,t\bar{t}}$ bins where it is up to 5%.

7.3 Detector modeling uncertainties

The uncertainties due to the detector modeling are estimated for each bin based on the methods described in Ref. [1]. They affect the detector response including signal reconstruction efficiency and the estimation of background events that passed all event selections and their kinematic distribution. The full analysis procedure is repeated with the varied detector modeling, and the difference between the results using the nominal and the varied modeling is taken as a systematic uncertainty.

The lepton reconstruction efficiency in simulation is calibrated by correction factors derived from measurements of these efficiencies in data using control regions enriched in $Z \rightarrow \ell\ell$ events. The lepton trigger and reconstruction efficiency correction factors, energy scale, and resolution are varied within the uncertainties in the $Z \rightarrow \ell\ell$ measurements [72, 73].

The jet energy scale (JES) uncertainty is derived using a combination of simulations, test beam data and *in situ* measurements [60, 74, 75]. Additional contributions from the jet flavor composition, calorimeter response to different jet flavors, and pileup are taken into account. Uncertainties in the jet energy resolution are obtained with an *in situ* measurement of the jet response balance in dijet events [76].

The difference in b -tagging efficiency between data and MC simulation is estimated in lepton+jets $t\bar{t}$ events with the selected jet containing a b -hadron on the leptonic side [77]. Correction factors are also applied for jets originating from light hadrons that are misidentified as jets containing b -hadrons. The associated systematic uncertainties are computed by varying the correction factors within their uncertainties.

The uncertainty associated with E_T^{miss} is calculated by propagating the energy scale and resolution systematic uncertainties to all jets and leptons in the E_T^{miss} calculation. Additional E_T^{miss} uncertainties arising from energy deposits not associated with any reconstructed objects are also included [64].

The uncertainty due to the finite size of the MC simulated samples are evaluated by varying the content of the migration matrix with a Poisson distribution. The standard deviation of the ensemble of results

unfolded with the varied matrices is taken as the uncertainty. The effect is more significant in the 7 TeV analysis (up to 3% in high- $m_{t\bar{t}}$ and high- $p_{T,t\bar{t}}$ bins), due to the smaller size of the MC simulation sample available at 7 TeV. In the 8 TeV analysis, while the MC statistical uncertainty is less significant (sub-percent overall), an additional uncertainty is included to account for the bias introduced by the unfolding procedure due to the observed deviation between data and the predicted $t\bar{t}$ events. The typical size of the bias is less than 1%, and increases towards higher $m_{t\bar{t}}$, $p_{T,t\bar{t}}$, and $|y_{t\bar{t}}|$ up to about 4%. The bias in the 7 TeV analysis is taken into account by choosing an unfolding parameter based on the level of bias for an observable, which is reflected in the data statistical uncertainty and thus not included as a systematic uncertainty.

The uncertainty in the integrated luminosity is estimated to be 1.8% for $\sqrt{s} = 7$ TeV [17] and 1.9% for $\sqrt{s} = 8$ TeV [18]. The effect of the uncertainty is substantially reduced in the normalized differential cross-sections due to large bin-to-bin correlations.

7.4 Summary of the main sources of systematic uncertainty

For $m_{t\bar{t}}$, the largest systematic uncertainties come from signal modeling (including generator choice, parton showering and hadronization, and extra radiation), JES, and Wt background modeling (at large $m_{t\bar{t}}$). The uncertainty due to signal modeling in $m_{t\bar{t}}$ is generally smaller at 7 TeV because of the requirement on the jet-lepton invariant mass, which reduces the fraction of wrong-jet events used to reconstruct the $t\bar{t}$ -system, is applied in the 7 TeV analysis but not in the 8 TeV analysis. For $p_{T,t\bar{t}}$, the uncertainty from signal modeling (including generator choice, parton showering and hadronization, and extra radiation) is the largest, followed by JES. The main uncertainties for $|y_{t\bar{t}}|$ come from PDF and signal generator choice.

8 Results

The unfolded parton-level normalized differential cross-sections for $\sqrt{s} = 7$ TeV and $\sqrt{s} = 8$ TeV are shown in Table 4 and Table 5, respectively. The total inclusive $t\bar{t}$ cross-sections, evaluated by integrating the spectra before the normalization, agree with the theoretical calculations and other inclusive measurements within uncertainties at both energies. The estimated uncertainties include all sources discussed in Section 7.

Comparisons of the data distributions with different SM predictions are quantified by computing χ^2 values and inferring p -values (probability of obtaining a χ^2 is larger than or equal to the observed value) from the χ^2 values and the number of degrees of freedom (NDF). The χ^2 is defined as

$$\chi^2 = V^T \cdot \text{Cov}^{-1} \cdot V \quad (2)$$

where V is the vector of the differences between the data and the theoretical predictions, and Cov^{-1} is the inverse of the full bin-to-bin covariance matrix. Due to the normalization constraint in the derivation of normalized differential cross-sections, the NDF and the rank of the covariance matrix is reduced by one unit to $N_b - 1$, where N_b is the number of bins in the spectrum being considered. Consequently, one of the N_b elements in V and the corresponding row and column in the $N_b \times N_b$ full covariance matrix Cov is discarded, and the $N_b - 1 \times N_b - 1$ submatrix obtained in this way is invertible, allowing the χ^2 to be computed. The χ^2 value does not depend on which element is discarded from the vector V_{N_b-1} and the

corresponding sub-matrix Cov_{N_b-1} . The evaluation of χ^2 under the normalization constraint follows the same procedure as described in Refs. [8, 11].

The comparison of the measured normalized distributions to predictions from different MC generators of $t\bar{t}$ production are shown graphically in Figure 4 for $\sqrt{s} = 7\text{TeV}$ and Figure 5 for $\sqrt{s} = 8\text{TeV}$, with the corresponding p -values comparing the measured spectra to the predictions from the MC generators in Table 6 and Table 7. Predictions from Powheg+Pythia with $h_{\text{damp}} = m_t$, MC@NLO+Herwig, Powheg+Pythia with $h_{\text{damp}} = \infty$, and Powheg+Herwig are used for comparison with data. In the 7 TeV analysis, Alpgen+Herwig is also used for the comparison, as it was the default sample used in the differential measurement in the $\ell+\text{jets}$ channel by ATLAS [8]. Both NLO generators (Powheg and MC@NLO) use the NLO CT10 [26] PDF set, while Alpgen+Herwig uses the LO CTEQ6L1 [78] PDF set.

Most of the generators agree with data in a wide kinematic range of the distributions. The $m_{t\bar{t}}$ spectrum is well described by most of the generators at both 7 TeV and 8 TeV, except for Powheg+Pythia in the highest $m_{t\bar{t}}$ bin in the 7 TeV analysis. For $p_{\text{T},t\bar{t}}$, agreement with Powheg+Pythia with $h_{\text{damp}} = \infty$ is particularly bad due to a harder $p_{\text{T},t\bar{t}}$ spectrum than data at both 7 TeV and 8 TeV. Better agreement with data is obtained from Powheg+Pythia with $h_{\text{damp}} = m_t$. This is consistent with the studies in Refs. [27, 28] using data from the $\sqrt{s} = 7\text{TeV}$ ATLAS parton-level measurement in the $\ell+\text{jets}$ channel [8]. In both the 7 TeV and 8 TeV analyses, MC@NLO+Herwig describes the $p_{\text{T},t\bar{t}}$ spectrum well also. Similar good agreement is also observed in 7 TeV and 8 TeV parton-level measurements by ATLAS in the $\ell+\text{jets}$ channel [8, 11]. For $|y_{t\bar{t}}|$, all the generators show fair agreement with data in the 7 TeV analysis, while at 8 TeV, none of the generators provides an adequate description of $|y_{t\bar{t}}|$. This difference in the level of agreement is due to the improved statistical precision and finer binning in $|y_{t\bar{t}}|$ for the 8 TeV analysis. The increasing discrepancy between data and MC prediction with increasing $|y_{t\bar{t}}|$ is also observed at the reconstructed level for both energies, as shown in Figure 1 and Figure 2. This observation is also consistent with the results of the ATLAS differential cross-section measurements in the $\ell+\text{jets}$ channel, at both 7 and 8 TeV [8, 11].

Figure 6 shows the normalized differential cross-sections at $\sqrt{s} = 8\text{TeV}$ compared with the predictions of MC@NLO+Herwig reweighted with different PDF sets: CT10, MSTW2008nlo68cl, NNPDF2.3, and HERAPDF15NLO. The hatched bands show the uncertainty of each PDF set. All predictions are compatible with the measured cross-sections within the uncertainties in the cases of $m_{t\bar{t}}$ and $p_{\text{T},t\bar{t}}$. However, for $|y_{t\bar{t}}|$, the MC@NLO+Herwig sample with the CT10 PDF set does not agree with the measured cross-sections at $|y_{t\bar{t}}| \sim 1.6$. Using NNPDF or HERAPDF significantly improves the agreement. The corresponding p -values are shown in Table 8.

Figure 7 and Table 9 show the comparison of the measured normalized differential cross-sections at $\sqrt{s} = 8\text{TeV}$ to Powheg+Pythia with different levels of radiation. The nominal sample (with $h_{\text{damp}} = m_t$) and two other samples, one with lower radiation ($h_{\text{damp}} = m_t$ and $\mu = 2.0$) and one with higher radiation ($h_{\text{damp}} = 2.0m_t$ and $\mu = 0.5$) than the nominal one, are used in the comparison. The $p_{\text{T},t\bar{t}}$ spectrum, particularly sensitive to radiation activity, shows that the nominal sample has better agreement with data. This observation is also consistent with the studies in Refs. [27, 28].

The parton-level measured distributions are also compared to fixed-order QCD calculations. Figure 8 and Figure 9 show the comparison with theoretical QCD NLO+NNLL predictions for $m_{t\bar{t}}$ [79] and $p_{\text{T},t\bar{t}}$ [80, 81] distributions at $\sqrt{s} = 7\text{TeV}$ and $\sqrt{s} = 8\text{TeV}$, respectively, and the corresponding p -values are given in Table 10. The predictions are calculated using the mass of the $t\bar{t}$ system as the dynamic scale of the process and the MSTW2008nnlo PDF [69] set. The NLO+NNLL calculation shows a good agreement in the $m_{t\bar{t}}$ spectrum and a large discrepancy for high values of $p_{\text{T},t\bar{t}}$ in measurements at both $\sqrt{s} = 7\text{TeV}$

and $\sqrt{s} = 8\text{TeV}$. Figure 10 shows the comparison of a full NNLO calculation [82] to the $m_{t\bar{t}}$ and $|y_{t\bar{t}}|$ measurements at $\sqrt{s} = 8\text{ TeV}$. The full NNLO calculation is evaluated using the fixed scale $\mu = m_t$ and the MSTW2008nnlo PDF [69]. The range of the NNLO prediction does not fully cover the highest bins in $m_{t\bar{t}}$ and $|y_{t\bar{t}}|$ and thus no prediction is shown in those bins.

The $\sqrt{s} = 7\text{TeV}$ results, together with previous results reported in $\ell+\text{jets}$ channel by ATLAS [8], are summarized with the SM predictions in Figure 11. This direct comparison can be performed due to the same bin widths of the $t\bar{t}$ -system observables used in both analyses. All distributions are plotted as ratios with respect to dilepton channel results. The normalized results from both the dilepton and $\ell+\text{jets}$ channels are consistent with each other in all $t\bar{t}$ -system variables within the uncertainties of the measurements.

$m_{t\bar{t}}$ [GeV]	$\frac{1}{\sigma} \frac{d\sigma}{dm_{t\bar{t}}}$ [10^{-3}GeV^{-1}]	Stat. [%]	Syst. [%]
250–450	2.41 ± 0.08	± 1.6	± 2.9
450–550	2.79 ± 0.05	± 1.4	± 1.0
550–700	1.09 ± 0.06	± 3.1	± 4.6
700–950	0.252 ± 0.023	± 5.7	± 7.2
950–2700	0.0066 ± 0.0014	± 16	± 14

$p_{T,t\bar{t}}$ [GeV]	$\frac{1}{\sigma} \frac{d\sigma}{dp_{T,t\bar{t}}}$ [10^{-3}GeV^{-1}]	Stat. [%]	Syst. [%]
0–40	13.5 ± 0.7	± 1.2	± 4.7
40–170	3.14 ± 0.17	± 1.5	± 5.1
170–340	0.269 ± 0.033	± 6.1	± 11
340–1000	0.0088 ± 0.0026	± 19	± 22

$ y_{t\bar{t}} $	$\frac{1}{\sigma} \frac{d\sigma}{dy_{t\bar{t}}}$	Stat. [%]	Syst. [%]
0–0.5	0.826 ± 0.019	± 1.9	± 1.4
0.5–1	0.643 ± 0.018	± 1.8	± 2.1
1–2.5	0.177 ± 0.007	± 2.8	± 3.0

Table 4: Normalized $t\bar{t}$ differential cross-sections for the different $t\bar{t}$ kinematic variables at $\sqrt{s} = 7\text{ TeV}$. The cross-sections in the last bins include events (if any) beyond of the bin edges. The uncertainties quoted in the second column represent the statistical and systematic uncertainties added in quadrature.

$m_{t\bar{t}}$ [GeV]	$\frac{1}{\sigma} \frac{d\sigma}{dm_{t\bar{t}}}$ [10^{-3}GeV^{-1}]	Stat. [%]	Syst. [%]
250–450	2.41 ± 0.07	± 1.1	± 6.0
450–570	2.56 ± 0.05	± 1.1	± 1.9
570–700	0.97 ± 0.08	± 1.6	± 8.4
700–850	0.35 ± 0.05	± 2.5	± 13
850–1000	0.129 ± 0.022	± 3.6	± 17
1000–2700	0.0086 ± 0.0024	± 6.6	± 23

$p_{T,t\bar{t}}$ [GeV]	$\frac{1}{\sigma} \frac{d\sigma}{dp_{T,t\bar{t}}}$ [10^{-3}GeV^{-1}]	Stat. [%]	Syst. [%]
0–30	14.3 ± 1.0	± 1.2	± 6.9
30–70	7.60 ± 0.16	± 1.1	± 1.9
70–120	2.94 ± 0.28	± 1.8	± 9.3
120–180	1.14 ± 0.12	± 2.7	± 9.5
180–250	0.42 ± 0.04	± 4.0	± 9.7
250–350	0.143 ± 0.018	± 6.0	± 11
350–1000	0.0099 ± 0.0015	± 8.9	± 12

$ y_{t\bar{t}} $	$\frac{1}{\sigma} \frac{d\sigma}{dy_{t\bar{t}}}$	Stat. [%]	Syst. [%]
0.0–0.4	0.821 ± 0.021	± 1.3	± 2.2
0.4–0.8	0.721 ± 0.018	± 1.3	± 2.1
0.8–1.2	0.499 ± 0.013	± 1.6	± 2.0
1.2–2.0	0.206 ± 0.006	± 2.4	± 1.9
2.0–2.8	0.0226 ± 0.0023	± 8.3	± 9.9

Table 5: Normalized $t\bar{t}$ differential cross-sections for the different $t\bar{t}$ kinematic variables at $\sqrt{s} = 8$ TeV. The uncertainties quoted in the second column represent the statistical and systematic uncertainties added in quadrature.

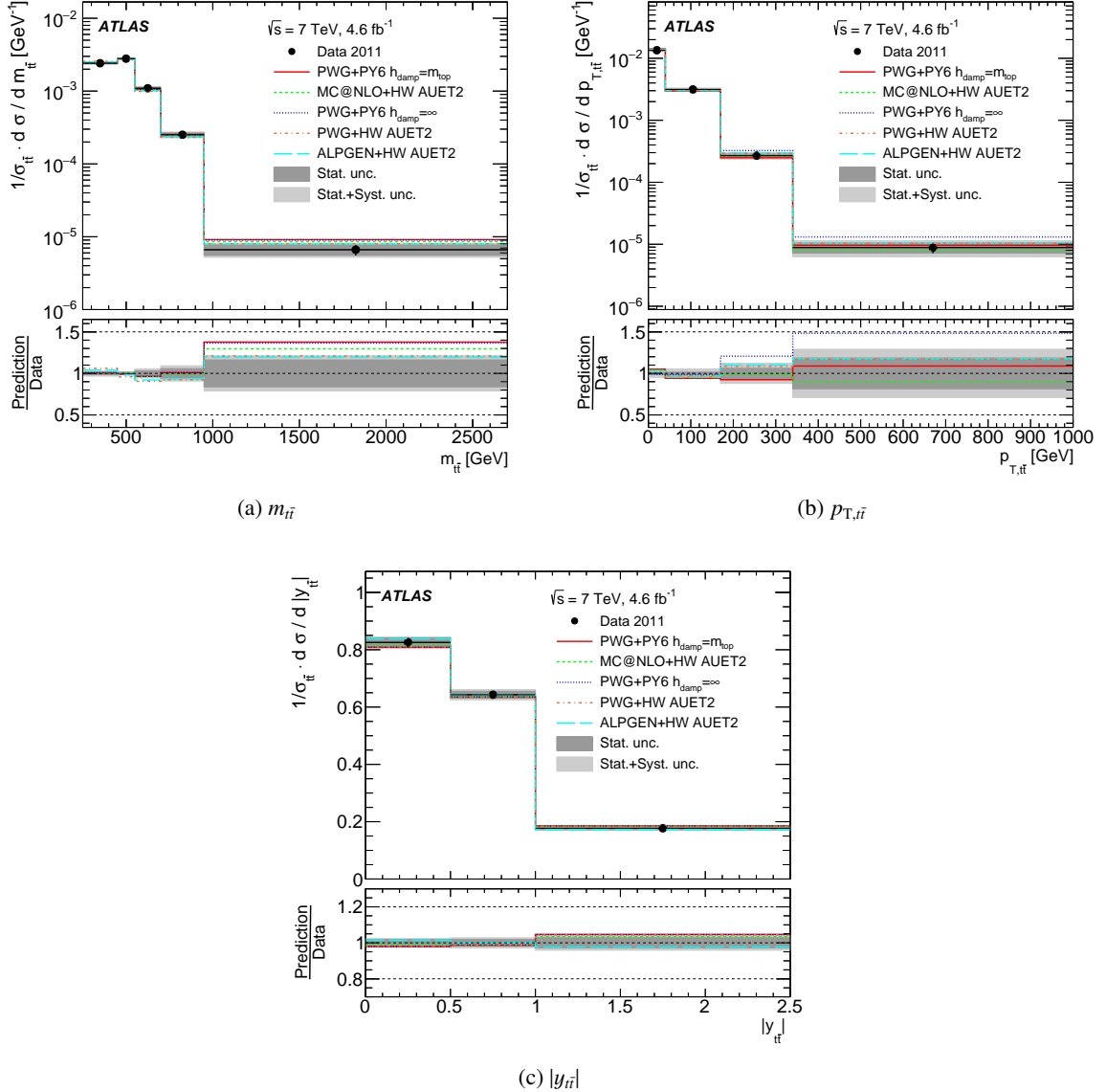


Figure 4: Normalized $t\bar{t}$ differential cross-sections as a function of the (a) invariant mass ($m_{t\bar{t}}$) (b) transverse momentum ($p_{T,t\bar{t}}$) and (c) absolute value of the rapidity ($|y_{t\bar{t}}|$) of the $t\bar{t}$ system at $\sqrt{s} = 7 \text{ TeV}$ measured in the dilepton channel compared to theoretical predictions from MC generators. All generators use the NLO CT10 [26] PDF, except for ALPGEN+HERWIG using the LO CTEQ6L1 PDF. The bottom panel shows the ratio of prediction to data. The light (dark) gray band includes the total (data statistical) uncertainty in the data in each bin.

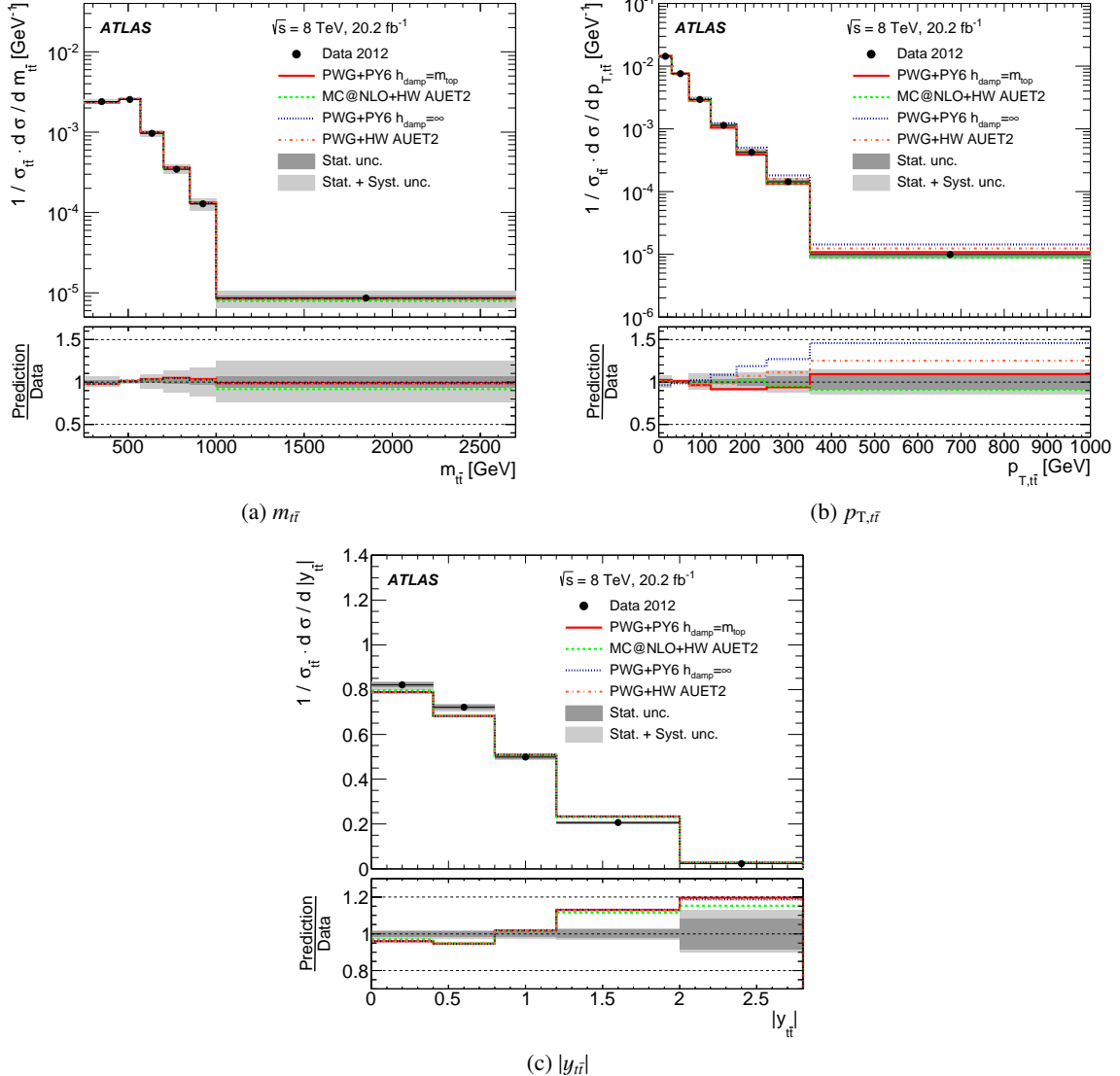


Figure 5: Normalized $t\bar{t}$ differential cross-sections as a function of the (a) invariant mass ($m_{t\bar{t}}$) (b) transverse momentum ($p_{T,t\bar{t}}$) and (c) absolute value of the rapidity ($|y_{t\bar{t}}|$) of the $t\bar{t}$ system at $\sqrt{s} = 8$ TeV measured in the dilepton $e\mu$ channel compared to theoretical predictions from MC generators. All generators use the NLO CT10 [26] PDF. The bottom panel shows the ratio of prediction to data. The light (dark) gray band includes the total (data statistical) uncertainty in the data in each bin.

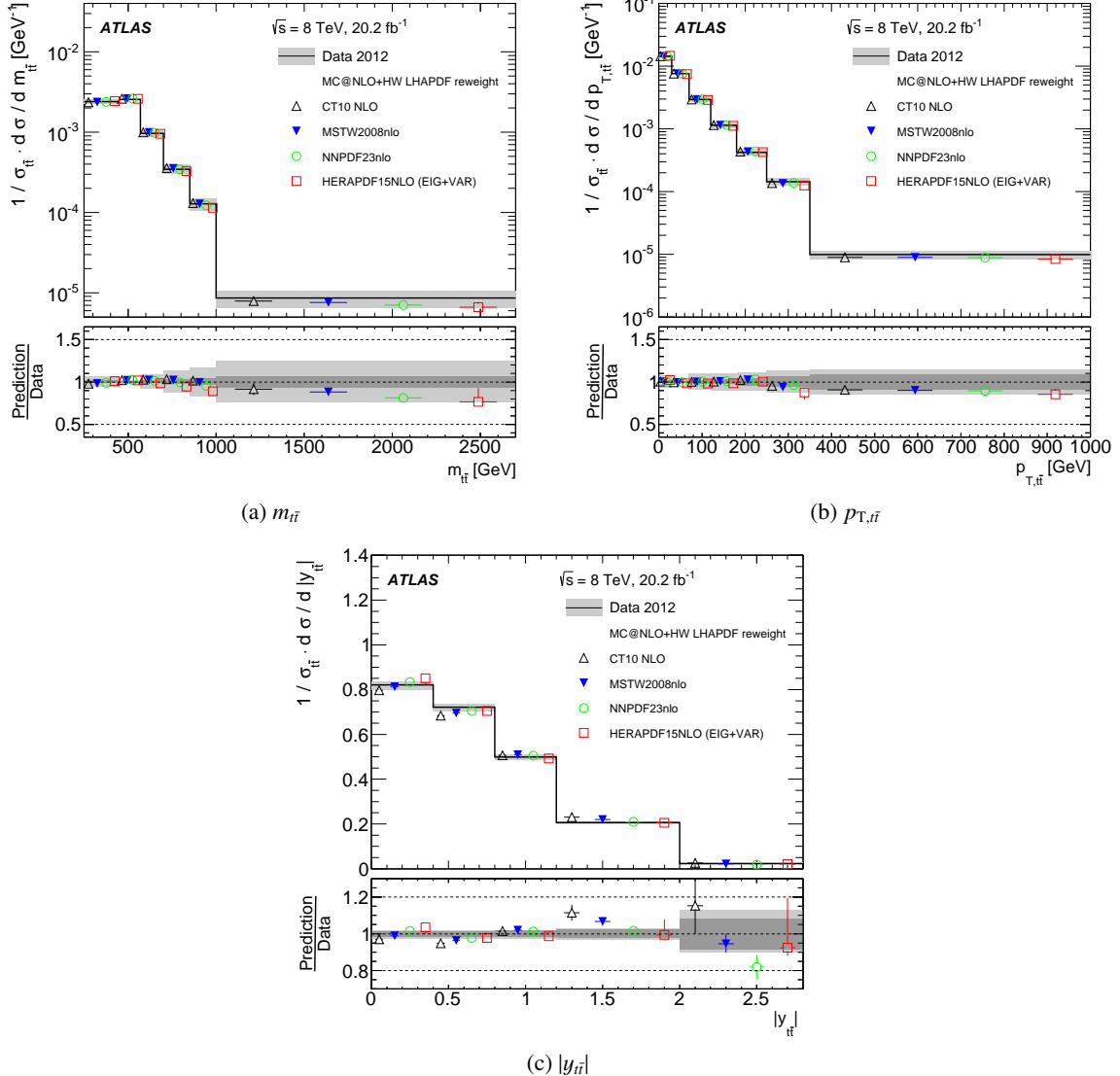


Figure 6: Normalized $t\bar{t}$ differential cross-sections as a function of the (a) invariant mass ($m_{t\bar{t}}$) (b) transverse momentum ($p_{T,t\bar{t}}$) and (c) absolute value of the rapidity ($|y_{t\bar{t}}|$) of the $t\bar{t}$ system at $\sqrt{s} = 8$ TeV measured in the dilepton $e\mu$ channel compared to different PDF sets. The MC@NLO+HERWIG generator is reweighted using the PDF sets to produce the different predictions. The bottom panel shows the ratio of prediction to data. The light (dark) gray band includes the total (data statistical) uncertainty in the data in each bin.

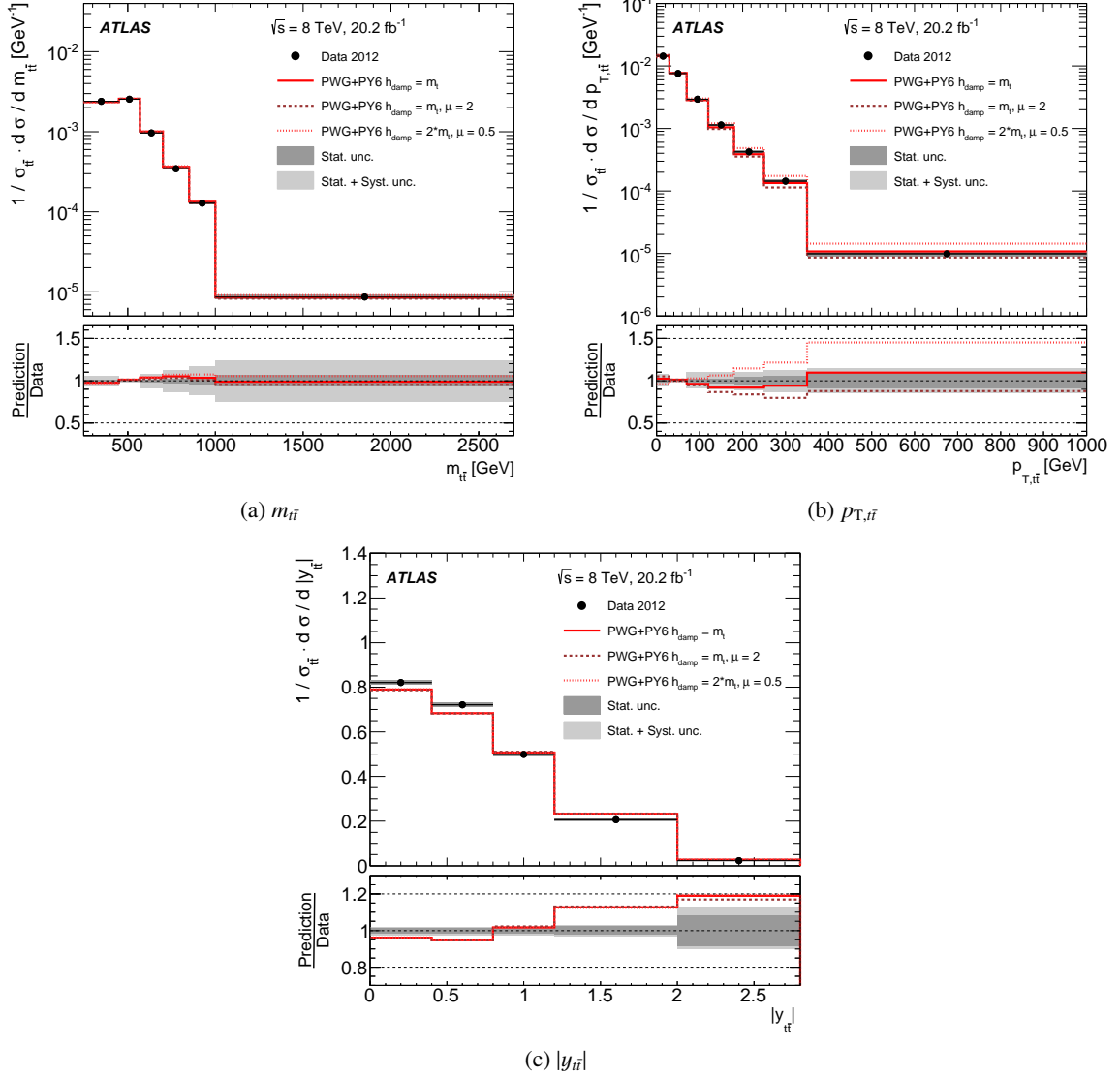


Figure 7: Normalized $t\bar{t}$ differential cross-sections as a function of the (a) invariant mass ($m_{t\bar{t}}$), (b) transverse momentum ($p_{T,t\bar{t}}$), and (c) absolute value of the rapidity ($|y_{t\bar{t}}|$), of the $t\bar{t}$ system at $\sqrt{s} = 8$ TeV measured in the dilepton $e\mu$ channel compared to theoretical predictions from MC generators. The Powheg+Pythia generator with different levels of radiation are used for the predictions. All generators use the NLO CT10 [26] PDF. The bottom panel shows the ratio of prediction to data. The light (dark) gray band includes the total (data statistical) uncertainty in the data in each bin.

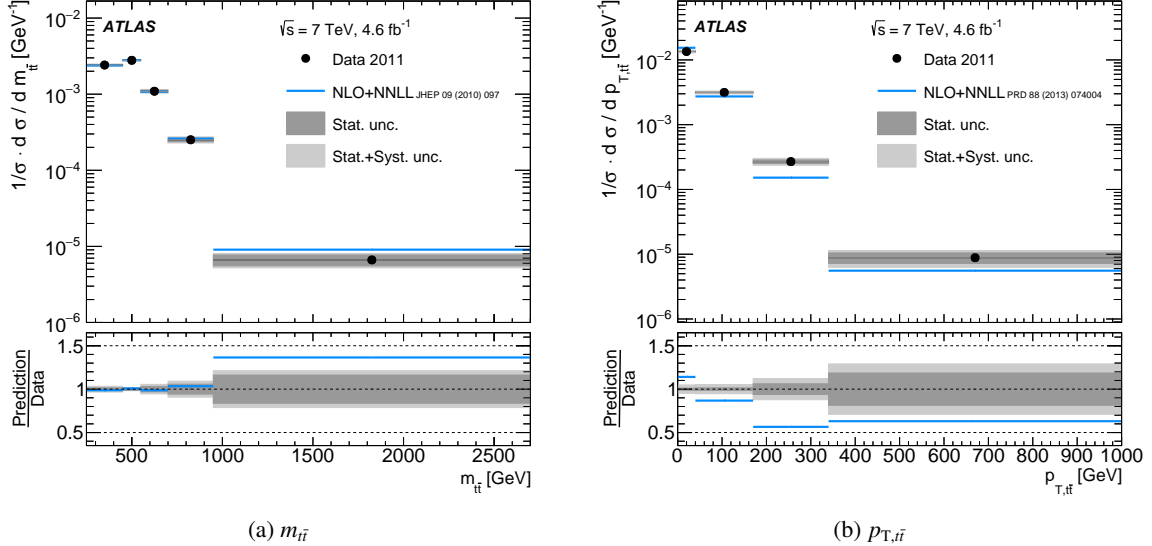


Figure 8: Normalized $t\bar{t}$ differential cross-sections as a function of the (a) invariant mass ($m_{t\bar{t}}$) and (b) transverse momentum ($p_{T,t\bar{t}}$) of the $t\bar{t}$ system at $\sqrt{s} = 7$ TeV measured in the dilepton channel compared with theoretical QCD calculations at NLO+NNLL level. The predictions are calculated using the MSTW2008nnlo PDF. The bottom panel shows the ratio of prediction to data. The light (dark) gray band includes the total (data statistical) uncertainty in the data in each bin.

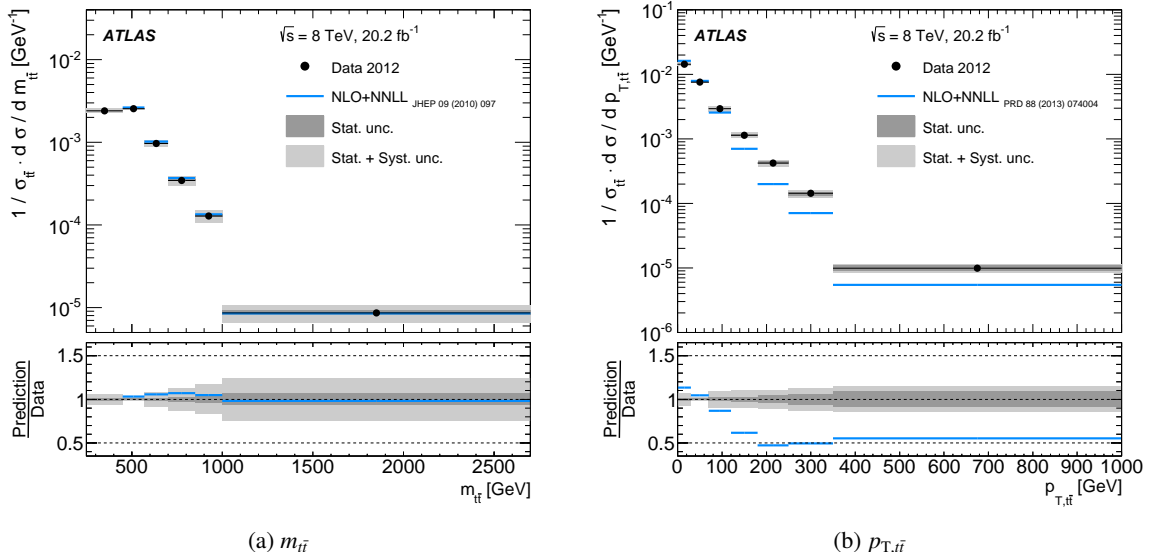


Figure 9: Normalized $t\bar{t}$ differential cross-sections as a function of the (a) invariant mass ($m_{t\bar{t}}$) and (b) transverse momentum ($p_{T,t\bar{t}}$) of the $t\bar{t}$ system at $\sqrt{s} = 8$ TeV measured in the dilepton $e\mu$ channel compared with theoretical QCD calculations at NLO+NNLL level. The predictions are calculated using the MSTW2008nnlo PDF. The bottom panel shows the ratio of prediction to data. The light (dark) gray band includes the total (data statistical) uncertainty in the data in each bin.

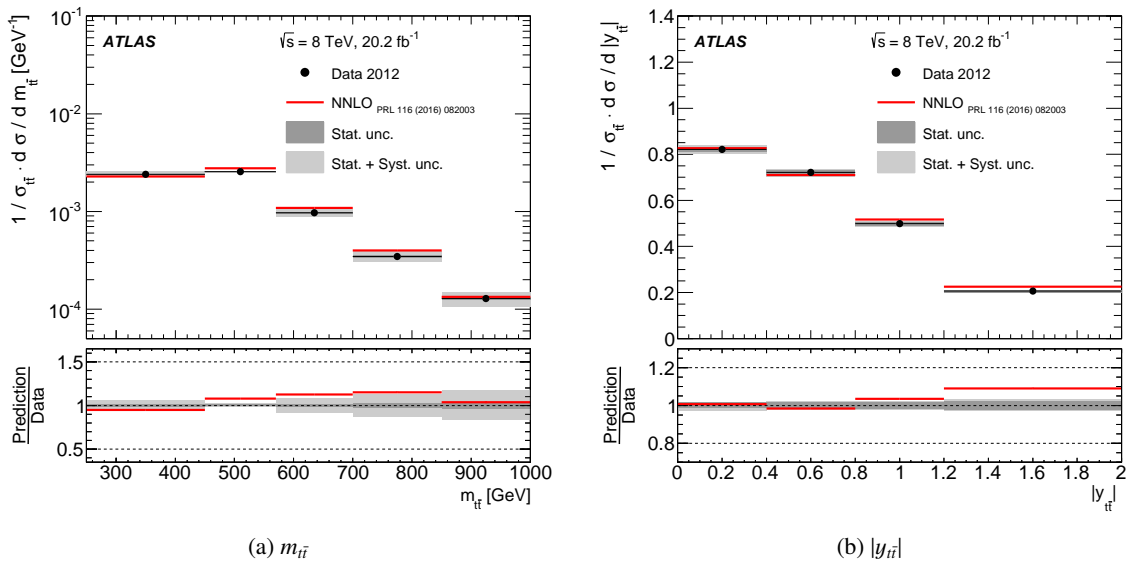


Figure 10: Normalized $t\bar{t}$ differential cross-sections as a function of the (a) invariant mass ($m_{t\bar{t}}$) and (b) absolute value of the rapidity ($|y_{t\bar{t}}|$) of the $t\bar{t}$ system at $\sqrt{s} = 8$ TeV measured in the dilepton $e\mu$ channel compared with theoretical QCD calculations at full NNLO accuracy. The predictions are calculated using the MSTW2008nnlo PDF. The bottom panel shows the ratio of prediction to data. The light (dark) gray band includes the total (data statistical) uncertainty in the data in each bin. The NNLO prediction does not cover the highest bins in $m_{t\bar{t}}$ and $|y_{t\bar{t}}|$.

	$m_{t\bar{t}}$		$p_{T,t\bar{t}}$		$ y_{t\bar{t}} $	
MC generator	χ^2/NDF	$p\text{-value}$	χ^2/NDF	$p\text{-value}$	χ^2/NDF	$p\text{-value}$
PWG+PY6 CT10 $h_{\text{damp}} = m_t$	4.7/4	0.32	2.2/3	0.52	1.3/2	0.52
PWG+PY6 CT10 $h_{\text{damp}} = \infty$	4.4/4	0.36	6.4/3	0.09	1.3/2	0.53
MC@NLO+HW CT10 AUET2	3.9/4	0.43	0.8/3	0.86	0.7/2	0.72
PWG+HW CT10 AUET2	9.1/4	0.06	1.9/3	0.60	1.2/2	0.56
ALPGEN+HW CTEQ6L1 AUET2	4.3/4	0.37	3.3/3	0.35	0.5/2	0.80

Table 6: Comparisons between the measured normalized cross-sections and the MC predictions at $\sqrt{s} = 7$ TeV. For each variable and prediction a χ^2 and a p -value are calculated using the covariance matrix of each measured spectrum. The number of degrees of freedom is equal to one less than the number of bins ($N_b - 1$). The abbreviations PWG, PY and HW correspond to Powheg, Pythia and Herwig respectively.

	$m_{t\bar{t}}$		$p_{T,t\bar{t}}$		$ y_{t\bar{t}} $	
MC generator	χ^2/NDF	$p\text{-value}$	χ^2/NDF	$p\text{-value}$	χ^2/NDF	$p\text{-value}$
PWG+PY6 CT10 $h_{\text{damp}} = m_t$	1.3/5	0.94	4.1/6	0.67	38.2/4	<0.01
PWG+PY6 CT10 $h_{\text{damp}} = \infty$	1.1/5	0.95	16.7/6	0.01	39.3/4	<0.01
MC@NLO+HW CT10 AUET2	2.0/5	0.85	0.4/6	1.00	29.8/4	<0.01
PWG+HW CT10 AUET2	1.2/5	0.95	3.3/6	0.77	37.0/4	<0.01

Table 7: Comparisons between the measured normalized cross-sections and the MC predictions at $\sqrt{s} = 8$ TeV. For each variable and prediction a χ^2 and a p -value are calculated using the covariance matrix of each measured spectrum. The number of degrees of freedom is equal to one less than the number of bins ($N_b - 1$). The abbreviations PWG, PY and HW correspond to Powheg, Pythia and Herwig respectively.

	$m_{t\bar{t}}$		$p_{T,t\bar{t}}$		$ y_{t\bar{t}} $	
PDF	χ^2/NDF	$p\text{-value}$	χ^2/NDF	$p\text{-value}$	χ^2/NDF	$p\text{-value}$
CT10 NLO	2.0/5	0.85	0.4/6	1.00	29.8/4	<0.01
MSTW2008nlo	2.1/5	0.83	0.6/6	1.00	11.6/4	0.02
NNPDF23nlo	2.3/5	0.81	0.4/6	1.00	3.2/4	0.53
HERAPDF15NLO	2.4/5	0.79	2.3/6	0.89	5.6/4	0.23

Table 8: Comparisons between the measured normalized cross-sections and the MC@NLO+Herwig predictions with varied PDF sets at $\sqrt{s} = 8$ TeV. For each variable and prediction a χ^2 and a p -value are calculated using the covariance matrix of each measured spectrum. The number of degrees of freedom is equal to one less than the number of bins ($N_b - 1$).

	$m_{t\bar{t}}$		$p_{T,t\bar{t}}$		$ y_{t\bar{t}} $	
MC generator	χ^2/NDF	$p\text{-value}$	χ^2/NDF	$p\text{-value}$	χ^2/NDF	$p\text{-value}$
PWG+PY6 CT10 $h_{\text{damp}} = m_t$	1.3/5	0.94	4.1/6	0.67	38.2/4	<0.01
PWG+PY6 CT10 $h_{\text{damp}} = m_t, \mu = 2m_t$	0.9/5	0.97	14.5/6	0.02	39.9/4	<0.01
PWG+PY6 CT10 $h_{\text{damp}} = 2.0m_t, \mu = 0.5m_t$	1.6/5	0.90	9.7/6	0.14	33.8/4	<0.01

Table 9: Comparisons between the measured normalized cross-sections and the Powheg+Pythia predictions with different levels of radiation at $\sqrt{s} = 8$ TeV. For each variable and prediction a χ^2 and a p -value are calculated using the covariance matrix of each measured spectrum. The number of degrees of freedom is equal to one less than the number of bins ($N_b - 1$). The abbreviations PWG and PY correspond to Powheg and Pythia respectively.

	$m_{t\bar{t}}$		$p_{T,t\bar{t}}$	
QCD calculation	χ^2/NDF	$p\text{-value}$	χ^2/NDF	$p\text{-value}$
NLO+NNLL ($\sqrt{s} = 7$ TeV)	5.0/4	0.29	14.3/3	<0.01
NLO+NNLL ($\sqrt{s} = 8$ TeV)	5.9/5	0.32	121.5/6	<0.01

Table 10: Comparisons between the measured normalized cross-sections and the QCD NLO+NNLL calculations at $\sqrt{s} = 7$ TeV and $\sqrt{s} = 8$ TeV. The NLO+NNLL predictions are calculated using the MSTW2008nnlo PDF. For each variable and prediction a χ^2 and a p -value are calculated using the covariance matrix of each measured spectrum. The number of degrees of freedom is equal to one less than the number of bins ($N_b - 1$).

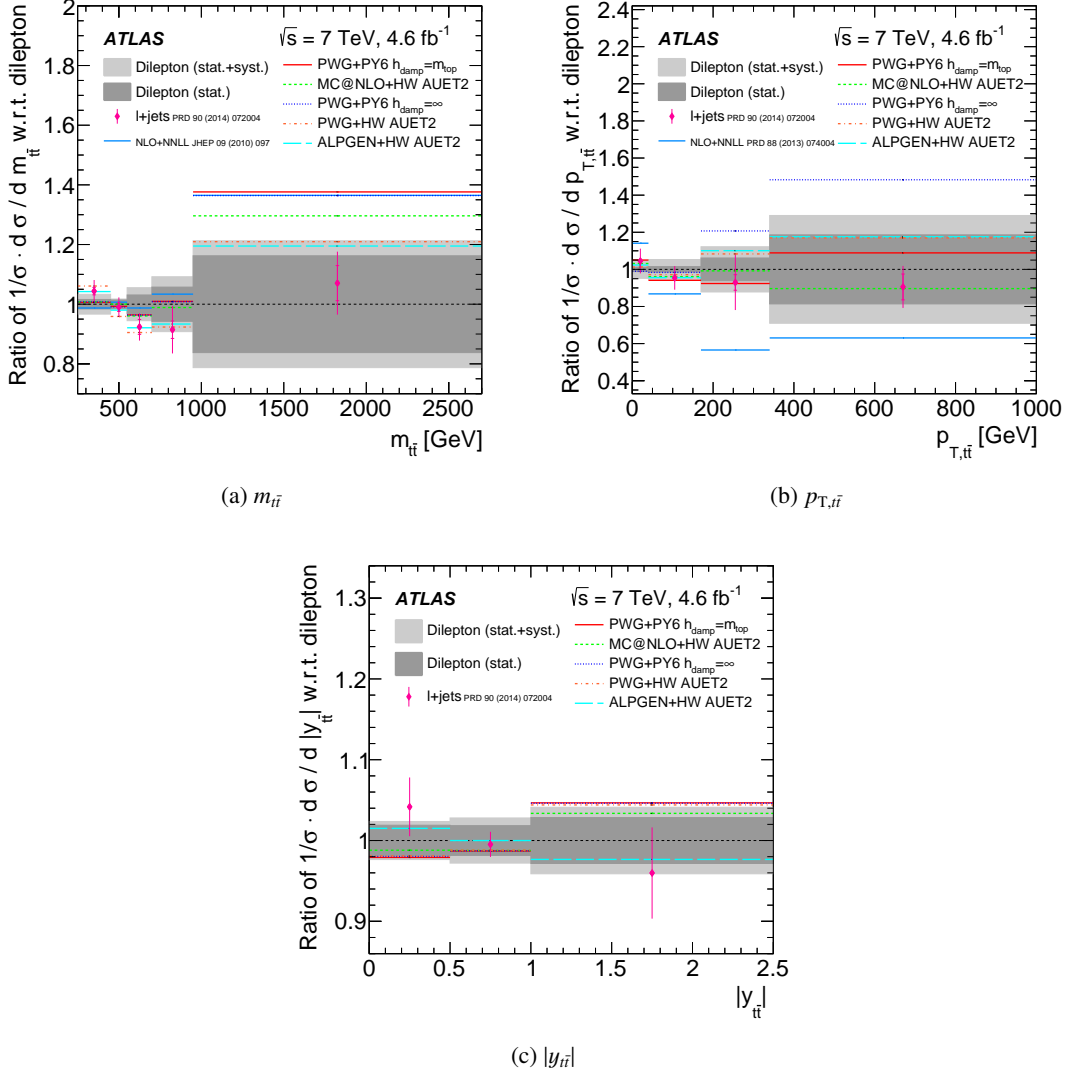


Figure 11: Ratio of different theoretical predictions and the lepton+jets measurement [8] to the measurement of the normalized $t\bar{t}$ differential cross-sections in the dilepton channel for (a) invariant mass ($m_{t\bar{t}}$) (b) transverse momentum ($p_{T,t\bar{t}}$) and (c) absolute value of the rapidity ($|y_{t\bar{t}}|$) of the $t\bar{t}$ system at $\sqrt{s} = 7$ TeV. Theoretical QCD calculations at NLO+NNLL level are also included in $m_{t\bar{t}}$ and $p_{T,t\bar{t}}$. All generators use the NLO CT10 [26] PDF, except for ALPGEN+HERWIG using the LO CTEQ6L1 PDF. The NLO+NNLL calculations use the MSTW2008nnlo PDF. The light (dark) gray band includes the total (data statistical) uncertainty in the data in each bin. The uncertainties on the two data measurements do not account for the correlations of the systematic uncertainties between the two channels.

9 Conclusions

Normalized differential $t\bar{t}$ production cross-sections have been measured as a function of the invariant mass, the transverse momentum, and the rapidity of the $t\bar{t}$ system in $\sqrt{s} = 7$ TeV and 8 TeV proton-proton collisions using the dilepton channel. The data correspond to an integrated luminosity of 4.6 fb^{-1} and

20.2 fb^{-1} for $\sqrt{s} = 7 \text{ TeV}$ and 8 TeV , respectively, collected by the ATLAS detector at the CERN LHC. The results complement the other ATLAS measurements in the lepton+jets channel using the 7 TeV and 8 TeV datasets.

The predictions from Monte Carlo and QCD calculations generally agree with data in a wide range of the kinematic distributions. Most of the generators describe the $m_{t\bar{t}}$ spectrum fairly well in 7 TeV and 8 TeV data. The $p_{T,t\bar{t}}$ spectrum in both 7 TeV and 8 TeV data is well described by PowHEG+PYTHIA with $h_{\text{damp}} = m_t$ and MC@NLO+HERWIG, but is particularly poorly described by PowHEG+PYTHIA with $h_{\text{damp}} = \infty$. For $|y_{t\bar{t}}|$, all of the generators predict higher cross-sections at large $|y_{t\bar{t}}|$ than observed in data, and the level of agreement is improved when using NNPDF2.3 and HERAPDF1.5 PDF sets instead of CT10. The QCD calculation agrees well with data in the $m_{t\bar{t}}$ spectrum at both NLO+NNLL and NNLO accuracy, while a large discrepancy for $p_{T,t\bar{t}}$ is seen at NLO+NNLL accuracy for both $\sqrt{s} = 7 \text{ TeV}$ and $\sqrt{s} = 8 \text{ TeV}$. The results at both 7 TeV and 8 TeV are consistent with the other ATLAS measurements in the lepton+jets channel.

Acknowledgements

We honor the memory of our colleague Irene Vichou, who made a large contribution to this work, but died shortly before its completion.

We thank CERN for the very successful operation of the LHC, as well as the support staff from our institutions without whom ATLAS could not be operated efficiently.

We acknowledge the support of ANPCyT, Argentina; YerPhI, Armenia; ARC, Australia; BMWFW and FWF, Austria; ANAS, Azerbaijan; SSTC, Belarus; CNPq and FAPESP, Brazil; NSERC, NRC and CFI, Canada; CERN; CONICYT, Chile; CAS, MOST and NSFC, China; COLCIENCIAS, Colombia; MSMT CR, MPO CR and VSC CR, Czech Republic; DNRF and DNSRC, Denmark; IN2P3-CNRS, CEA-DSM/IRFU, France; GNSF, Georgia; BMBF, HGF, and MPG, Germany; GSRT, Greece; RGC, Hong Kong SAR, China; ISF, I-CORE and Benoziyo Center, Israel; INFN, Italy; MEXT and JSPS, Japan; CNRST, Morocco; FOM and NWO, Netherlands; RCN, Norway; MNiSW and NCN, Poland; FCT, Portugal; MNE/IFA, Romania; MES of Russia and NRC KI, Russian Federation; JINR; MESTD, Serbia; MSSR, Slovakia; ARRS and MIZŠ, Slovenia; DST/NRF, South Africa; MINECO, Spain; SRC and Wallenberg Foundation, Sweden; SERI, SNSF and Cantons of Bern and Geneva, Switzerland; MOST, Taiwan; TAEK, Turkey; STFC, United Kingdom; DOE and NSF, United States of America. In addition, individual groups and members have received support from BCKDF, the Canada Council, CANARIE, CRC, Compute Canada, FQRNT, and the Ontario Innovation Trust, Canada; EPLANET, ERC, FP7, Horizon 2020 and Marie Skłodowska-Curie Actions, European Union; Investissements d’Avenir Labex and Idex, ANR, Région Auvergne and Fondation Partager le Savoir, France; DFG and AvH Foundation, Germany; Herakleitos, Thales and Aristea programmes co-financed by EU-ESF and the Greek NSRF; BSF, GIF and Minerva, Israel; BRF, Norway; Generalitat de Catalunya, Generalitat Valenciana, Spain; the Royal Society and Leverhulme Trust, United Kingdom.

The crucial computing support from all WLCG partners is acknowledged gratefully, in particular from CERN, the ATLAS Tier-1 facilities at TRIUMF (Canada), NDGF (Denmark, Norway, Sweden), CC-IN2P3 (France), KIT/GridKA (Germany), INFN-CNAF (Italy), NL-T1 (Netherlands), PIC (Spain), ASGC (Taiwan), RAL (UK) and BNL (USA), the Tier-2 facilities worldwide and large non-WLCG resource providers. Major contributors of computing resources are listed in Ref. [83].

References

- [1] ATLAS Collaboration, *Measurement of the $t\bar{t}$ production cross-section using $e\mu$ events with b -tagged jets in pp collisions at $\sqrt{s} = 7$ and 8 TeV with the ATLAS detector*, *Eur. Phys. J. C* **74** (2014) 3109, arXiv:[1406.5375 \[hep-ex\]](#).
- [2] CMS Collaboration, *Measurement of the $t\bar{t}$ production cross section in the dilepton channel in pp collisions at $\sqrt{s} = 7$ TeV*, *JHEP* **11** (2012) 067, arXiv:[1208.2671 \[hep-ex\]](#).
- [3] CMS Collaboration, *Measurement of the $t\bar{t}$ production cross section in the dilepton channel in pp collisions at $\sqrt{s} = 8$ TeV*, *JHEP* **02** (2014) 024, arXiv:[1312.7582 \[hep-ex\]](#).
- [4] CMS Collaboration, *Measurement of the $t\bar{t}$ production cross section in the $e\mu$ channel in proton–proton collisions at $\sqrt{s} = 7$ and 8 TeV*, *JHEP* **08** (2016) 029, arXiv:[1603.02303 \[hep-ex\]](#).
- [5] ATLAS Collaboration, *Measurement of the $t\bar{t}$ production cross-section using $e\mu$ events with b -tagged jets in pp collisions at $\sqrt{s} = 13$ TeV with the ATLAS detector*, *Phys. Lett. B* **761** (2016) 136, arXiv:[1606.02699 \[hep-ex\]](#).
- [6] CMS Collaboration, *Measurement of the top quark pair production cross section in proton–proton collisions at $\sqrt{s} = 13$ TeV*, *Phys. Rev. Lett.* **116** (2016) 052002, arXiv:[1510.05302 \[hep-ex\]](#).
- [7] ATLAS Collaboration, *Measurements of top quark pair relative differential cross-sections with ATLAS in pp collisions at $\sqrt{s} = 7$ TeV*, *Eur. Phys. J. C* **73** (2013) 2261, arXiv:[1207.5644 \[hep-ex\]](#).
- [8] ATLAS Collaboration, *Measurements of normalized differential cross-sections for $t\bar{t}$ production in pp collisions at $\sqrt{s} = 7$ TeV using the ATLAS detector*, *Phys. Rev. D* **90** (2014) 072004, arXiv:[1407.0371 \[hep-ex\]](#).
- [9] ATLAS Collaboration, *Differential top-antitop cross-section measurements as a function of observables constructed from final-state particles using pp collisions at $\sqrt{s} = 7$ TeV in the ATLAS detector*, *JHEP* **06** (2015) 100, arXiv:[1502.05923 \[hep-ex\]](#).
- [10] ATLAS Collaboration, *Measurement of the differential cross-section of highly boosted top quarks as a function of their transverse momentum in $\sqrt{s} = 8$ TeV proton–proton collisions using the ATLAS detector*, *Phys. Rev. D* **93** (2016) 032009, arXiv:[1510.03818 \[hep-ex\]](#).
- [11] ATLAS Collaboration, *Measurements of top-quark pair differential cross-sections in the lepton+jets channel in pp collisions at $\sqrt{s} = 8$ TeV using the ATLAS detector*, *Eur. Phys. J. C* **76** (2015) 538, arXiv:[1511.04716 \[hep-ex\]](#).
- [12] CMS Collaboration, *Measurement of differential top-quark-pair production cross sections in pp collisions at $\sqrt{s} = 7$ TeV*, *Eur. Phys. J. C* **73** (2013) 2339, arXiv:[1211.2220 \[hep-ex\]](#).
- [13] CMS Collaboration, *Measurement of the differential cross section for top quark pair production in pp collisions at $\sqrt{s} = 8$ TeV*, *Eur. Phys. J. C* **75** (2015) 542, arXiv:[1505.04480 \[hep-ex\]](#).
- [14] CMS Collaboration, *Measurement of the integrated and differential $t\bar{t}$ production cross sections for high- p_T top quarks in pp collisions at $\sqrt{s} = 8$ TeV*, *Phys. Rev. D* (2016), arXiv:[1605.00116 \[hep-ex\]](#).

- [15] CMS Collaboration, *Measurement of the $t\bar{t}$ production cross section in the all-jets final state in pp collisions at $\sqrt{s} = 8$ TeV*, *Eur. Phys. J. C* **76** (2016) 128, arXiv:1509.06076 [hep-ex].
- [16] ATLAS Collaboration, *The ATLAS Experiment at the CERN Large Hadron Collider*, *JINST* **3** (2008) S08003.
- [17] ATLAS Collaboration, *Improved luminosity determination in pp collisions at $\sqrt{s} = 7$ TeV using the ATLAS detector at the LHC*, *Eur. Phys. J. C* **73** (2013) 2518, arXiv:1302.4393 [hep-ex].
- [18] ATLAS Collaboration, *Luminosity determination in pp collisions at $\sqrt{s} = 8$ TeV using the ATLAS detector at the LHC*, (2016), arXiv:1608.03953 [hep-ex].
- [19] S. Agostinelli et al., *GEANT4: A Simulation toolkit*, *Nucl. Instrum. Methods Phys. Res., Sect. A* **506** (2003) 250–303.
- [20] ATLAS Collaboration, *The ATLAS Simulation Infrastructure*, *Eur. Phys. J. C* **70** (2010) 823, arXiv:1005.4568 [hep-ex].
- [21] ATLAS Collaboration, *Performance of the Fast ATLAS Tracking Simulation (FATRAS) and the ATLAS Fast Calorimeter Simulation (FastCaloSim) with single particles*, ATL-SOFT-PUB-2014-01, 2014, URL: <https://cds.cern.ch/record/1669341>.
- [22] P. Nason, *A New method for combining NLO QCD with shower Monte Carlo algorithms*, *JHEP* **0411** (2004) 040, arXiv:hep-ph/0409146 [hep-ph].
- [23] S. Frixione, P. Nason, and C. Oleari, *Matching NLO QCD computations with Parton Shower simulations: the POWHEG method*, *JHEP* **0711** (2007) 070, arXiv:0709.2092 [hep-ph].
- [24] S. Alioli et al., *A general framework for implementing NLO calculations in shower Monte Carlo programs: the POWHEG BOX*, *JHEP* **1006** (2010) 043, arXiv:1002.2581 [hep-ph].
- [25] S. Frixione, P. Nason, and G. Ridolfi, *A Positive-weight next-to-leading-order Monte Carlo for heavy flavour hadroproduction*, *JHEP* **0709** (2007) 126, arXiv:0707.3088 [hep-ph].
- [26] H.-L. Lai et al., *New parton distributions for collider physics*, *Phys. Rev. D* **82** (2010) 074024, arXiv:1007.2241 [hep-ph].
- [27] ATLAS Collaboration, *Comparison of Monte Carlo generator predictions to ATLAS measurements of top pair production at 7 TeV*, ATL-PHYS-PUB-2015-002, 2015, URL: <https://cds.cern.ch/record/1981319>.
- [28] ATLAS Collaboration, *Comparison of Monte Carlo generator predictions from Powheg and Sherpa to ATLAS measurements of top pair production at 7 TeV*, ATL-PHYS-PUB-2015-011, 2015, URL: <https://cds.cern.ch/record/2020602>.
- [29] T. Sjöstrand, S. Mrenna, and P. Z. Skands, *PYTHIA 6.4 physics and manual*, *JHEP* **0605** (2006) 026, arXiv:hep-ph/0603175 [hep-ph].
- [30] P. Z. Skands, *Tuning Monte Carlo Generators: The Perugia Tunes*, *Phys. Rev. D* **82** (2010) 074018, arXiv:1005.3457 [hep-ph].
- [31] J. Pumplin et al., *New generation of parton distributions with uncertainties from global QCD analysis*, *JHEP* **0207** (2002) 012, arXiv:hep-ph/0201195 [hep-ph].

- [32] S. Frixione and B. R. Webber, *Matching NLO QCD computations and parton shower simulations*, JHEP **06** (2002) 029, arXiv:[hep-ph/0204244 \[hep-ph\]](#).
- [33] S. Frixione, P. Nason, and B. R. Webber, *Matching NLO QCD and parton showers in heavy flavor production*, JHEP **0308** (2003) 007, arXiv:[hep-ph/0305252 \[hep-ph\]](#).
- [34] G. Corcella et al., *HERWIG 6: An Event generator for hadron emission reactions with interfering gluons (including supersymmetric processes)*, JHEP **0101** (2001) 010, arXiv:[hep-ph/0011363 \[hep-ph\]](#).
- [35] J. M. Butterworth, J. R. Forshaw, and M. H. Seymour, *Multiparton interactions in photoproduction at HERA*, Z. Phys. C **72** (1996) 637–646, arXiv:[hep-ph/9601371 \[hep-ph\]](#).
- [36] ATLAS Collaboration, *New ATLAS event generator tunes to 2010 data*, ATL-PHYS-PUB-2011-008, 2011, URL: <https://cds.cern.ch/record/1345343>.
- [37] M. L. Mangano et al., *ALPGEN, a generator for hard multiparton processes in hadronic collisions*, JHEP **0307** (2003) 001, arXiv:[hep-ph/0206293 \[hep-ph\]](#).
- [38] H. L. Lai et al., *Global QCD analysis of parton structure of the nucleon: CTEQ5 parton distributions*, Eur. Phys. J. C **12** (2000) 375–392, arXiv:[hep-ph/9903282 \[hep-ph\]](#).
- [39] ATLAS Collaboration, *Measurement of $t\bar{t}$ production with a veto on additional central jet activity in pp collisions at $\sqrt{s} = 7$ TeV using the ATLAS detector*, Eur. Phys. J. C **72** (2012) 2043, arXiv:[1203.5015 \[hep-ex\]](#).
- [40] ATLAS Collaboration, *Measurement of the $t\bar{t}$ production cross-section as a function of jet multiplicity and jet transverse momentum in 7 TeV proton–proton collisions with the ATLAS detector*, JHEP **01** (2015) 020, arXiv:[1407.0891 \[hep-ex\]](#).
- [41] M. Cacciari et al., *Top-pair production at hadron colliders with next-to-next-to-leading logarithmic soft-gluon resummation*, Phys. Lett. B **710** (2012) 612–622, arXiv:[1111.5869 \[hep-ph\]](#).
- [42] P. Baernreuther, M. Czakon, and A. Mitov, *Percent Level Precision Physics at the Tevatron: Next-to-Next-to-Leading Order QCD Corrections to $q\bar{q} \rightarrow t\bar{t} + X$* , Phys. Rev. Lett. **109** (2012) 132001, arXiv:[1204.5201 \[hep-ph\]](#).
- [43] M. Czakon and A. Mitov, *NNLO corrections to top pair production at hadron colliders: the quark-gluon reaction*, JHEP **1301** (2013) 080, arXiv:[1210.6832 \[hep-ph\]](#).
- [44] M. Czakon and A. Mitov, *NNLO corrections to top-pair production at hadron colliders: the all-fermionic scattering channels*, JHEP **1212** (2012) 054, arXiv:[1207.0236 \[hep-ph\]](#).
- [45] M. Czakon, P. Fiedler, and A. Mitov, *Total Top-Quark Pair-Production Cross Section at Hadron Colliders Through $O(\alpha_S^4)$* , Phys. Rev. Lett. **110** (2013) 252004, arXiv:[1303.6254 \[hep-ph\]](#).
- [46] M. Czakon and A. Mitov, *Top++: A Program for the Calculation of the Top-Pair Cross-Section at Hadron Colliders*, Comput. Phys. Commun. **185** (2014) 2930, arXiv:[1112.5675 \[hep-ph\]](#).

- [47] E. Re,
Single-top Wt-channel production matched with parton showers using the POWHEG method, *Eur. Phys. J. C* **71** (2011) 1547, arXiv:[1009.2450 \[hep-ph\]](#).
- [48] S. Frixione et al., *Single-top hadroproduction in association with a W boson*, *JHEP* **0807** (2008) 029, arXiv:[0805.3067 \[hep-ph\]](#).
- [49] N. Kidonakis,
Two-loop soft anomalous dimensions for single top quark associated production with a W- or H-, *Phys. Rev. D* **82** (2010) 054018, arXiv:[1005.4451 \[hep-ph\]](#).
- [50] R. Gavin et al., *FEWZ 2.0: A code for hadronic Z production at next-to-next-to-leading order*, *Comput. Phys. Commun.* **182** (2011) 2388–2403, arXiv:[1011.3540 \[hep-ph\]](#).
- [51] ATLAS Collaboration, *Measurement of the top quark-pair production cross section with ATLAS in pp collisions at $\sqrt{s} = 7$ TeV*, *Eur. Phys. J. C* **71** (2011) 1577, arXiv:[1012.1792 \[hep-ex\]](#).
- [52] ATLAS Collaboration, *Measurement of the top quark pair production cross section in pp collisions at $\sqrt{s} = 7$ TeV in dilepton final states with ATLAS*, *Phys. Lett. B* **707** (2012) 459, arXiv:[1108.3699 \[hep-ex\]](#).
- [53] J. M. Campbell, R. K. Ellis, and C. Williams, *Vector boson pair production at the LHC*, *JHEP* **1107** (2011) 018, arXiv:[1105.0020 \[hep-ph\]](#).
- [54] J. Alwall et al., *MadGraph 5 : Going Beyond*, *JHEP* **1106** (2011) 128.
- [55] B. P. Kersevan and E. Richter-Was, *The Monte Carlo event generator AcerMC versions 2.0 to 3.8 with interfaces to PYTHIA 6.4, HERWIG 6.5 and ARIADNE 4.1*, *Comput. Phys. Commun.* **184** (2013) 919–985, arXiv:[hep-ph/0405247 \[hep-ph\]](#).
- [56] ATLAS Collaboration, *Electron reconstruction and identification efficiency measurements with the ATLAS detector using the 2011 LHC proton–proton collision data*, *Eur. Phys. J. C* **74** (2014) 2941, arXiv:[1404.2240 \[hep-ex\]](#).
- [57] K. Rehermann and B. Tweedie,
Efficient Identification of Boosted Semileptonic Top Quarks at the LHC, *JHEP* **1103** (2011) 059, arXiv:[1007.2221 \[hep-ph\]](#).
- [58] M. Cacciari, G. P. Salam, and G. Soyez, *The Anti- $k(t)$ jet clustering algorithm*, *JHEP* **0804** (2008) 063.
- [59] ATLAS Collaboration,
Topological cell clustering in the ATLAS calorimeters and its performance in LHC Run 1, (2016), arXiv:[1603.02934](#).
- [60] ATLAS Collaboration,
Jet energy measurement with the ATLAS detector in proton–proton collisions at $\sqrt{s} = 7$ TeV, *Eur. Phys. J. C* **73** (2013) 2304, arXiv:[1112.6426 \[hep-ex\]](#).
- [61] ATLAS Collaboration, *Pile-up subtraction and suppression for jets in ATLAS*, ATLAS-CONF-2013-083, 2013, URL: <https://cds.cern.ch/record/1570994>.
- [62] ATLAS Collaboration, *Measurement of the b-tag Efficiency in a Sample of Jets Containing Muons with 5 fb^{-1} of data from the ATLAS detector*, ATLAS-CONF-2012-043, 2012, URL: <https://cds.cern.ch/record/1435197>.

- [63] ATLAS Collaboration, *Calibration of the performance of b-tagging for c and light-flavour jets in the 2012 ATLAS data*, ATLAS-CONF-2014-046, 2014, URL: <https://cds.cern.ch/record/1741020>.
- [64] ATLAS Collaboration, *Performance of missing transverse momentum reconstruction in proton–proton collisions at $\sqrt{s} = 7$ TeV with ATLAS*, *Eur. Phys. J. C* **72** (2012) 1844, arXiv:[1108.5602 \[hep-ex\]](https://arxiv.org/abs/1108.5602).
- [65] T. Adye, *Unfolding algorithms and tests using RooUnfold*, (2011), arXiv:[1105.1160 \[physics.data-an\]](https://arxiv.org/abs/1105.1160).
- [66] G. D’Agostini, *A Multidimensional unfolding method based on Bayes’ theorem*, *Nucl. Instrum. Meth. A* **362** (1995) 487–498.
- [67] ATLAS Collaboration, *Comparison of Monte Carlo generator predictions for gap fraction and jet multiplicity observables in $t\bar{t}$ events*, ATL-PHYS-PUB-2014-005, 2014, URL: <https://cds.cern.ch/record/1703034>.
- [68] M. Botje et al., *The PDF4LHC Working Group Interim Recommendations*, (2011), arXiv:[1101.0538 \[hep-ph\]](https://arxiv.org/abs/1101.0538).
- [69] A. Martin et al., *Parton distributions for the LHC*, *Eur. Phys. J. C* **63** (2009) 189–285, arXiv:[0901.0002 \[hep-ph\]](https://arxiv.org/abs/0901.0002).
- [70] R. D. Ball et al., *Parton distributions with LHC data*, *Nucl. Phys. B* **867** (2013) 244–289, arXiv:[1207.1303 \[hep-ex\]](https://arxiv.org/abs/1207.1303).
- [71] J. Alwall et al., *Comparative study of various algorithms for the merging of parton showers and matrix elements in hadronic collisions*, *Eur. Phys. J. C* **53** (2008) 473–500, arXiv:[0706.2569 \[hep-ph\]](https://arxiv.org/abs/0706.2569).
- [72] ATLAS Collaboration, *Electron performance measurements with the ATLAS detector using the 2010 LHC proton–proton collision data*, *Eur. Phys. J. C* **72** (2012) 1909, arXiv:[1110.3174 \[hep-ex\]](https://arxiv.org/abs/1110.3174).
- [73] ATLAS Collaboration, *Preliminary results on the muon reconstruction efficiency, momentum resolution, and momentum scale in ATLAS 2012 pp collision data*, ATLAS-CONF-2013-088, 2013, URL: <https://cds.cern.ch/record/1580207>.
- [74] ATLAS Collaboration, *Jet energy measurement and its systematic uncertainty in proton–proton collisions at $\sqrt{s} = 7$ TeV with the ATLAS detector*, *Eur. Phys. J. C* **75** (2015) 17, arXiv:[1406.0076 \[hep-ex\]](https://arxiv.org/abs/1406.0076).
- [75] ATLAS Collaboration, *Single hadron response measurement and calorimeter jet energy scale uncertainty with the ATLAS detector at the LHC*, *Eur. Phys. J. C* **73** (2013) 2305, arXiv:[1203.1302 \[hep-ex\]](https://arxiv.org/abs/1203.1302).
- [76] ATLAS Collaboration, *Jet energy resolution in proton–proton collisions at $\sqrt{s} = 7$ TeV recorded in 2010 with the ATLAS detector*, *Eur. Phys. J. C* **73** (2013) 2306, arXiv:[1210.6210 \[hep-ex\]](https://arxiv.org/abs/1210.6210).
- [77] ATLAS Collaboration, *Measuring the b-tag efficiency in a $t\bar{t}$ sample with 4.7 fb^{-1} of data from the ATLAS detector*, ATLAS-CONF-2012-097, 2012, URL: <https://cds.cern.ch/record/1460443>.
- [78] W. Tung et al., *Heavy Quark Mass Effects in Deep Inelastic Scattering and Global QCD Analysis*, *JHEP* **0702** (2007) 053.

- [79] V. Ahrens et al., *Renormalization-Group Improved Predictions for Top-Quark Pair Production at Hadron Colliders*, JHEP **1009** (2010) 097, arXiv:[1003.5827](https://arxiv.org/abs/1003.5827) [hep-ph].
- [80] H. X. Zhu et al., *Transverse-momentum resummation for top-quark pairs at hadron colliders*, Phys. Rev. Lett. **110** (2013) 082001, arXiv:[1208.5774](https://arxiv.org/abs/1208.5774) [hep-ph].
- [81] H. T. Li et al., *Top quark pair production at small transverse momentum in hadronic collisions*, Phys. Rev. D **88** (2013) 074004, arXiv:[1307.2464](https://arxiv.org/abs/1307.2464).
- [82] M. Czakon, D. Heymes, and A. Mitov,
High-precision differential predictions for top-quark pairs at the LHC,
Phys. Rev. Lett. **116** (2016) 082003, arXiv:[1511.00549](https://arxiv.org/abs/1511.00549) [hep-ph].
- [83] ATLAS Collaboration, *ATLAS Computing Acknowledgements 2016–2017*, ATL-GEN-PUB-2016-002, 2016, URL: <https://cds.cern.ch/record/2202407>.

The ATLAS Collaboration

M. Aaboud^{136d}, G. Aad⁸⁷, B. Abbott¹¹⁴, J. Abdallah⁶⁵, O. Abdinov¹², B. Abelsoos¹¹⁸, R. Aben¹⁰⁸, O.S. AbouZeid¹³⁸, N.L. Abraham¹⁵², H. Abramowicz¹⁵⁶, H. Abreu¹⁵⁵, R. Abreu¹¹⁷, Y. Abulaiti^{149a,149b}, B.S. Acharya^{167a,167b,a}, L. Adamczyk^{40a}, D.L. Adams²⁷, J. Adelman¹⁰⁹, S. Adomeit¹⁰¹, T. Adye¹³², A.A. Affolder⁷⁶, T. Agatonovic-Jovin¹⁴, J. Agricola⁵⁶, J.A. Aguilar-Saavedra^{127a,127f}, S.P. Ahlen²⁴, F. Ahmadov^{67,b}, G. Aielli^{134a,134b}, H. Akerstedt^{149a,149b}, T.P.A. Åkesson⁸³, A.V. Akimov⁹⁷, G.L. Alberghi^{22a,22b}, J. Albert¹⁷², S. Albrand⁵⁷, M.J. Alconada Verzini⁷³, M. Alekса³², I.N. Aleksandrov⁶⁷, C. Alexa^{28b}, G. Alexander¹⁵⁶, T. Alexopoulos¹⁰, M. Alhroob¹¹⁴, B. Ali¹²⁹, M. Aliev^{75a,75b}, G. Alimonti^{93a}, J. Alison³³, S.P. Alkire³⁷, B.M.M. Allbrooke¹⁵², B.W. Allen¹¹⁷, P.P. Allport¹⁹, A. Aloisio^{105a,105b}, A. Alonso³⁸, F. Alonso⁷³, C. Alpigiani¹³⁹, M. Alstaty⁸⁷, B. Alvarez Gonzalez³², D. Álvarez Piqueras¹⁷⁰, M.G. Alviggi^{105a,105b}, B.T. Amadio¹⁶, K. Amako⁶⁸, Y. Amaral Coutinho^{26a}, C. Amelung²⁵, D. Amidei⁹¹, S.P. Amor Dos Santos^{127a,127c}, A. Amorim^{127a,127b}, S. Amoroso³², G. Amundsen²⁵, C. Anastopoulos¹⁴², L.S. Ancu⁵¹, N. Andari¹⁰⁹, T. Andeen¹¹, C.F. Anders^{60b}, G. Anders³², J.K. Anders⁷⁶, K.J. Anderson³³, A. Andreazza^{93a,93b}, V. Andrei^{60a}, S. Angelidakis⁹, I. Angelozzi¹⁰⁸, P. Anger⁴⁶, A. Angerami³⁷, F. Anghinolfi³², A.V. Anisenkov^{110,c}, N. Anjos¹³, A. Annovi^{125a,125b}, C. Antel^{60a}, M. Antonelli⁴⁹, A. Antonov^{99,*}, F. Anulli^{133a}, M. Aoki⁶⁸, L. Aperio Bella¹⁹, G. Arabidze⁹², Y. Arai⁶⁸, J.P. Araque^{127a}, A.T.H. Arce⁴⁷, F.A. Arduh⁷³, J.-F. Arguin⁹⁶, S. Argyropoulos⁶⁵, M. Arik^{20a}, A.J. Armbruster¹⁴⁶, L.J. Armitage⁷⁸, O. Arnaez³², H. Arnold⁵⁰, M. Arratia³⁰, O. Arslan²³, A. Artamonov⁹⁸, G. Artoni¹²¹, S. Artz⁸⁵, S. Asai¹⁵⁸, N. Asbah⁴⁴, A. Ashkenazi¹⁵⁶, B. Åsman^{149a,149b}, L. Asquith¹⁵², K. Assamagan²⁷, R. Astalos^{147a}, M. Atkinson¹⁶⁹, N.B. Atlay¹⁴⁴, K. Augsten¹²⁹, G. Avolio³², B. Axen¹⁶, M.K. Ayoub¹¹⁸, G. Azuelos^{96,d}, M.A. Baak³², A.E. Baas^{60a}, M.J. Baca¹⁹, H. Bachacou¹³⁷, K. Bachas^{75a,75b}, M. Backes³², M. Backhaus³², P. Bagiacchi^{133a,133b}, P. Bagnaia^{133a,133b}, Y. Bai^{35a}, J.T. Barnes¹³², O.K. Baker¹⁷⁹, E.M. Baldin^{110,c}, P. Balek¹⁷⁵, T. Balestri¹⁵¹, F. Balli¹³⁷, W.K. Balunas¹²³, E. Banas⁴¹, Sw. Banerjee^{176,e}, A.A.E. Bannoura¹⁷⁸, L. Barak³², E.L. Barberio⁹⁰, D. Barberis^{52a,52b}, M. Barbero⁸⁷, T. Barillari¹⁰², M-S Barisits³², T. Barklow¹⁴⁶, N. Barlow³⁰, S.L. Barnes⁸⁶, B.M. Barnett¹³², R.M. Barnett¹⁶, Z. Barnovska-Blenessy⁵, A. Baroncelli^{135a}, G. Barone²⁵, A.J. Barr¹²¹, L. Barranco Navarro¹⁷⁰, F. Barreiro⁸⁴, J. Barreiro Guimarães da Costa^{35a}, R. Bartoldus¹⁴⁶, A.E. Barton⁷⁴, P. Bartos^{147a}, A. Basalaev¹²⁴, A. Bassalat^{118,f}, R.L. Bates⁵⁵, S.J. Batista¹⁶², J.R. Batley³⁰, M. Battaglia¹³⁸, M. Bauce^{133a,133b}, F. Bauer¹³⁷, H.S. Bawa^{146,g}, J.B. Beacham¹¹², M.D. Beattie⁷⁴, T. Beau⁸², P.H. Beauchemin¹⁶⁵, P. Bechtle²³, H.P. Beck^{18,h}, K. Becker¹²¹, M. Becker⁸⁵, M. Beckingham¹⁷³, C. Becot¹¹¹, A.J. Beddall^{20e}, A. Beddall^{20b}, V.A. Bednyakov⁶⁷, M. Bedognetti¹⁰⁸, C.P. Bee¹⁵¹, L.J. Beemster¹⁰⁸, T.A. Beermann³², M. Begel²⁷, J.K. Behr⁴⁴, C. Belanger-Champagne⁸⁹, A.S. Bell⁸⁰, G. Bella¹⁵⁶, L. Bellagamba^{22a}, A. Bellerive³¹, M. Bellomo⁸⁸, K. Belotskiy⁹⁹, O. Beltramello³², N.L. Belyaev⁹⁹, O. Benary^{156,*}, D. Benchekroun^{136a}, M. Bender¹⁰¹, K. Bendtz^{149a,149b}, N. Benekos¹⁰, Y. Benhammou¹⁵⁶, E. Benhar Noccioli¹⁷⁹, J. Benitez⁶⁵, D.P. Benjamin⁴⁷, J.R. Bensinger²⁵, S. Bentvelsen¹⁰⁸, L. Beresford¹²¹, M. Beretta⁴⁹, D. Berge¹⁰⁸, E. Bergeaas Kuutmann¹⁶⁸, N. Berger⁵, J. Beringer¹⁶, S. Berlendis⁵⁷, N.R. Bernard⁸⁸, C. Bernius¹¹¹, F.U. Bernlochner²³, T. Berry⁷⁹, P. Berta¹³⁰, C. Bertella⁸⁵, G. Bertoli^{149a,149b}, F. Bertolucci^{125a,125b}, I.A. Bertram⁷⁴, C. Bertsche⁴⁴, D. Bertsche¹¹⁴, G.J. Besjes³⁸, O. Bessidskaia Bylund^{149a,149b}, M. Bessner⁴⁴, N. Besson¹³⁷, C. Betancourt⁵⁰, S. Bethke¹⁰², A.J. Bevan⁷⁸, R.M. Bianchi¹²⁶, L. Bianchini²⁵, M. Bianco³², O. Biebel¹⁰¹, D. Biedermann¹⁷, R. Bielski⁸⁶, N.V. Biesuz^{125a,125b}, M. Biglietti^{135a}, J. Bilbao De Mendizabal⁵¹, T.R.V. Billoud⁹⁶, H. Bilokon⁴⁹, M. Bindi⁵⁶, S. Binet¹¹⁸, A. Bingul^{20b}, C. Bini^{133a,133b}, S. Biondi^{22a,22b}, D.M. Bjergaard⁴⁷, C.W. Black¹⁵³, J.E. Black¹⁴⁶, K.M. Black²⁴, D. Blackburn¹³⁹, R.E. Blair⁶, J.-B. Blanchard¹³⁷, T. Blazek^{147a}, I. Bloch⁴⁴, C. Blocker²⁵, W. Blum^{85,*}, U. Blumenschein⁵⁶,

S. Blunier^{34a}, G.J. Bobbink¹⁰⁸, V.S. Bobrovnikov^{110,c}, S.S. Bocchetta⁸³, A. Bocci⁴⁷, C. Bock¹⁰¹,
 M. Boehler⁵⁰, D. Boerner¹⁷⁸, J.A. Bogaerts³², D. Bogavac¹⁴, A.G. Bogdanchikov¹¹⁰, C. Bohm^{149a},
 V. Boisvert⁷⁹, P. Bokan¹⁴, T. Bold^{40a}, A.S. Boldyrev^{167a,167c}, M. Bomben⁸², M. Bona⁷⁸,
 M. Boonekamp¹³⁷, A. Borisov¹³¹, G. Borissov⁷⁴, J. Bortfeldt³², D. Bortoletto¹²¹, V. Bortolotto^{62a,62b,62c},
 K. Bos¹⁰⁸, D. Boscherini^{22a}, M. Bosman¹³, J.D. Bossio Sola²⁹, J. Boudreau¹²⁶, J. Bouffard²,
 E.V. Bouhova-Thacker⁷⁴, D. Boumediene³⁶, C. Bourdarios¹¹⁸, S.K. Boutle⁵⁵, A. Boveia³², J. Boyd³²,
 I.R. Boyko⁶⁷, J. Bracinik¹⁹, A. Brandt⁸, G. Brandt⁵⁶, O. Brandt^{60a}, U. Bratzler¹⁵⁹, B. Brau⁸⁸,
 J.E. Brau¹¹⁷, H.M. Braun^{178,*}, W.D. Breaden Madden⁵⁵, K. Brendlinger¹²³, A.J. Brennan⁹⁰,
 L. Brenner¹⁰⁸, R. Brenner¹⁶⁸, S. Bressler¹⁷⁵, T.M. Bristow⁴⁸, D. Britton⁵⁵, D. Britzger⁴⁴, F.M. Brochu³⁰,
 I. Brock²³, R. Brock⁹², G. Brooijmans³⁷, T. Brooks⁷⁹, W.K. Brooks^{34b}, J. Brosamer¹⁶, E. Brost¹⁰⁹,
 J.H. Broughton¹⁹, P.A. Bruckman de Renstrom⁴¹, D. Bruncko^{147b}, R. Bruneliere⁵⁰, A. Bruni^{22a},
 G. Bruni^{22a}, L.S. Bruni¹⁰⁸, BH Brunt³⁰, M. Bruschi^{22a}, N. Bruscino²³, P. Bryant³³, L. Bryngemark⁸³,
 T. Buanes¹⁵, Q. Buat¹⁴⁵, P. Buchholz¹⁴⁴, A.G. Buckley⁵⁵, I.A. Budagov⁶⁷, F. Buehrer⁵⁰, M.K. Bugge¹²⁰,
 O. Bulekov⁹⁹, D. Bullock⁸, H. Burckhart³², S. Burdin⁷⁶, C.D. Burgard⁵⁰, B. Burghgrave¹⁰⁹, K. Burka⁴¹,
 S. Burke¹³², I. Burmeister⁴⁵, J.T.P. Burr¹²¹, E. Busato³⁶, D. Büscher⁵⁰, V. Büscher⁸⁵, P. Bussey⁵⁵,
 J.M. Butler²⁴, C.M. Buttar⁵⁵, J.M. Butterworth⁸⁰, P. Butti¹⁰⁸, W. Buttlinger²⁷, A. Buzatu⁵⁵,
 A.R. Buzykaev^{110,c}, S. Cabrera Urbán¹⁷⁰, D. Caforio¹²⁹, V.M. Cairo^{39a,39b}, O. Cakir^{4a}, N. Calace⁵¹,
 P. Calafiura¹⁶, A. Calandri⁸⁷, G. Calderini⁸², P. Calfayan¹⁰¹, G. Callea^{39a,39b}, L.P. Caloba^{26a},
 S. Calvente Lopez⁸⁴, D. Calvet³⁶, S. Calvet³⁶, T.P. Calvet⁸⁷, R. Camacho Toro³³, S. Camarda³²,
 P. Camarri^{134a,134b}, D. Cameron¹²⁰, R. Caminal Armadans¹⁶⁹, C. Camincher⁵⁷, S. Campana³²,
 M. Campanelli⁸⁰, A. Camplani^{93a,93b}, A. Campoverde¹⁴⁴, V. Canale^{105a,105b}, A. Canepa^{163a},
 M. Cano Bret¹⁴¹, J. Cantero¹¹⁵, R. Cantrill^{127a}, T. Cao⁴², M.D.M. Capeans Garrido³², I. Caprini^{28b},
 M. Caprini^{28b}, M. Capua^{39a,39b}, R. Caputo⁸⁵, R.M. Carbone³⁷, R. Cardarelli^{134a}, F. Cardillo⁵⁰,
 I. Carli¹³⁰, T. Carli³², G. Carlino^{105a}, L. Carminati^{93a,93b}, S. Caron¹⁰⁷, E. Carquin^{34b},
 G.D. Carrillo-Montoya³², J.R. Carter³⁰, J. Carvalho^{127a,127c}, D. Casadei¹⁹, M.P. Casado^{13,i},
 M. Casolino¹³, D.W. Casper¹⁶⁶, E. Castaneda-Miranda^{148a}, R. Castelijn¹⁰⁸, A. Castelli¹⁰⁸,
 V. Castillo Gimenez¹⁷⁰, N.F. Castro^{127a,j}, A. Catinaccio³², J.R. Catmore¹²⁰, A. Cattai³², J. Caudron⁸⁵,
 V. Cavaliere¹⁶⁹, E. Cavallaro¹³, D. Cavalli^{93a}, M. Cavalli-Sforza¹³, V. Cavasinni^{125a,125b},
 F. Ceradini^{135a,135b}, L. Cerdá Alberich¹⁷⁰, B.C. Cerio⁴⁷, A.S. Cerqueira^{26b}, A. Cerri¹⁵², L. Cerrito⁷⁸,
 F. Cerutti¹⁶, M. Cerv³², A. Cervelli¹⁸, S.A. Cetin^{20d}, A. Chafaq^{136a}, D. Chakraborty¹⁰⁹, S.K. Chan⁵⁸,
 Y.L. Chan^{62a}, P. Chang¹⁶⁹, J.D. Chapman³⁰, D.G. Charlton¹⁹, A. Chatterjee⁵¹, C.C. Chau¹⁶²,
 C.A. Chavez Barajas¹⁵², S. Che¹¹², S. Cheatham⁷⁴, A. Chegwidden⁹², S. Chekanov⁶,
 S.V. Chekulaev^{163a}, G.A. Chelkov^{67,k}, M.A. Chelstowska⁹¹, C. Chen⁶⁶, H. Chen²⁷, K. Chen¹⁵¹,
 S. Chen^{35b}, S. Chen¹⁵⁸, X. Chen^{35c}, Y. Chen⁶⁹, H.C. Cheng⁹¹, H.J. Cheng^{35a}, Y. Cheng³³,
 A. Cheplakov⁶⁷, E. Cheremushkina¹³¹, R. Cherkaoui El Moursli^{136e}, V. Chernyatin^{27,*}, E. Cheu⁷,
 L. Chevalier¹³⁷, V. Chiarella⁴⁹, G. Chiarelli^{125a,125b}, G. Chiodini^{75a}, A.S. Chisholm¹⁹, A. Chitan^{28b},
 M.V. Chizhov⁶⁷, K. Choi⁶³, A.R. Chomont³⁶, S. Chouridou⁹, B.K.B. Chow¹⁰¹, V. Christodoulou⁸⁰,
 D. Chromeck-Burckhart³², J. Chudoba¹²⁸, A.J. Chuinard⁸⁹, J.J. Chwastowski⁴¹, L. Chytka¹¹⁶,
 G. Ciapetti^{133a,133b}, A.K. Ciftci^{4a}, D. Cinca⁴⁵, V. Cindro⁷⁷, I.A. Cioara²³, C. Ciocca^{22a,22b}, A. Ciocio¹⁶,
 F. Cirotto^{105a,105b}, Z.H. Citron¹⁷⁵, M. Citterio^{93a}, M. Ciubancan^{28b}, A. Clark⁵¹, B.L. Clark⁵⁸,
 M.R. Clark³⁷, P.J. Clark⁴⁸, R.N. Clarke¹⁶, C. Clement^{149a,149b}, Y. Coadou⁸⁷, M. Cobal^{167a,167c},
 A. Coccaro⁵¹, J. Cochran⁶⁶, L. Colasurdo¹⁰⁷, B. Cole³⁷, A.P. Colijn¹⁰⁸, J. Collot⁵⁷, T. Colombo³²,
 G. Compostella¹⁰², P. Conde Muiño^{127a,127b}, E. Coniavitis⁵⁰, S.H. Connell^{148b}, I.A. Connolly⁷⁹,
 V. Consorti⁵⁰, S. Constantinescu^{28b}, G. Conti³², F. Conventi^{105a,l}, M. Cooke¹⁶, B.D. Cooper⁸⁰,
 A.M. Cooper-Sarkar¹²¹, K.J.R. Cormier¹⁶², T. Cornelissen¹⁷⁸, M. Corradi^{133a,133b}, F. Corriveau^{89,m},
 A. Corso-Radu¹⁶⁶, A. Cortes-Gonzalez¹³, G. Cortiana¹⁰², G. Costa^{93a}, M.J. Costa¹⁷⁰, D. Costanzo¹⁴²,
 G. Cottin³⁰, G. Cowan⁷⁹, B.E. Cox⁸⁶, K. Cranmer¹¹¹, S.J. Crawley⁵⁵, G. Cree³¹, S. Crépé-Renaudin⁵⁷,

F. Crescioli⁸², W.A. Cribbs^{149a,149b}, M. Crispin Ortuzar¹²¹, M. Cristinziani²³, V. Croft¹⁰⁷,
 G. Crosetti^{39a,39b}, A. Cueto⁸⁴, T. Cuhadar Donszelmann¹⁴², J. Cummings¹⁷⁹, M. Curatolo⁴⁹, J. Cúth⁸⁵,
 H. Czirr¹⁴⁴, P. Czodrowski³, G. D'amen^{22a,22b}, S. D'Auria⁵⁵, M. D'Onofrio⁷⁶,
 M.J. Da Cunha Sargedas De Sousa^{127a,127b}, C. Da Via⁸⁶, W. Dabrowski^{40a}, T. Dado^{147a}, T. Dai⁹¹,
 O. Dale¹⁵, F. Dallaire⁹⁶, C. Dallapiccola⁸⁸, M. Dam³⁸, J.R. Dandoy³³, N.P. Dang⁵⁰, A.C. Daniells¹⁹,
 N.S. Dann⁸⁶, M. Danninger¹⁷¹, M. Dano Hoffmann¹³⁷, V. Dao⁵⁰, G. Darbo^{52a}, S. Darmora⁸,
 J. Dassoulas³, A. Dattagupta⁶³, W. Davey²³, C. David¹⁷², T. Davidek¹³⁰, M. Davies¹⁵⁶, P. Davison⁸⁰,
 E. Dawe⁹⁰, I. Dawson¹⁴², R.K. Daya-Ishmukhametova⁸⁸, K. De⁸, R. de Asmundis^{105a},
 A. De Benedetti¹¹⁴, S. De Castro^{22a,22b}, S. De Cecco⁸², N. De Groot¹⁰⁷, P. de Jong¹⁰⁸, H. De la Torre⁸⁴,
 F. De Lorenzi⁶⁶, A. De Maria⁵⁶, D. De Pedis^{133a}, A. De Salvo^{133a}, U. De Sanctis¹⁵², A. De Santo¹⁵²,
 J.B. De Vivie De Regie¹¹⁸, W.J. Dearnaley⁷⁴, R. Debbe²⁷, C. Debenedetti¹³⁸, D.V. Dedovich⁶⁷,
 N. Dehghanian³, I. Deigaard¹⁰⁸, M. Del Gaudio^{39a,39b}, J. Del Peso⁸⁴, T. Del Prete^{125a,125b},
 D. Delgove¹¹⁸, F. Deliot¹³⁷, C.M. Delitzsch⁵¹, M. Deliyergiyev⁷⁷, A. Dell'Acqua³², L. Dell'Asta²⁴,
 M. Dell'Orso^{125a,125b}, M. Della Pietra^{105a,l}, D. della Volpe⁵¹, M. Delmastro⁵, P.A. Delsart⁵⁷,
 D.A. DeMarco¹⁶², S. Demers¹⁷⁹, M. Demichev⁶⁷, A. Demilly⁸², S.P. Denisov¹³¹, D. Denysiuk¹³⁷,
 D. Derendarz⁴¹, J.E. Derkaoui^{136d}, F. Derue⁸², P. Dervan⁷⁶, K. Desch²³, C. Deterre⁴⁴, K. Dette⁴⁵,
 P.O. Deviveiros³², A. Dewhurst¹³², S. Dhaliwal²⁵, A. Di Ciaccio^{134a,134b}, L. Di Ciaccio⁵,
 W.K. Di Clemente¹²³, C. Di Donato^{133a,133b}, A. Di Girolamo³², B. Di Girolamo³², B. Di Micco^{135a,135b},
 R. Di Nardo³², A. Di Simone⁵⁰, R. Di Sipio¹⁶², D. Di Valentino³¹, C. Diaconu⁸⁷, M. Diamond¹⁶²,
 F.A. Dias⁴⁸, M.A. Diaz^{34a}, E.B. Diehl⁹¹, J. Dietrich¹⁷, S. Diglio⁸⁷, A. Dimitrieva¹⁴, J. Dingfelder²³,
 P. Dita^{28b}, S. Dita^{28b}, F. Dittus³², F. Djama⁸⁷, T. Djobava^{53b}, J.I. Djuvsland^{60a}, M.A.B. do Vale^{26c},
 D. Dobos³², M. Dobre^{28b}, C. Doglioni⁸³, J. Dolejsi¹³⁰, Z. Dolezal¹³⁰, B.A. Dolgoshein^{99,*},
 M. Donadelli^{26d}, S. Donati^{125a,125b}, P. Dondero^{122a,122b}, J. Donini³⁶, J. Dopke¹³², A. Doria^{105a},
 M.T. Dova⁷³, A.T. Doyle⁵⁵, E. Drechsler⁵⁶, M. Dris¹⁰, Y. Du¹⁴⁰, J. Duarte-Campderros¹⁵⁶,
 E. Duchovni¹⁷⁵, G. Duckeck¹⁰¹, O.A. Ducu^{96,n}, D. Duda¹⁰⁸, A. Dudarev³², E.M. Duffield¹⁶,
 L. Duflot¹¹⁸, M. Dührssen³², M. Dumancic¹⁷⁵, M. Dunford^{60a}, H. Duran Yildiz^{4a}, M. Düren⁵⁴,
 A. Durglishvili^{53b}, D. Duschinger⁴⁶, B. Dutta⁴⁴, M. Dyndal⁴⁴, C. Eckardt⁴⁴, K.M. Ecker¹⁰²,
 R.C. Edgar⁹¹, N.C. Edwards⁴⁸, T. Eifert³², G. Eigen¹⁵, K. Einsweiler¹⁶, T. Ekelof¹⁶⁸, M. El Kacimi^{136c},
 V. Ellajosyula⁸⁷, M. Ellert¹⁶⁸, S. Elles⁵, F. Ellinghaus¹⁷⁸, A.A. Elliot¹⁷², N. Ellis³², J. Elmsheuser²⁷,
 M. Elsing³², D. Emelyanov¹³², Y. Enari¹⁵⁸, O.C. Endner⁸⁵, J.S. Ennis¹⁷³, J. Erdmann⁴⁵, A. Ereditato¹⁸,
 G. Ernis¹⁷⁸, J. Ernst², M. Ernst²⁷, S. Errede¹⁶⁹, E. Ertel⁸⁵, M. Escalier¹¹⁸, H. Esch⁴⁵, C. Escobar¹²⁶,
 B. Esposito⁴⁹, A.I. Etienne¹³⁷, E. Etzion¹⁵⁶, H. Evans⁶³, A. Ezhilov¹²⁴, F. Fabbri^{22a,22b}, L. Fabbri^{22a,22b},
 G. Facini³³, R.M. Fakhrutdinov¹³¹, S. Falciano^{133a}, R.J. Falla⁸⁰, J. Faltova³², Y. Fang^{35a}, M. Fanti^{93a,93b},
 A. Farbin⁸, A. Farilla^{135a}, C. Farina¹²⁶, E.M. Farina^{122a,122b}, T. Farooque¹³, S. Farrell¹⁶,
 S.M. Farrington¹⁷³, P. Farthouat³², F. Fassi^{136e}, P. Fassnacht³², D. Fassouliotis⁹, M. Faucci Giannelli⁷⁹,
 A. Favareto^{52a,52b}, W.J. Fawcett¹²¹, L. Fayard¹¹⁸, O.L. Fedin^{124,o}, W. Fedorko¹⁷¹, S. Feigl¹²⁰,
 L. Feligioni⁸⁷, C. Feng¹⁴⁰, E.J. Feng³², H. Feng⁹¹, A.B. Fenyuk¹³¹, L. Feremenga⁸,
 P. Fernandez Martinez¹⁷⁰, S. Fernandez Perez¹³, J. Ferrando⁵⁵, A. Ferrari¹⁶⁸, P. Ferrari¹⁰⁸, R. Ferrari^{122a},
 D.E. Ferreira de Lima^{60b}, A. Ferrer¹⁷⁰, D. Ferrere⁵¹, C. Ferretti⁹¹, A. Ferretto Parodi^{52a,52b}, F. Fiedler⁸⁵,
 A. Filipčić⁷⁷, M. Filipuzzi⁴⁴, F. Filthaut¹⁰⁷, M. Fincke-Keeler¹⁷², K.D. Finelli¹⁵³,
 M.C.N. Fiolhais^{127a,127c}, L. Fiorini¹⁷⁰, A. Firan⁴², A. Fischer², C. Fischer¹³, J. Fischer¹⁷⁸, W.C. Fisher⁹²,
 N. Flasche¹⁴⁴, I. Fleck¹⁴⁴, P. Fleischmann⁹¹, G.T. Fletcher¹⁴², R.R.M. Fletcher¹²³, T. Flick¹⁷⁸,
 A. Floderus⁸³, L.R. Flores Castillo^{62a}, M.J. Flowerdew¹⁰², G.T. Forcolin⁸⁶, A. Formica¹³⁷, A. Forti⁸⁶,
 A.G. Foster¹⁹, D. Fournier¹¹⁸, H. Fox⁷⁴, S. Fracchia¹³, P. Francavilla⁸², M. Franchini^{22a,22b},
 D. Francis³², L. Franconi¹²⁰, M. Franklin⁵⁸, M. Frate¹⁶⁶, M. Fraternali^{122a,122b}, D. Freeborn⁸⁰,
 S.M. Fressard-Batraneanu³², F. Friedrich⁴⁶, D. Froidevaux³², J.A. Frost¹²¹, C. Fukunaga¹⁵⁹,
 E. Fullana Torregrosa⁸⁵, T. Fusayasu¹⁰³, J. Fuster¹⁷⁰, C. Gabaldon⁵⁷, O. Gabizon¹⁷⁸, A. Gabrielli^{22a,22b},

A. Gabrielli¹⁶, G.P. Gach^{40a}, S. Gadatsch³², S. Gadomski⁵¹, G. Gagliardi^{52a,52b}, L.G. Gagnon⁹⁶,
 P. Gagnon⁶³, C. Galea¹⁰⁷, B. Galhardo^{127a,127c}, E.J. Gallas¹²¹, B.J. Gallop¹³², P. Gallus¹²⁹, G. Galster³⁸,
 K.K. Gan¹¹², J. Gao⁵⁹, Y. Gao⁴⁸, Y.S. Gao^{146,g}, F.M. Garay Walls⁴⁸, C. García¹⁷⁰,
 J.E. García Navarro¹⁷⁰, M. Garcia-Sciveres¹⁶, R.W. Gardner³³, N. Garelli¹⁴⁶, V. Garonne¹²⁰,
 A. Gascon Bravo⁴⁴, C. Gatti⁴⁹, A. Gaudiello^{52a,52b}, G. Gaudio^{122a}, L. Gauthier⁹⁶, I.L. Gavrilenco⁹⁷,
 C. Gay¹⁷¹, G. Gaycken²³, E.N. Gazis¹⁰, Z. Gecse¹⁷¹, C.N.P. Gee¹³², Ch. Geich-Gimbel²³, M. Geisen⁸⁵,
 M.P. Geisler^{60a}, C. Gemme^{52a}, M.H. Genest⁵⁷, C. Geng^{59,p}, S. Gentile^{133a,133b}, C. Gentsos¹⁵⁷,
 S. George⁷⁹, D. Gerbaudo¹³, A. Gershon¹⁵⁶, S. Ghasemi¹⁴⁴, H. Ghazlane^{136b}, M. Ghneimat²³,
 B. Giacobbe^{22a}, S. Giagu^{133a,133b}, P. Giannetti^{125a,125b}, B. Gibbard²⁷, S.M. Gibson⁷⁹, M. Gignac¹⁷¹,
 M. Gilchriese¹⁶, T.P.S. Gillam³⁰, D. Gillberg³¹, G. Gilles¹⁷⁸, D.M. Gingrich^{3,d}, N. Giokaris^{9,*},
 M.P. Giordani^{167a,167c}, F.M. Giorgi^{22a}, F.M. Giorgi¹⁷, P.F. Giraud¹³⁷, P. Giromini⁵⁸, D. Giugni^{93a},
 F. Giulì¹²¹, C. Giuliani¹⁰², M. Giuliani^{60b}, B.K. Gjelsten¹²⁰, S. Gkaitatzis¹⁵⁷, I. Gkialas⁹,
 E.L. Gkougkousis¹¹⁸, L.K. Gladilin¹⁰⁰, C. Glasman⁸⁴, J. Glatzer⁵⁰, P.C.F. Glaysher⁴⁸, A. Glazov⁴⁴,
 M. Goblirsch-Kolb²⁵, J. Godlewski⁴¹, S. Goldfarb⁹⁰, T. Golling⁵¹, D. Golubkov¹³¹,
 A. Gomes^{127a,127b,127d}, R. Gonçalo^{127a}, J. Goncalves Pinto Firmino Da Costa¹³⁷, G. Gonella⁵⁰,
 L. Gonella¹⁹, A. Gongadze⁶⁷, S. González de la Hoz¹⁷⁰, G. Gonzalez Parra¹³, S. Gonzalez-Sevilla⁵¹,
 L. Goossens³², P.A. Gorbounov⁹⁸, H.A. Gordon²⁷, I. Gorelov¹⁰⁶, B. Gorini³², E. Gorini^{75a,75b},
 A. Gorišek⁷⁷, E. Gornicki⁴¹, A.T. Goshaw⁴⁷, C. Gössling⁴⁵, M.I. Gostkin⁶⁷, C.R. Goudet¹¹⁸,
 D. Goujdami^{136c}, A.G. Goussiou¹³⁹, N. Govender^{148b,q}, E. Gozani¹⁵⁵, L. Graber⁵⁶,
 I. Grabowska-Bold^{40a}, P.O.J. Gradin⁵⁷, P. Grafström^{22a,22b}, J. Gramling⁵¹, E. Gramstad¹²⁰,
 S. Grancagnolo¹⁷, V. Gratchev¹²⁴, P.M. Gravila^{28e}, H.M. Gray³², E. Graziani^{135a}, Z.D. Greenwood^{81,r},
 C. Grefe²³, K. Gregersen⁸⁰, I.M. Gregor⁴⁴, P. Grenier¹⁴⁶, K. Grevtsov⁵, J. Griffiths⁸, A.A. Grillo¹³⁸,
 K. Grimm⁷⁴, S. Grinstein^{13,s}, Ph. Gris³⁶, J.-F. Grivaz¹¹⁸, S. Groh⁸⁵, J.P. Grohs⁴⁶, E. Gross¹⁷⁵,
 J. Grosse-Knetter⁵⁶, G.C. Grossi⁸¹, Z.J. Grout¹⁵², L. Guan⁹¹, W. Guan¹⁷⁶, J. Guenther⁶⁴, F. Gescini⁵¹,
 D. Guest¹⁶⁶, O. Gueta¹⁵⁶, E. Guido^{52a,52b}, T. Guillemin⁵, S. Guindon², U. Gul⁵⁵, C. Gumpert³²,
 J. Guo¹⁴¹, Y. Guo^{59,p}, R. Gupta⁴², S. Gupta¹²¹, G. Gustavino^{133a,133b}, P. Gutierrez¹¹⁴,
 N.G. Gutierrez Ortiz⁸⁰, C. Gutschow⁴⁶, C. Guyot¹³⁷, C. Gwenlan¹²¹, C.B. Gwilliam⁷⁶, A. Haas¹¹¹,
 C. Haber¹⁶, H.K. Hadavand⁸, N. Haddad^{136e}, A. Hadef⁸⁷, P. Haefner²³, S. Hageböck²³, Z. Hajduk⁴¹,
 H. Hakobyan^{180,*}, M. Haleem⁴⁴, J. Haley¹¹⁵, G. Halladjian⁹², G.D. Hallewell⁸⁷, K. Hamacher¹⁷⁸,
 P. Hamal¹¹⁶, K. Hamano¹⁷², A. Hamilton^{148a}, G.N. Hamity¹⁴², P.G. Hamnett⁴⁴, L. Han⁵⁹,
 K. Hanagaki^{68,t}, K. Hanawa¹⁵⁸, M. Hance¹³⁸, B. Haney¹²³, P. Hanke^{60a}, R. Hanna¹³⁷, J.B. Hansen³⁸,
 J.D. Hansen³⁸, M.C. Hansen²³, P.H. Hansen³⁸, K. Hara¹⁶⁴, A.S. Hard¹⁷⁶, T. Harenberg¹⁷⁸, F. Hariri¹¹⁸,
 S. Harkusha⁹⁴, R.D. Harrington⁴⁸, P.F. Harrison¹⁷³, F. Hartjes¹⁰⁸, N.M. Hartmann¹⁰¹, M. Hasegawa⁶⁹,
 Y. Hasegawa¹⁴³, A. Hasib¹¹⁴, S. Hassani¹³⁷, S. Haug¹⁸, R. Hauser⁹², L. Hauswald⁴⁶, M. Havranek¹²⁸,
 C.M. Hawkes¹⁹, R.J. Hawkings³², D. Hayden⁹², C.P. Hays¹²¹, J.M. Hays⁷⁸, H.S. Hayward⁷⁶,
 S.J. Haywood¹³², S.J. Head¹⁹, T. Heck⁸⁵, V. Hedberg⁸³, L. Heelan⁸, S. Heim¹²³, T. Heim¹⁶,
 B. Heinemann¹⁶, J.J. Heinrich¹⁰¹, L. Heinrich¹¹¹, C. Heinz⁵⁴, J. Hejbal¹²⁸, L. Helary²⁴,
 S. Hellman^{149a,149b}, C. Helsens³², J. Henderson¹²¹, R.C.W. Henderson⁷⁴, Y. Heng¹⁷⁶, S. Henkelmann¹⁷¹,
 A.M. Henriques Correia³², S. Henrot-Versille¹¹⁸, G.H. Herbert¹⁷, Y. Hernández Jiménez¹⁷⁰, G. Herten⁵⁰,
 R. Hertenberger¹⁰¹, L. Hervas³², G.G. Hesketh⁸⁰, N.P. Hessey¹⁰⁸, J.W. Hetherly⁴², R. Hickling⁷⁸,
 E. Higón-Rodríguez¹⁷⁰, E. Hill¹⁷², J.C. Hill³⁰, K.H. Hiller⁴⁴, S.J. Hillier¹⁹, I. Hincliffe¹⁶, E. Hines¹²³,
 R.R. Hinman¹⁶, M. Hirose⁵⁰, D. Hirschbuehl¹⁷⁸, J. Hobbs¹⁵¹, N. Hod^{163a}, M.C. Hodgkinson¹⁴²,
 P. Hodgson¹⁴², A. Hoecker³², M.R. Hoeferkamp¹⁰⁶, F. Hoenig¹⁰¹, D. Hohn²³, T.R. Holmes¹⁶,
 M. Homann⁴⁵, T.M. Hong¹²⁶, B.H. Hooberman¹⁶⁹, W.H. Hopkins¹¹⁷, Y. Horii¹⁰⁴, A.J. Horton¹⁴⁵,
 J.-Y. Hostachy⁵⁷, S. Hou¹⁵⁴, A. Hoummada^{136a}, J. Howarth⁴⁴, M. Hrabovsky¹¹⁶, I. Hristova¹⁷,
 J. Hrvnac¹¹⁸, T. Hrynevich⁹⁵, A. Hrynevich⁹⁵, C. Hsu^{148c}, P.J. Hsu^{154,u}, S.-C. Hsu¹³⁹, D. Hu³⁷, Q. Hu⁵⁹,
 Y. Huang⁴⁴, Z. Hubacek¹²⁹, F. Hubaut⁸⁷, F. Huegging²³, T.B. Huffman¹²¹, E.W. Hughes³⁷, G. Hughes⁷⁴,

M. Huhtinen³², P. Huo¹⁵¹, N. Huseynov^{67,b}, J. Huston⁹², J. Huth⁵⁸, G. Iacobucci⁵¹, G. Iakovidis²⁷,
 I. Ibragimov¹⁴⁴, L. Iconomidou-Fayard¹¹⁸, E. Ideal¹⁷⁹, Z. Idrissi^{136e}, P. Iengo³², O. Igonkina^{108,v},
 T. Iizawa¹⁷⁴, Y. Ikegami⁶⁸, M. Ikeno⁶⁸, Y. Ilchenko^{11,w}, D. Iliadis¹⁵⁷, N. Ilic¹⁴⁶, T. Ince¹⁰²,
 G. Introzzi^{122a,122b}, P. Ioannou^{9,*}, M. Iodice^{135a}, K. Iordanidou³⁷, V. Ippolito⁵⁸, N. Ishijima¹¹⁹,
 M. Ishino⁷⁰, M. Ishitsuka¹⁶⁰, R. Ishmukhametov¹¹², C. Issever¹²¹, S. Isti^{20a}, F. Ito¹⁶⁴,
 J.M. Iturbe Ponce⁸⁶, R. Iuppa^{134a,134b}, W. Iwanski⁶⁴, H. Iwasaki⁶⁸, J.M. Izen⁴³, V. Izzo^{105a}, S. Jabbar³,
 B. Jackson¹²³, P. Jackson¹, V. Jain², K.B. Jakobi⁸⁵, K. Jakobs⁵⁰, S. Jakobsen³², T. Jakoubek¹²⁸,
 D.O. Jamin¹¹⁵, D.K. Jana⁸¹, E. Jansen⁸⁰, R. Jansky⁶⁴, J. Janssen²³, M. Janus⁵⁶, G. Jarlskog⁸³,
 N. Javadov^{67,b}, T. Javůrek⁵⁰, M. Javurkova⁵⁰, F. Jeanneau¹³⁷, L. Jeanty¹⁶, G.-Y. Jeng¹⁵³, D. Jennens⁹⁰,
 P. Jenni^{50,x}, C. Jeske¹⁷³, S. Jézéquel⁵, H. Ji¹⁷⁶, J. Jia¹⁵¹, H. Jiang⁶⁶, Y. Jiang⁵⁹, S. Jiggins⁸⁰,
 J. Jimenez Pena¹⁷⁰, S. Jin^{35a}, A. Jinaru^{28b}, O. Jinnouchi¹⁶⁰, P. Johansson¹⁴², K.A. Johns⁷,
 W.J. Johnson¹³⁹, K. Jon-And^{149a,149b}, G. Jones¹⁷³, R.W.L. Jones⁷⁴, S. Jones⁷, T.J. Jones⁷⁶,
 J. Jongmanns^{60a}, P.M. Jorge^{127a,127b}, J. Jovicevic^{163a}, X. Ju¹⁷⁶, A. Juste Rozas^{13,s}, M.K. Köhler¹⁷⁵,
 A. Kaczmar ska⁴¹, M. Kado¹¹⁸, H. Kagan¹¹², M. Kagan¹⁴⁶, S.J. Kahn⁸⁷, E. Kajomovitz⁴⁷,
 C.W. Kalderon¹²¹, A. Kaluza⁸⁵, S. Kama⁴², A. Kamenshchikov¹³¹, N. Kanaya¹⁵⁸, S. Kaneti³⁰,
 L. Kanjir⁷⁷, V.A. Kantserov⁹⁹, J. Kanzaki⁶⁸, B. Kaplan¹¹¹, L.S. Kaplan¹⁷⁶, A. Kapliy³³, D. Kar^{148c},
 K. Karakostas¹⁰, A. Karamaoun³, N. Karastathis¹⁰, M.J. Kareem⁵⁶, E. Karentzos¹⁰, M. Karnevskiy⁸⁵,
 S.N. Karpov⁶⁷, Z.M. Karpova⁶⁷, K. Karthik¹¹¹, V. Kartvelishvili⁷⁴, A.N. Karyukhin¹³¹, K. Kasahara¹⁶⁴,
 L. Kashif¹⁷⁶, R.D. Kass¹¹², A. Kastanas¹⁵, Y. Kataoka¹⁵⁸, C. Kato¹⁵⁸, A. Katre⁵¹, J. Katzy⁴⁴,
 K. Kawade¹⁰⁴, K. Kawagoe⁷², T. Kawamoto¹⁵⁸, G. Kawamura⁵⁶, V.F. Kazanin^{110,c}, R. Keeler¹⁷²,
 R. Kehoe⁴², J.S. Keller⁴⁴, J.J. Kempster⁷⁹, H. Keoshkerian¹⁶², O. Kepka¹²⁸, B.P. Kerševan⁷⁷,
 S. Kersten¹⁷⁸, R.A. Keyes⁸⁹, M. Khader¹⁶⁹, F. Khalil-zada¹², A. Khanov¹¹⁵, A.G. Kharlamov^{110,c},
 T.J. Khoo⁵¹, V. Khovanskiy⁹⁸, E. Khramov⁶⁷, J. Khubua^{53b,y}, S. Kido⁶⁹, H.Y. Kim⁸, S.H. Kim¹⁶⁴,
 Y.K. Kim³³, N. Kimura¹⁵⁷, O.M. Kind¹⁷, B.T. King⁷⁶, M. King¹⁷⁰, S.B. King¹⁷¹, J. Kirk¹³²,
 A.E. Kiryunin¹⁰², T. Kishimoto⁶⁹, D. Kisielewska^{40a}, F. Kiss⁵⁰, K. Kiuchi¹⁶⁴, O. Kivernyk¹³⁷,
 E. Kladiva^{147b}, M.H. Klein³⁷, M. Klein⁷⁶, U. Klein⁷⁶, K. Kleinknecht⁸⁵, P. Klimek¹⁰⁹, A. Klimentov²⁷,
 R. Klingenberg⁴⁵, J.A. Klinger¹⁴², T. Klioutchnikova³², E.-E. Kluge^{60a}, P. Kluit¹⁰⁸, S. Kluth¹⁰²,
 J. Knapik⁴¹, E. Kneringer⁶⁴, E.B.F.G. Knoops⁸⁷, A. Knue¹⁰², A. Kobayashi¹⁵⁸, D. Kobayashi¹⁶⁰,
 T. Kobayashi¹⁵⁸, M. Kobel⁴⁶, M. Kocian¹⁴⁶, P. Kodys¹³⁰, T. Koffas³¹, E. Koffeman¹⁰⁸, T. Koi¹⁴⁶,
 H. Kolanoski¹⁷, M. Kolb^{60b}, I. Koletsou⁵, A.A. Komar^{97,*}, Y. Komori¹⁵⁸, T. Kondo⁶⁸,
 N. Kondrashova⁴⁴, K. Köneke⁵⁰, A.C. König¹⁰⁷, T. Kono^{68,z}, R. Konoplich^{111,aa}, N. Konstantinidis⁸⁰,
 R. Kopeliansky⁶³, S. Koperny^{40a}, L. Köpke⁸⁵, A.K. Kopp⁵⁰, K. Korcyl⁴¹, K. Kordas¹⁵⁷, A. Korn⁸⁰,
 A.A. Korol^{110,c}, I. Korolkov¹³, E.V. Korolkova¹⁴², O. Kortner¹⁰², S. Kortner¹⁰², T. Kosek¹³⁰,
 V.V. Kostyukhin²³, A. Kotwal⁴⁷, A. Kourkoumeli-Charalampidi⁹, C. Kourkoumelis⁹, V. Kouskoura²⁷,
 A.B. Kowalewska⁴¹, R. Kowalewski¹⁷², T.Z. Kowalski^{40a}, C. Kozakai¹⁵⁸, W. Kozanecki¹³⁷,
 A.S. Kozhin¹³¹, V.A. Kramarenko¹⁰⁰, G. Kramberger⁷⁷, D. Krasnopevtsev⁹⁹, M.W. Krasny⁸²,
 A. Krasznahorkay³², A. Kravchenko²⁷, M. Kretz^{60c}, J. Kretzschmar⁷⁶, K. Kreutzfeldt⁵⁴, P. Krieger¹⁶²,
 K. Krizka³³, K. Kroeninger⁴⁵, H. Kroha¹⁰², J. Kroll¹²³, J. Kroseberg²³, J. Krstic¹⁴, U. Kruchonak⁶⁷,
 H. Krüger²³, N. Krumnack⁶⁶, A. Kruse¹⁷⁶, M.C. Kruse⁴⁷, M. Kruskal²⁴, T. Kubota⁹⁰, H. Kucuk⁸⁰,
 S. Kuday^{4b}, J.T. Kuechler¹⁷⁸, S. Kuehn⁵⁰, A. Kugel^{60c}, F. Kuger¹⁷⁷, A. Kuhl¹³⁸, T. Kuhl¹⁴⁴, V. Kukhtin⁶⁷,
 R. Kukla¹³⁷, Y. Kulchitsky⁹⁴, S. Kuleshov^{34b}, M. Kuna^{133a,133b}, T. Kunigo⁷⁰, A. Kupco¹²⁸,
 H. Kurashige⁶⁹, Y.A. Kurochkin⁹⁴, V. Kus¹²⁸, E.S. Kuwertz¹⁷², M. Kuze¹⁶⁰, J. Kvita¹¹⁶, T. Kwan¹⁷²,
 D. Kyriazopoulos¹⁴², A. La Rosa¹⁰², J.L. La Rosa Navarro^{26d}, L. La Rotonda^{39a,39b}, C. Lacasta¹⁷⁰,
 F. Lacava^{133a,133b}, J. Lacey³¹, H. Lacker¹⁷, D. Lacour⁸², V.R. Lacuesta¹⁷⁰, E. Ladygin⁶⁷, R. Lafaye⁵,
 B. Laforge⁸², T. Lagouri¹⁷⁹, S. Lai⁵⁶, S. Lammers⁶³, W. Lampl⁷, E. Lançon¹³⁷, U. Landgraf⁵⁰,
 M.P.J. Landon⁷⁸, M.C. Lanfermann⁵¹, V.S. Lang^{60a}, J.C. Lange¹³, A.J. Lankford¹⁶⁶, F. Lanni²⁷,
 K. Lantzsch²³, A. Lanza^{122a}, S. Laplace⁸², C. Lapoire³², J.F. Laporte¹³⁷, T. Lari^{93a},

F. Lasagni Manghi^{22a,22b}, M. Lassnig³², P. Laurelli⁴⁹, W. Lavrijsen¹⁶, A.T. Law¹³⁸, P. Laycock⁷⁶,
 T. Lazovich⁵⁸, M. Lazzaroni^{93a,93b}, B. Le⁹⁰, O. Le Dertz⁸², E. Le Guiriec⁸⁷, E.P. Le Quilleuc¹³⁷,
 M. LeBlanc¹⁷², T. LeCompte⁶, F. Ledroit-Guillon⁵⁷, C.A. Lee²⁷, S.C. Lee¹⁵⁴, L. Lee¹, B. Lefebvre⁸⁹,
 G. Lefebvre⁸², M. Lefebvre¹⁷², F. Legger¹⁰¹, C. Leggett¹⁶, A. Lehan⁷⁶, G. Lehmann Miotto³², X. Lei⁷,
 W.A. Leight³¹, A.G. Leister¹⁷⁹, M.A.L. Leite^{26d}, R. Leitner¹³⁰, D. Lellouch¹⁷⁵, B. Lemmer⁵⁶,
 K.J.C. Leney⁸⁰, T. Lenz²³, B. Lenzi³², R. Leone⁷, S. Leone^{125a,125b}, C. Leonidopoulos⁴⁸,
 S. Leontsinis¹⁰, G. Lerner¹⁵², C. Leroy⁹⁶, A.A.J. Lesage¹³⁷, C.G. Lester³⁰, M. Levchenko¹²⁴,
 J. Levêque⁵, D. Levin⁹¹, L.J. Levinson¹⁷⁵, M. Levy¹⁹, D. Lewis⁷⁸, A.M. Leyko²³, M. Leyton⁴³,
 B. Li^{59,p}, H. Li¹⁵¹, H.L. Li³³, L. Li⁴⁷, L. Li¹⁴¹, Q. Li^{35a}, S. Li⁴⁷, X. Li⁸⁶, Y. Li¹⁴⁴, Z. Liang^{35a},
 B. Liberti^{134a}, A. Liblong¹⁶², P. Lichard³², K. Lie¹⁶⁹, J. Liebal²³, W. Liebig¹⁵, A. Limosani¹⁵³,
 S.C. Lin^{154,ab}, T.H. Lin⁸⁵, B.E. Lindquist¹⁵¹, A.E. Lioni⁵¹, E. Lipeles¹²³, A. Lipniacka¹⁵, M. Lisovyi^{60b},
 T.M. Liss¹⁶⁹, A. Lister¹⁷¹, A.M. Litke¹³⁸, B. Liu^{154,ac}, D. Liu¹⁵⁴, H. Liu⁹¹, H. Liu²⁷, J. Liu⁸⁷, J.B. Liu⁵⁹,
 K. Liu⁸⁷, L. Liu¹⁶⁹, M. Liu⁴⁷, M. Liu⁵⁹, Y.L. Liu⁵⁹, Y. Liu⁵⁹, M. Livan^{122a,122b}, A. Lleres⁵⁷,
 J. Llorente Merino^{35a}, S.L. Lloyd⁷⁸, F. Lo Sterzo¹⁵⁴, E.M. Lobodzinska⁴⁴, P. Loch⁷, W.S. Lockman¹³⁸,
 F.K. Loebinger⁸⁶, A.E. Loevschall-Jensen³⁸, K.M. Loew²⁵, A. Loginov^{179,*}, T. Lohse¹⁷,
 K. Lohwasser⁴⁴, M. Lokajicek¹²⁸, B.A. Long²⁴, J.D. Long¹⁶⁹, R.E. Long⁷⁴, L. Longo^{75a,75b},
 K.A.Looper¹¹², L. Lopes^{127a}, D. Lopez Mateos⁵⁸, B. Lopez Paredes¹⁴², I. Lopez Paz¹³,
 A. Lopez Solis⁸², J. Lorenz¹⁰¹, N. Lorenzo Martinez⁶³, M. Losada²¹, P.J. Lösel¹⁰¹, X. Lou^{35a},
 A. Lounis¹¹⁸, J. Love⁶, P.A. Love⁷⁴, H. Lu^{62a}, N. Lu⁹¹, H.J. Lubatti¹³⁹, C. Luci^{133a,133b}, A. Lucotte⁵⁷,
 C. Luedtke⁵⁰, F. Luehring⁶³, W. Lukas⁶⁴, L. Luminari^{133a}, O. Lundberg^{149a,149b}, B. Lund-Jensen¹⁵⁰,
 P.M. Luzi⁸², D. Lynn²⁷, R. Lysak¹²⁸, E. Lytken⁸³, V. Lyubushkin⁶⁷, H. Ma²⁷, L.L. Ma¹⁴⁰, Y. Ma¹⁴⁰,
 G. Maccarrone⁴⁹, A. Macchiolo¹⁰², C.M. Macdonald¹⁴², B. Maček⁷⁷, J. Machado Miguens^{123,127b},
 D. Madaffari⁸⁷, R. Madar³⁶, H.J. Maddocks¹⁶⁸, W.F. Mader⁴⁶, A. Madsen⁴⁴, J. Maeda⁶⁹, S. Maeland¹⁵,
 T. Maeno²⁷, A. Maevskiy¹⁰⁰, E. Magradze⁵⁶, J. Mahlstedt¹⁰⁸, C. Maiani¹¹⁸, C. Maidantchik^{26a},
 A.A. Maier¹⁰², T. Maier¹⁰¹, A. Maio^{127a,127b,127d}, S. Majewski¹¹⁷, Y. Makida⁶⁸, N. Makovec¹¹⁸,
 B. Malaescu⁸², Pa. Malecki⁴¹, V.P. Maleev¹²⁴, F. Malek⁵⁷, U. Mallik⁶⁵, D. Malon⁶, C. Malone¹⁴⁶,
 S. Maltezos¹⁰, S. Malyukov³², J. Mamuzic¹⁷⁰, G. Mancini⁴⁹, B. Mandelli³², L. Mandelli^{93a}, I. Mandić⁷⁷,
 J. Maneira^{127a,127b}, L. Manhaes de Andrade Filho^{26b}, J. Manjarres Ramos^{163b}, A. Mann¹⁰¹,
 A. Manousos³², B. Mansoulie¹³⁷, J.D. Mansour^{35a}, R. Mantifel⁸⁹, M. Mantoani⁵⁶, S. Manzoni^{93a,93b},
 L. Mapelli³², G. Marceca²⁹, L. March⁵¹, G. Marchiori⁸², M. Marcisovsky¹²⁸, M. Marjanovic¹⁴,
 D.E. Marley⁹¹, F. Marroquim^{26a}, S.P. Marsden⁸⁶, Z. Marshall¹⁶, S. Marti-Garcia¹⁷⁰, B. Martin⁹²,
 T.A. Martin¹⁷³, V.J. Martin⁴⁸, B. Martin dit Latour¹⁵, M. Martinez^{13,s}, V.I. Martinez Outschoorn¹⁶⁹,
 S. Martin-Haugh¹³², V.S. Martoiu^{28b}, A.C. Martyniuk⁸⁰, M. Marx¹³⁹, A. Marzin³², L. Masetti⁸⁵,
 T. Mashimo¹⁵⁸, R. Mashinistov⁹⁷, J. Masik⁸⁶, A.L. Maslenikov^{110,c}, I. Massa^{22a,22b}, L. Massa^{22a,22b},
 P. Mastrandrea⁵, A. Mastroberardino^{39a,39b}, T. Masubuchi¹⁵⁸, P. Mättig¹⁷⁸, J. Mattmann⁸⁵, J. Maurer^{28b},
 S.J. Maxfield⁷⁶, D.A. Maximov^{110,c}, R. Mazini¹⁵⁴, S.M. Mazza^{93a,93b}, N.C. Mc Fadden¹⁰⁶,
 G. Mc Goldrick¹⁶², S.P. Mc Kee⁹¹, A. McCarn⁹¹, R.L. McCarthy¹⁵¹, T.G. McCarthy¹⁰²,
 L.I. McClymont⁸⁰, E.F. McDonald⁹⁰, J.A. McFayden⁸⁰, G. Mchedlidze⁵⁶, S.J. McMahon¹³²,
 R.A. McPherson^{172,m}, M. Medinnis⁴⁴, S. Meehan¹³⁹, S. Mehlhase¹⁰¹, A. Mehta⁷⁶, K. Meier^{60a},
 C. Meineck¹⁰¹, B. Meirose⁴³, D. Melini^{170,ad}, B.R. Mellado Garcia^{148c}, M. Melo^{147a}, F. Meloni¹⁸,
 A. Mengarelli^{22a,22b}, S. Menke¹⁰², E. Meoni¹⁶⁵, S. Mergelmeyer¹⁷, P. Mermod⁵¹, L. Merola^{105a,105b},
 C. Meroni^{93a}, F.S. Merritt³³, A. Messina^{133a,133b}, J. Metcalfe⁶, A.S. Mete¹⁶⁶, C. Meyer⁸⁵, C. Meyer¹²³,
 J-P. Meyer¹³⁷, J. Meyer¹⁰⁸, H. Meyer Zu Theenhausen^{60a}, F. Miano¹⁵², R.P. Middleton¹³²,
 S. Miglioranzi^{52a,52b}, L. Mijović²³, G. Mikenberg¹⁷⁵, M. Mikestikova¹²⁸, M. Mikuž⁷⁷, M. Milesi⁹⁰,
 A. Milic⁶⁴, D.W. Miller³³, C. Mills⁴⁸, A. Milov¹⁷⁵, D.A. Milstead^{149a,149b}, A.A. Minaenko¹³¹,
 Y. Minami¹⁵⁸, I.A. Minashvili⁶⁷, A.I. Mincer¹¹¹, B. Mindur^{40a}, M. Mineev⁶⁷, Y. Ming¹⁷⁶, L.M. Mir¹³,
 K.P. Mistry¹²³, T. Mitani¹⁷⁴, J. Mitrevski¹⁰¹, V.A. Mitsou¹⁷⁰, A. Miucci⁵¹, P.S. Miyagawa¹⁴²,

J.U. Mjörnmark⁸³, T. Moa^{149a,149b}, K. Mochizuki⁹⁶, S. Mohapatra³⁷, S. Molander^{149a,149b},
 R. Moles-Valls²³, R. Monden⁷⁰, M.C. Mondragon⁹², K. Mönig⁴⁴, J. Monk³⁸, E. Monnier⁸⁷,
 A. Montalbano¹⁵¹, J. Montejo Berlingen³², F. Monticelli⁷³, S. Monzani^{93a,93b}, R.W. Moore³,
 N. Morange¹¹⁸, D. Moreno²¹, M. Moreno Llácer⁵⁶, P. Morettini^{52a}, S. Morgenstern³², D. Mori¹⁴⁵,
 T. Mori¹⁵⁸, M. Morii⁵⁸, M. Morinaga¹⁵⁸, V. Morisbak¹²⁰, S. Moritz⁸⁵, A.K. Morley¹⁵³, G. Mornacchi³²,
 J.D. Morris⁷⁸, L. Morvaj¹⁵¹, M. Mosidze^{53b}, J. Moss^{146,ae}, K. Motohashi¹⁶⁰, R. Mount¹⁴⁶,
 E. Mountricha²⁷, S.V. Mouraviev^{97,*}, E.J.W. Moyse⁸⁸, S. Muanza⁸⁷, R.D. Mudd¹⁹, F. Mueller¹⁰²,
 J. Mueller¹²⁶, R.S.P. Mueller¹⁰¹, T. Mueller³⁰, D. Muenstermann⁷⁴, P. Mullen⁵⁵, G.A. Mullier¹⁸,
 F.J. Munoz Sanchez⁸⁶, J.A. Murillo Quijada¹⁹, W.J. Murray^{173,132}, H. Musheghyan⁵⁶, M. Muškinja⁷⁷,
 A.G. Myagkov^{131,af}, M. Myska¹²⁹, B.P. Nachman¹⁴⁶, O. Nackenhorst⁵¹, K. Nagai¹²¹, R. Nagai^{68,z},
 K. Nagano⁶⁸, Y. Nagasaka⁶¹, K. Nagata¹⁶⁴, M. Nagel⁵⁰, E. Nagy⁸⁷, A.M. Nairz³², Y. Nakahama³²,
 K. Nakamura⁶⁸, T. Nakamura¹⁵⁸, I. Nakano¹¹³, H. Namasivayam⁴³, R.F. Naranjo Garcia⁴⁴,
 R. Narayan¹¹, D.I. Narrias Villar^{60a}, I. Naryshkin¹²⁴, T. Naumann⁴⁴, G. Navarro²¹, R. Nayyar⁷,
 H.A. Neal⁹¹, P.Yu. Nechaeva⁹⁷, T.J. Neep⁸⁶, A. Negri^{122a,122b}, M. Negrini^{22a}, S. Nektarijevic¹⁰⁷,
 C. Nellist¹¹⁸, A. Nelson¹⁶⁶, S. Nemecek¹²⁸, P. Nemethy¹¹¹, A.A. Nepomuceno^{26a}, M. Nesi^{32,ag},
 M.S. Neubauer¹⁶⁹, M. Neumann¹⁷⁸, R.M. Neves¹¹¹, P. Nevski²⁷, P.R. Newman¹⁹, D.H. Nguyen⁶,
 T. Nguyen Manh⁹⁶, R.B. Nickerson¹²¹, R. Nicolaidou¹³⁷, J. Nielsen¹³⁸, A. Nikiforov¹⁷,
 V. Nikolaenko^{131,af}, I. Nikolic-Audit⁸², K. Nikolopoulos¹⁹, J.K. Nilsen¹²⁰, P. Nilsson²⁷, Y. Ninomiya¹⁵⁸,
 A. Nisati^{133a}, R. Nisius¹⁰², T. Nobe¹⁵⁸, M. Nomachi¹¹⁹, I. Nomidis³¹, T. Nooney⁷⁸, S. Norberg¹¹⁴,
 M. Nordberg³², N. Norjoharuddeen¹²¹, O. Novgorodova⁴⁶, S. Nowak¹⁰², M. Nozaki⁶⁸, L. Nozka¹¹⁶,
 K. Ntekas¹⁰, E. Nurse⁸⁰, F. Nuti⁹⁰, F. O'grady⁷, D.C. O'Neil¹⁴⁵, A.A. O'Rourke⁴⁴, V. O'Shea⁵⁵,
 F.G. Oakham^{31,d}, H. Oberlack¹⁰², T. Obermann²³, J. Ocariz⁸², A. Ochi⁶⁹, I. Ochoa³⁷,
 J.P. Ochoa-Ricoux^{34a}, S. Oda⁷², S. Odaka⁶⁸, H. Ogren⁶³, A. Oh⁸⁶, S.H. Oh⁴⁷, C.C. Ohm¹⁶,
 H. Ohman¹⁶⁸, H. Oide³², H. Okawa¹⁶⁴, Y. Okumura³³, T. Okuyama⁶⁸, A. Olariu^{28b},
 L.F. Oleiro Seabra^{127a}, S.A. Olivares Pino⁴⁸, D. Oliveira Damazio²⁷, A. Olszewski⁴¹, J. Olszowska⁴¹,
 A. Onofre^{127a,127e}, K. Onogi¹⁰⁴, P.U.E. Onyisi^{11,w}, M.J. Oreglia³³, Y. Oren¹⁵⁶, D. Orestano^{135a,135b},
 N. Orlando^{62b}, R.S. Orr¹⁶², B. Osculati^{52a,52b,*}, R. Ospanov⁸⁶, G. Otero y Garzon²⁹, H. Otono⁷²,
 M. Ouchrif^{136d}, F. Ould-Saada¹²⁰, A. Ouraou¹³⁷, K.P. Oussoren¹⁰⁸, Q. Ouyang^{35a}, M. Owen⁵⁵,
 R.E. Owen¹⁹, V.E. Ozcan^{20a}, N. Ozturk⁸, K. Pachal¹⁴⁵, A. Pacheco Pages¹³, L. Pacheco Rodriguez¹³⁷,
 C. Padilla Aranda¹³, S. Pagan Griso¹⁶, F. Paige²⁷, P. Pais⁸⁸, K. Pajchel¹²⁰, G. Palacino^{163b},
 S. Palazzo^{39a,39b}, S. Palestini³², M. Palka^{40b}, D. Pallin³⁶, E.St. Panagiotopoulou¹⁰, C.E. Pandini⁸²,
 J.G. Panduro Vazquez⁷⁹, P. Pani^{149a,149b}, S. Panitkin²⁷, D. Pantea^{28b}, L. Paolozzi⁵¹,
 Th.D. Papadopoulou¹⁰, K. Papageorgiou⁹, A. Paramonov⁶, D. Paredes Hernandez¹⁷⁹, A.J. Parker⁷⁴,
 M.A. Parker³⁰, K.A. Parker¹⁴², F. Parodi^{52a,52b}, J.A. Parsons³⁷, U. Parzefall⁵⁰, V.R. Pascuzzi¹⁶²,
 E. Pasqualucci^{133a}, S. Passaggio^{52a}, Fr. Pastore⁷⁹, G. Pásztor^{31,ah}, S. Pataraia¹⁷⁸, J.R. Pater⁸⁶, T. Pauly³²,
 J. Pearce¹⁷², B. Pearson¹¹⁴, L.E. Pedersen³⁸, M. Pedersen¹²⁰, S. Pedraza Lopez¹⁷⁰, R. Pedro^{127a,127b},
 S.V. Peleganchuk^{110,c}, O. Penc¹²⁸, C. Peng^{35a}, H. Peng⁵⁹, J. Penwell⁶³, B.S. Peralva^{26b}, M.M. Perego¹³⁷,
 D.V. Perepelitsa²⁷, E. Perez Codina^{163a}, L. Perini^{93a,93b}, H. Pernegger³², S. Perrella^{105a,105b},
 R. Peschke⁴⁴, V.D. Peshekhanov⁶⁷, K. Peters⁴⁴, R.F.Y. Peters⁸⁶, B.A. Petersen³², T.C. Petersen³⁸,
 E. Petit⁵⁷, A. Petridis¹, C. Petridou¹⁵⁷, P. Petroff¹¹⁸, E. Petrolo^{133a}, M. Petrov¹²¹, F. Petrucci^{135a,135b},
 N.E. Pettersson⁸⁸, A. Peyaud¹³⁷, R. Pezoa^{34b}, P.W. Phillips¹³², G. Piacquadio^{146,ai}, E. Pianori¹⁷³,
 A. Picazio⁸⁸, E. Piccaro⁷⁸, M. Piccinini^{22a,22b}, M.A. Pickering¹²¹, R. Piegaia²⁹, J.E. Pilcher³³,
 A.D. Pilkington⁸⁶, A.W.J. Pin⁸⁶, M. Pinamonti^{167a,167c,aj}, J.L. Pinfold³, A. Pingel³⁸, S. Pires⁸²,
 H. Pirumov⁴⁴, M. Pitt¹⁷⁵, L. Plazak^{147a}, M.-A. Pleier²⁷, V. Pleskot⁸⁵, E. Plotnikova⁶⁷, P. Plucinski⁹²,
 D. Pluth⁶⁶, R. Poettgen^{149a,149b}, L. Poggiali¹¹⁸, D. Pohl²³, G. Polesello^{122a}, A. Poley⁴⁴,
 A. Policicchio^{39a,39b}, R. Polifka¹⁶², A. Polini^{22a}, C.S. Pollard⁵⁵, V. Polychronakos²⁷, K. Pommès³²,
 L. Pontecorvo^{133a}, B.G. Pope⁹², G.A. Popenecriu^{28c}, D.S. Popovic¹⁴, A. Poppleton³², S. Pospisil¹²⁹,

K. Potamianos¹⁶, I.N. Potrap⁶⁷, C.J. Potter³⁰, C.T. Potter¹¹⁷, G. Poulard³², J. Poveda³²,
 V. Pozdnyakov⁶⁷, M.E. Pozo Astigarraga³², P. Pralavorio⁸⁷, A. Pranko¹⁶, S. Prell⁶⁶, D. Price⁸⁶,
 L.E. Price⁶, M. Primavera^{75a}, S. Prince⁸⁹, K. Prokofiev^{62c}, F. Prokoshin^{34b}, S. Protopopescu²⁷,
 J. Proudfoot⁶, M. Przybycien^{40a}, D. Puddu^{135a,135b}, M. Purohit^{27,ak}, P. Puzo¹¹⁸, J. Qian⁹¹, G. Qin⁵⁵,
 Y. Qin⁸⁶, A. Quadt⁵⁶, W.B. Quayle^{167a,167b}, M. Queitsch-Maitland⁸⁶, D. Quilty⁵⁵, S. Raddum¹²⁰,
 V. Radeka²⁷, V. Radescu^{60b}, S.K. Radhakrishnan¹⁵¹, P. Radloff¹¹⁷, P. Rados⁹⁰, F. Ragusa^{93a,93b},
 G. Rahal¹⁸¹, J.A. Raine⁸⁶, S. Rajagopalan²⁷, M. Rammensee³², C. Rangel-Smith¹⁶⁸, M.G. Ratti^{93a,93b},
 F. Rauscher¹⁰¹, S. Rave⁸⁵, T. Ravenscroft⁵⁵, I. Ravinovich¹⁷⁵, M. Raymond³², A.L. Read¹²⁰,
 N.P. Readioff⁷⁶, M. Reale^{75a,75b}, D.M. Rebuzzi^{122a,122b}, A. Redelbach¹⁷⁷, G. Redlinger²⁷, R. Reece¹³⁸,
 K. Reeves⁴³, L. Rehnisch¹⁷, J. Reichert¹²³, H. Reisin²⁹, C. Rembser³², H. Ren^{35a}, M. Rescigno^{133a},
 S. Resconi^{93a}, O.L. Rezanova^{110,c}, P. Reznicek¹³⁰, R. Rezvani⁹⁶, R. Richter¹⁰², S. Richter⁸⁰,
 E. Richter-Was^{40b}, O. Ricken²³, M. Ridel⁸², P. Rieck¹⁷, C.J. Riegel¹⁷⁸, J. Rieger⁵⁶, O. Rifki¹¹⁴,
 M. Rijssenbeek¹⁵¹, A. Rimoldi^{122a,122b}, M. Rimoldi¹⁸, L. Rinaldi^{22a}, B. Ristic⁵¹, E. Ritsch³², I. Riu¹³,
 F. Rizatdinova¹¹⁵, E. Rizvi⁷⁸, C. Rizzi¹³, S.H. Robertson^{89,m}, A. Robichaud-Veronneau⁸⁹,
 D. Robinson³⁰, J.E.M. Robinson⁴⁴, A. Robson⁵⁵, C. Roda^{125a,125b}, Y. Rodina^{87,al}, A. Rodriguez Perez¹³,
 D. Rodriguez Rodriguez¹⁷⁰, S. Roe³², C.S. Rogan⁵⁸, O. Røhne¹²⁰, A. Romaniouk⁹⁹, M. Romano^{22a,22b},
 S.M. Romano Saez³⁶, E. Romero Adam¹⁷⁰, N. Rompotis¹³⁹, M. Ronzani⁵⁰, L. Roos⁸², E. Ros¹⁷⁰,
 S. Rosati^{133a}, K. Rosbach⁵⁰, P. Rose¹³⁸, O. Rosenthal¹⁴⁴, N.-A. Rosien⁵⁶, V. Rossetti^{149a,149b},
 E. Rossi^{105a,105b}, L.P. Rossi^{52a}, J.H.N. Rosten³⁰, R. Rosten¹³⁹, M. Rotaru^{28b}, I. Roth¹⁷⁵, J. Rothberg¹³⁹,
 D. Rousseau¹¹⁸, C.R. Royon¹³⁷, A. Rozanov⁸⁷, Y. Rozen¹⁵⁵, X. Ruan^{148c}, F. Rubbo¹⁴⁶,
 M.S. Rudolph¹⁶², F. Rühr⁵⁰, A. Ruiz-Martinez³¹, Z. Rurikova⁵⁰, N.A. Rusakovich⁶⁷, A. Ruschke¹⁰¹,
 H.L. Russell¹³⁹, J.P. Rutherford⁷, N. Ruthmann³², Y.F. Ryabov¹²⁴, M. Rybar¹⁶⁹, G. Rybkin¹¹⁸, S. Ryu⁶,
 A. Ryzhov¹³¹, G.F. Rzehorz⁵⁶, A.F. Saavedra¹⁵³, G. Sabato¹⁰⁸, S. Sacerdoti²⁹, H.F-W. Sadrozinski¹³⁸,
 R. Sadykov⁶⁷, F. Safai Tehrani^{133a}, P. Saha¹⁰⁹, M. Sahinsoy^{60a}, M. Saimpert¹³⁷, T. Saito¹⁵⁸,
 H. Sakamoto¹⁵⁸, Y. Sakurai¹⁷⁴, G. Salamanna^{135a,135b}, A. Salamon^{134a,134b}, J.E. Salazar Loyola^{34b},
 D. Salek¹⁰⁸, P.H. Sales De Bruin¹³⁹, D. Salihagic¹⁰², A. Salnikov¹⁴⁶, J. Salt¹⁷⁰, D. Salvatore^{39a,39b},
 F. Salvatore¹⁵², A. Salvucci^{62a}, A. Salzburger³², D. Sammel⁵⁰, D. Sampsonidis¹⁵⁷, J. Sánchez¹⁷⁰,
 V. Sanchez Martinez¹⁷⁰, A. Sanchez Pineda^{105a,105b}, H. Sandaker¹²⁰, R.L. Sandbach⁷⁸, H.G. Sander⁸⁵,
 M. Sandhoff¹⁷⁸, C. Sandoval²¹, R. Sandstroem¹⁰², D.P.C. Sankey¹³², M. Sannino^{52a,52b}, A. Sansoni⁴⁹,
 C. Santoni³⁶, R. Santonico^{134a,134b}, H. Santos^{127a}, I. Santoyo Castillo¹⁵², K. Sapp¹²⁶, A. Sapronov⁶⁷,
 J.G. Saraiva^{127a,127d}, B. Sarrazin²³, O. Sasaki⁶⁸, Y. Sasaki¹⁵⁸, K. Sato¹⁶⁴, G. Sauvage^{5,*}, E. Sauvan⁵,
 G. Savage⁷⁹, P. Savard^{162,d}, C. Sawyer¹³², L. Sawyer^{81,r}, J. Saxon³³, C. Sbarra^{22a}, A. Sbrizzi^{22a,22b},
 T. Scanlon⁸⁰, D.A. Scannicchio¹⁶⁶, M. Scarcella¹⁵³, V. Scarfone^{39a,39b}, J. Schaarschmidt¹⁷⁵,
 P. Schacht¹⁰², B.M. Schachtner¹⁰¹, D. Schaefer³², R. Schaefer⁴⁴, J. Schaeffer⁸⁵, S. Schaepe²³,
 S. Schaetzl^{60b}, U. Schäfer⁸⁵, A.C. Schaffer¹¹⁸, D. Schaile¹⁰¹, R.D. Schamberger¹⁵¹, V. Scharf^{60a},
 V.A. Schegelsky¹²⁴, D. Scheirich¹³⁰, M. Schernau¹⁶⁶, C. Schiavi^{52a,52b}, S. Schier¹³⁸, C. Schillo⁵⁰,
 M. Schioppa^{39a,39b}, S. Schlenker³², K.R. Schmidt-Sommerfeld¹⁰², K. Schmieden³², C. Schmitt⁸⁵,
 S. Schmitt⁴⁴, S. Schmitz⁸⁵, B. Schneider^{163a}, U. Schnoor⁵⁰, L. Schoeffel¹³⁷, A. Schoening^{60b},
 B.D. Schoenrock⁹², E. Schopf²³, M. Schott⁸⁵, J. Schovancova⁸, S. Schramm⁵¹, M. Schreyer¹⁷⁷,
 N. Schuh⁸⁵, A. Schulte⁸⁵, M.J. Schultens²³, H.-C. Schultz-Coulon^{60a}, H. Schulz¹⁷, M. Schumacher⁵⁰,
 B.A. Schumm¹³⁸, Ph. Schune¹³⁷, A. Schwartzman¹⁴⁶, T.A. Schwarz⁹¹, H. Schweiger⁸⁶,
 Ph. Schwemling¹³⁷, R. Schwienhorst⁹², J. Schwindling¹³⁷, T. Schwindt²³, G. Sciolla²⁵, F. Scuri^{125a,125b},
 F. Scutti⁹⁰, J. Searcy⁹¹, P. Seema²³, S.C. Seidel¹⁰⁶, A. Seiden¹³⁸, F. Seifert¹²⁹, J.M. Seixas^{26a},
 G. Sekhniaidze^{105a}, K. Sekhon⁹¹, S.J. Sekula⁴², D.M. Seliverstov^{124,*}, N. Semprini-Cesari^{22a,22b},
 C. Serfon¹²⁰, L. Serin¹¹⁸, L. Serkin^{167a,167b}, M. Sessa^{135a,135b}, R. Seuster¹⁷², H. Severini¹¹⁴, T. Sfiligoj⁷⁷,
 F. Sforza³², A. Sfyrla⁵¹, E. Shabalina⁵⁶, N.W. Shaikh^{149a,149b}, L.Y. Shan^{35a}, R. Shang¹⁶⁹, J.T. Shank²⁴,
 M. Shapiro¹⁶, P.B. Shatalov⁹⁸, K. Shaw^{167a,167b}, S.M. Shaw⁸⁶, A. Shcherbakova^{149a,149b}, C.Y. Shehu¹⁵²,

P. Sherwood⁸⁰, L. Shi^{154,am}, S. Shimizu⁶⁹, C.O. Shimmin¹⁶⁶, M. Shimojima¹⁰³, M. Shiyakova^{67,an},
 A. Shmeleva⁹⁷, D. Shoaleh Saadi⁹⁶, M.J. Shochet³³, S. Shojaii^{93a}, S. Shrestha¹¹², E. Shulga⁹⁹,
 M.A. Shupe⁷, P. Sicho¹²⁸, A.M. Sickles¹⁶⁹, P.E. Sidebo¹⁵⁰, O. Sidiropoulou¹⁷⁷, D. Sidorov¹¹⁵,
 A. Sidoti^{22a,22b}, F. Siegert⁴⁶, Dj. Sijacki¹⁴, J. Silva^{127a,127d}, S.B. Silverstein^{149a}, V. Simak¹²⁹, O. Simard⁵,
 Lj. Simic¹⁴, S. Simion¹¹⁸, E. Simioni⁸⁵, B. Simmons⁸⁰, D. Simon³⁶, M. Simon⁸⁵, P. Sinervo¹⁶²,
 N.B. Sinev¹¹⁷, M. Sioli^{22a,22b}, G. Siragusa¹⁷⁷, S.Yu. Sivoklokov¹⁰⁰, J. Sjölin^{149a,149b}, M.B. Skinner⁷⁴,
 H.P. Skottowe⁵⁸, P. Skubic¹¹⁴, M. Slater¹⁹, T. Slavicek¹²⁹, M. Slawinska¹⁰⁸, K. Sliwa¹⁶⁵, R. Slovak¹³⁰,
 V. Smakhtin¹⁷⁵, B.H. Smart⁵, L. Smestad¹⁵, J. Smiesko^{147a}, S.Yu. Smirnov⁹⁹, Y. Smirnov⁹⁹,
 L.N. Smirnova^{100,ao}, O. Smirnova⁸³, M.N.K. Smith³⁷, R.W. Smith³⁷, M. Smizanska⁷⁴, K. Smolek¹²⁹,
 A.A. Snesarev⁹⁷, S. Snyder²⁷, R. Sobie^{172,m}, F. Socher⁴⁶, A. Soffer¹⁵⁶, D.A. Soh¹⁵⁴, G. Sokhrannyi⁷⁷,
 C.A. Solans Sanchez³², M. Solar¹²⁹, E.Yu. Soldatov⁹⁹, U. Soldevila¹⁷⁰, A.A. Solodkov¹³¹,
 A. Soloshenko⁶⁷, O.V. Solovyanov¹³¹, V. Solovyev¹²⁴, P. Sommer⁵⁰, H. Son¹⁶⁵, H.Y. Song^{59,ap},
 A. Sood¹⁶, A. Sopczak¹²⁹, V. Sopko¹²⁹, V. Sorin¹³, D. Sosa^{60b}, C.L. Sotiropoulou^{125a,125b},
 R. Soualah^{167a,167c}, A.M. Soukharev^{110,c}, D. South⁴⁴, B.C. Sowden⁷⁹, S. Spagnolo^{75a,75b},
 M. Spalla^{125a,125b}, M. Spangenberg¹⁷³, F. Spanò⁷⁹, D. Sperlich¹⁷, F. Spettel¹⁰², R. Spighi^{22a}, G. Spigo³²,
 L.A. Spiller⁹⁰, M. Spousta¹³⁰, R.D. St. Denis^{55,*}, A. Stabile^{93a}, R. Stamen^{60a}, S. Stamm¹⁷,
 E. Stanecka⁴¹, R.W. Stanek⁶, C. Stanescu^{135a}, M. Stanescu-Bellu⁴⁴, M.M. Stanitzki⁴⁴, S. Stapnes¹²⁰,
 E.A. Starchenko¹³¹, G.H. Stark³³, J. Stark⁵⁷, S.H Stark³⁸, P. Staroba¹²⁸, P. Starovoitov^{60a}, S. Stärz³²,
 R. Staszewski⁴¹, P. Steinberg²⁷, B. Stelzer¹⁴⁵, H.J. Stelzer³², O. Stelzer-Chilton^{163a}, H. Stenzel⁵⁴,
 G.A. Stewart⁵⁵, J.A. Stillings²³, M.C. Stockton⁸⁹, M. Stoebe⁸⁹, G. Stoica^{28b}, P. Stolte⁵⁶, S. Stonjek¹⁰²,
 A.R. Stradling⁸, A. Straessner⁴⁶, M.E. Stramaglia¹⁸, J. Strandberg¹⁵⁰, S. Strandberg^{149a,149b},
 A. Strandlie¹²⁰, M. Strauss¹¹⁴, P. Strizenec^{147b}, R. Ströhmer¹⁷⁷, D.M. Strom¹¹⁷, R. Stroynowski⁴²,
 A. Strubig¹⁰⁷, S.A. Stucci¹⁸, B. Stugu¹⁵, N.A. Styles⁴⁴, D. Su¹⁴⁶, J. Su¹²⁶, S. Suchek^{60a}, Y. Sugaya¹¹⁹,
 M. Suk¹²⁹, V.V. Sulin⁹⁷, S. Sultansoy^{4c}, T. Sumida⁷⁰, S. Sun⁵⁸, X. Sun^{35a}, J.E. Sundermann⁵⁰,
 K. Suruliz¹⁵², G. Susinno^{39a,39b}, M.R. Sutton¹⁵², S. Suzuki⁶⁸, M. Svatos¹²⁸, M. Swiatlowski³³,
 I. Sykora^{147a}, T. Sykora¹³⁰, D. Ta⁵⁰, C. Taccini^{135a,135b}, K. Tackmann⁴⁴, J. Taenzer¹⁶², A. Taffard¹⁶⁶,
 R. Tafirout^{163a}, N. Taiblum¹⁵⁶, H. Takai²⁷, R. Takashima⁷¹, T. Takeshita¹⁴³, Y. Takubo⁶⁸, M. Talby⁸⁷,
 A.A. Talyshев^{110,c}, K.G. Tan⁹⁰, J. Tanaka¹⁵⁸, R. Tanaka¹¹⁸, S. Tanaka⁶⁸, B.B. Tannenwald¹¹²,
 S. Tapia Araya^{34b}, S. Tapprogge⁸⁵, S. Tarem¹⁵⁵, G.F. Tartarelli^{93a}, P. Tas¹³⁰, M. Tasevsky¹²⁸,
 T. Tashiro⁷⁰, E. Tassi^{39a,39b}, A. Tavares Delgado^{127a,127b}, Y. Tayalati^{136e}, A.C. Taylor¹⁰⁶, G.N. Taylor⁹⁰,
 P.T.E. Taylor⁹⁰, W. Taylor^{163b}, F.A. Teischinger³², P. Teixeira-Dias⁷⁹, K.K. Temming⁵⁰, D. Temple¹⁴⁵,
 H. Ten Kate³², P.K. Teng¹⁵⁴, J.J. Teoh¹¹⁹, F. Tepel¹⁷⁸, S. Terada⁶⁸, K. Terashi¹⁵⁸, J. Terron⁸⁴, S. Terzo¹⁰²,
 M. Testa⁴⁹, R.J. Teuscher^{162,m}, T. Theveneaux-Pelzer⁸⁷, J.P. Thomas¹⁹, J. Thomas-Wilsker⁷⁹,
 E.N. Thompson³⁷, P.D. Thompson¹⁹, A.S. Thompson⁵⁵, L.A. Thomsen¹⁷⁹, E. Thomson¹²³,
 M. Thomson³⁰, M.J. Tibbetts¹⁶, R.E. Ticse Torres⁸⁷, V.O. Tikhomirov^{97,aq}, Yu.A. Tikhonov^{110,c},
 S. Timoshenko⁹⁹, P. Tipton¹⁷⁹, S. Tisserant⁸⁷, K. Todome¹⁶⁰, T. Todorov^{5,*}, S. Todorova-Nova¹³⁰,
 J. Tojo⁷², S. Tokár^{147a}, K. Tokushuku⁶⁸, E. Tolley⁵⁸, L. Tomlinson⁸⁶, M. Tomoto¹⁰⁴, L. Tompkins^{146,ar},
 K. Toms¹⁰⁶, B. Tong⁵⁸, E. Torrence¹¹⁷, H. Torres¹⁴⁵, E. Torró Pastor¹³⁹, J. Toth^{87,as}, F. Touchard⁸⁷,
 D.R. Tovey¹⁴², T. Trefzger¹⁷⁷, A. Tricoli²⁷, I.M. Trigger^{163a}, S. Trincaz-Duvold⁸², M.F. Tripiana¹³,
 W. Trischuk¹⁶², B. Trocmé⁵⁷, A. Trofymov⁴⁴, C. Troncon^{93a}, M. Trottier-McDonald¹⁶, M. Trovatelli¹⁷²,
 L. Truong^{167a,167c}, M. Trzebinski⁴¹, A. Trzupek⁴¹, J.C.-L. Tseng¹²¹, P.V. Tsiareshka⁹⁴, G. Tsipolitis¹⁰,
 N. Tsirintanis⁹, S. Tsiskaridze¹³, V. Tsiskaridze⁵⁰, E.G. Tskhadadze^{53a}, K.M. Tsui^{62a}, I.I. Tsukerman⁹⁸,
 V. Tsulaia¹⁶, S. Tsuno⁶⁸, D. Tsybychev¹⁵¹, Y. Tu^{62b}, A. Tudorache^{28b}, V. Tudorache^{28b}, A.N. Tuna⁵⁸,
 S.A. Tupputi^{22a,22b}, S. Turchikhin⁶⁷, D. Turecek¹²⁹, D. Turgeman¹⁷⁵, R. Turra^{93a,93b}, A.J. Turvey⁴²,
 P.M. Tuts³⁷, M. Tyndel¹³², G. Ucchielli^{22a,22b}, I. Ueda¹⁵⁸, M. Ughetto^{149a,149b}, F. Ukegawa¹⁶⁴, G. Unal³²,
 A. Undrus²⁷, G. Unel¹⁶⁶, F.C. Ungaro⁹⁰, Y. Unno⁶⁸, C. Unverdorben¹⁰¹, J. Urban^{147b}, P. Urquijo⁹⁰,
 P. Urrejola⁸⁵, G. Usai⁸, A. Usanova⁶⁴, L. Vacavant⁸⁷, V. Vacek¹²⁹, B. Vachon⁸⁹, C. Valderanis¹⁰¹,

E. Valdes Santurio^{149a,149b}, N. Valencic¹⁰⁸, S. Valentinetto^{22a,22b}, A. Valero¹⁷⁰, L. Valery¹³, S. Valkar¹³⁰,
 J.A. Valls Ferrer¹⁷⁰, W. Van Den Wollenberg¹⁰⁸, P.C. Van Der Deijl¹⁰⁸, R. van der Geer¹⁰⁸,
 H. van der Graaf¹⁰⁸, N. van Eldik¹⁵⁵, P. van Gemmeren⁶, J. Van Nieuwkoop¹⁴⁵, I. van Vulpen¹⁰⁸,
 M.C. van Woerden³², M. Vanadia^{133a,133b}, W. Vandelli³², R. Vanguri¹²³, A. Vaniachine¹⁶¹, P. Vankov¹⁰⁸,
 G. Vardanyan¹⁸⁰, R. Vari^{133a}, E.W. Varnes⁷, T. Varol⁴², D. Varouchas⁸², A. Vartapetian⁸, K.E. Varvell¹⁵³,
 J.G. Vasquez¹⁷⁹, F. Vazeille³⁶, T. Vazquez Schroeder⁸⁹, J. Veatch⁵⁶, V. Veeraraghavan⁷, L.M. Veloce¹⁶²,
 F. Veloso^{127a,127c}, S. Veneziano^{133a}, A. Ventura^{75a,75b}, M. Venturi¹⁷², N. Venturi¹⁶², A. Venturini²⁵,
 V. Vercesi^{122a}, M. Verducci^{133a,133b}, W. Verkerke¹⁰⁸, J.C. Vermeulen¹⁰⁸, A. Vest^{46,at}, M.C. Vetterli^{145,d},
 O. Viazlo⁸³, I. Vichou^{169,*}, T. Vickey¹⁴², O.E. Vickey Boeriu¹⁴², G.H.A. Viehhauser¹²¹, S. Viel¹⁶,
 L. Vigani¹²¹, M. Villa^{22a,22b}, M. Villaplana Perez^{93a,93b}, E. Vilucchi⁴⁹, M.G. Vincter³¹,
 V.B. Vinogradov⁶⁷, C. Vittori^{22a,22b}, I. Vivarelli¹⁵², S. Vlachos¹⁰, M. Vlasak¹²⁹, M. Vogel¹⁷⁸,
 P. Vokac¹²⁹, G. Volpi^{125a,125b}, M. Volpi⁹⁰, H. von der Schmitt¹⁰², E. von Toerne²³, V. Vorobel¹³⁰,
 K. Vorobev⁹⁹, M. Vos¹⁷⁰, R. Voss³², J.H. Vossebeld⁷⁶, N. Vranjes¹⁴, M. Vranjes Milosavljevic¹⁴,
 V. Vrba¹²⁸, M. Vreeswijk¹⁰⁸, R. Vuillermet³², I. Vukotic³³, Z. Vykydal¹²⁹, P. Wagner²³, W. Wagner¹⁷⁸,
 H. Wahlberg⁷³, S. Wahrmund⁴⁶, J. Wakabayashi¹⁰⁴, J. Walder⁷⁴, R. Walker¹⁰¹, W. Walkowiak¹⁴⁴,
 V. Wallangen^{149a,149b}, C. Wang^{35b}, C. Wang^{140,au}, F. Wang¹⁷⁶, H. Wang¹⁶, H. Wang⁴², J. Wang⁴⁴,
 J. Wang¹⁵³, K. Wang⁸⁹, R. Wang⁶, S.M. Wang¹⁵⁴, T. Wang²³, T. Wang³⁷, W. Wang⁵⁹, X. Wang¹⁷⁹,
 C. Wanotayaroj¹¹⁷, A. Warburton⁸⁹, C.P. Ward³⁰, D.R. Wardrop⁸⁰, A. Washbrook⁴⁸, P.M. Watkins¹⁹,
 A.T. Watson¹⁹, M.F. Watson¹⁹, G. Watts¹³⁹, S. Watts⁸⁶, B.M. Waugh⁸⁰, S. Webb⁸⁵, M.S. Weber¹⁸,
 S.W. Weber¹⁷⁷, J.S. Webster⁶, A.R. Weidberg¹²¹, B. Weinert⁶³, J. Weingarten⁵⁶, C. Weiser⁵⁰,
 H. Weits¹⁰⁸, P.S. Wells³², T. Wenaus²⁷, T. Wengler³², S. Wenig³², N. Wermes²³, M. Werner⁵⁰,
 M.D. Werner⁶⁶, P. Werner³², M. Wessels^{60a}, J. Wetter¹⁶⁵, K. Whalen¹¹⁷, N.L. Whallon¹³⁹,
 A.M. Wharton⁷⁴, A. White⁸, M.J. White¹, R. White^{34b}, D. Whiteson¹⁶⁶, F.J. Wickens¹³²,
 W. Wiedenmann¹⁷⁶, M. Wielers¹³², P. Wienemann²³, C. Wiglesworth³⁸, L.A.M. Wiik-Fuchs²³,
 A. Wildauer¹⁰², F. Wilk⁸⁶, H.G. Wilkens³², H.H. Williams¹²³, S. Williams¹⁰⁸, C. Willis⁹², S. Willocq⁸⁸,
 J.A. Wilson¹⁹, I. Wingerter-Seez⁵, F. Winklmeier¹¹⁷, O.J. Winston¹⁵², B.T. Winter²³, M. Wittgen¹⁴⁶,
 J. Wittkowski¹⁰¹, T.M.H. Wolf¹⁰⁸, M.W. Wolter⁴¹, H. Wolters^{127a,127c}, S.D. Worm¹³², B.K. Wosiek⁴¹,
 J. Wotschack³², M.J. Woudstra⁸⁶, K.W. Wozniak⁴¹, M. Wu⁵⁷, M. Wu³³, S.L. Wu¹⁷⁶, X. Wu⁵¹, Y. Wu⁹¹,
 T.R. Wyatt⁸⁶, B.M. Wynne⁴⁸, S. Xella³⁸, D. Xu^{35a}, L. Xu²⁷, B. Yabsley¹⁵³, S. Yacoob^{148a},
 D. Yamaguchi¹⁶⁰, Y. Yamaguchi¹¹⁹, A. Yamamoto⁶⁸, S. Yamamoto¹⁵⁸, T. Yamanaka¹⁵⁸, K. Yamauchi¹⁰⁴,
 Y. Yamazaki⁶⁹, Z. Yan²⁴, H. Yang¹⁴¹, H. Yang¹⁷⁶, Y. Yang¹⁵⁴, Z. Yang¹⁵, W-M. Yao¹⁶, Y.C. Yap⁸²,
 Y. Yasu⁶⁸, E. Yatsenko⁵, K.H. Yau Wong²³, J. Ye⁴², S. Ye²⁷, I. Yeletskikh⁶⁷, A.L. Yen⁵⁸, E. Yildirim⁸⁵,
 K. Yorita¹⁷⁴, R. Yoshida⁶, K. Yoshihara¹²³, C. Young¹⁴⁶, C.J.S. Young³², S. Youssef²⁴, D.R. Yu¹⁶,
 J. Yu⁸, J.M. Yu⁹¹, J. Yu⁶⁶, L. Yuan⁶⁹, S.P.Y. Yuen²³, I. Yusuff^{30,aw}, B. Zabinski⁴¹, R. Zaidan¹⁴⁰,
 A.M. Zaitsev^{131,af}, N. Zakharchuk⁴⁴, J. Zalieckas¹⁵, A. Zaman¹⁵¹, S. Zambito⁵⁸, L. Zanello^{133a,133b},
 D. Zanzi⁹⁰, C. Zeitnitz¹⁷⁸, M. Zeman¹²⁹, A. Zemla^{40a}, J.C. Zeng¹⁶⁹, Q. Zeng¹⁴⁶, K. Zengel²⁵,
 O. Zenin¹³¹, T. Ženiš^{147a}, D. Zerwas¹¹⁸, D. Zhang⁹¹, F. Zhang¹⁷⁶, G. Zhang^{59,ap}, H. Zhang^{35b},
 J. Zhang⁶, L. Zhang⁵⁰, R. Zhang²³, R. Zhang^{59,au}, X. Zhang¹⁴⁰, Z. Zhang¹¹⁸, X. Zhao⁴², Y. Zhao^{140,aw},
 Z. Zhao⁵⁹, A. Zhemchugov⁶⁷, J. Zhong¹²¹, B. Zhou⁹¹, C. Zhou⁴⁷, L. Zhou³⁷, L. Zhou⁴², M. Zhou¹⁵¹,
 N. Zhou^{35c}, C.G. Zhu¹⁴⁰, H. Zhu^{35a}, J. Zhu⁹¹, Y. Zhu⁵⁹, X. Zhuang^{35a}, K. Zhukov⁹⁷, A. Zibell¹⁷⁷,
 D. Ziemińska⁶³, N.I. Zimine⁶⁷, C. Zimmermann⁸⁵, S. Zimmermann⁵⁰, Z. Zinonos⁵⁶, M. Zinser⁸⁵,
 M. Ziolkowski¹⁴⁴, L. Živković¹⁴, G. Zobernig¹⁷⁶, A. Zoccoli^{22a,22b}, M. zur Nedden¹⁷, L. Zwalinski³².

¹ Department of Physics, University of Adelaide, Adelaide, Australia

² Physics Department, SUNY Albany, Albany NY, United States of America

³ Department of Physics, University of Alberta, Edmonton AB, Canada

⁴ ^(a) Department of Physics, Ankara University, Ankara; ^(b) Istanbul Aydin University, Istanbul; ^(c)

- Division of Physics, TOBB University of Economics and Technology, Ankara, Turkey
- ⁵ LAPP, CNRS/IN2P3 and Université Savoie Mont Blanc, Annecy-le-Vieux, France
- ⁶ High Energy Physics Division, Argonne National Laboratory, Argonne IL, United States of America
- ⁷ Department of Physics, University of Arizona, Tucson AZ, United States of America
- ⁸ Department of Physics, The University of Texas at Arlington, Arlington TX, United States of America
- ⁹ Physics Department, National and Kapodistrian University of Athens, Athens, Greece
- ¹⁰ Physics Department, National Technical University of Athens, Zografou, Greece
- ¹¹ Department of Physics, The University of Texas at Austin, Austin TX, United States of America
- ¹² Institute of Physics, Azerbaijan Academy of Sciences, Baku, Azerbaijan
- ¹³ Institut de Física d'Altes Energies (IFAE), The Barcelona Institute of Science and Technology, Barcelona, Spain
- ¹⁴ Institute of Physics, University of Belgrade, Belgrade, Serbia
- ¹⁵ Department for Physics and Technology, University of Bergen, Bergen, Norway
- ¹⁶ Physics Division, Lawrence Berkeley National Laboratory and University of California, Berkeley CA, United States of America
- ¹⁷ Department of Physics, Humboldt University, Berlin, Germany
- ¹⁸ Albert Einstein Center for Fundamental Physics and Laboratory for High Energy Physics, University of Bern, Bern, Switzerland
- ¹⁹ School of Physics and Astronomy, University of Birmingham, Birmingham, United Kingdom
- ²⁰ ^(a) Department of Physics, Bogazici University, Istanbul; ^(b) Department of Physics Engineering, Gaziantep University, Gaziantep; ^(d) Istanbul Bilgi University, Faculty of Engineering and Natural Sciences, Istanbul, Turkey; ^(e) Bahcesehir University, Faculty of Engineering and Natural Sciences, Istanbul, Turkey, Turkey
- ²¹ Centro de Investigaciones, Universidad Antonio Narino, Bogota, Colombia
- ²² ^(a) INFN Sezione di Bologna; ^(b) Dipartimento di Fisica e Astronomia, Università di Bologna, Bologna, Italy
- ²³ Physikalisches Institut, University of Bonn, Bonn, Germany
- ²⁴ Department of Physics, Boston University, Boston MA, United States of America
- ²⁵ Department of Physics, Brandeis University, Waltham MA, United States of America
- ²⁶ ^(a) Universidade Federal do Rio De Janeiro COPPE/EE/IF, Rio de Janeiro; ^(b) Electrical Circuits Department, Federal University of Juiz de Fora (UFJF), Juiz de Fora; ^(c) Federal University of Sao Joao del Rei (UFSJ), Sao Joao del Rei; ^(d) Instituto de Fisica, Universidade de Sao Paulo, Sao Paulo, Brazil
- ²⁷ Physics Department, Brookhaven National Laboratory, Upton NY, United States of America
- ²⁸ ^(a) Transilvania University of Brasov, Brasov, Romania; ^(b) Horia Hulubei National Institute of Physics and Nuclear Engineering, Bucharest; ^(c) National Institute for Research and Development of Isotopic and Molecular Technologies, Physics Department, Cluj Napoca; ^(d) University Politehnica Bucharest, Bucharest; ^(e) West University in Timisoara, Timisoara, Romania
- ²⁹ Departamento de Física, Universidad de Buenos Aires, Buenos Aires, Argentina
- ³⁰ Cavendish Laboratory, University of Cambridge, Cambridge, United Kingdom
- ³¹ Department of Physics, Carleton University, Ottawa ON, Canada
- ³² CERN, Geneva, Switzerland
- ³³ Enrico Fermi Institute, University of Chicago, Chicago IL, United States of America
- ³⁴ ^(a) Departamento de Física, Pontificia Universidad Católica de Chile, Santiago; ^(b) Departamento de Física, Universidad Técnica Federico Santa María, Valparaíso, Chile
- ³⁵ ^(a) Institute of High Energy Physics, Chinese Academy of Sciences, Beijing; ^(b) Department of Physics, Nanjing University, Jiangsu; ^(c) Physics Department, Tsinghua University, Beijing 100084, China

- ³⁶ Laboratoire de Physique Corpusculaire, Université Clermont Auvergne, Université Blaise Pascal, CNRS/IN2P3, Clermont-Ferrand, France
- ³⁷ Nevis Laboratory, Columbia University, Irvington NY, United States of America
- ³⁸ Niels Bohr Institute, University of Copenhagen, Kobenhavn, Denmark
- ³⁹ ^(a) INFN Gruppo Collegato di Cosenza, Laboratori Nazionali di Frascati; ^(b) Dipartimento di Fisica, Università della Calabria, Rende, Italy
- ⁴⁰ ^(a) AGH University of Science and Technology, Faculty of Physics and Applied Computer Science, Krakow; ^(b) Marian Smoluchowski Institute of Physics, Jagiellonian University, Krakow, Poland
- ⁴¹ Institute of Nuclear Physics Polish Academy of Sciences, Krakow, Poland
- ⁴² Physics Department, Southern Methodist University, Dallas TX, United States of America
- ⁴³ Physics Department, University of Texas at Dallas, Richardson TX, United States of America
- ⁴⁴ DESY, Hamburg and Zeuthen, Germany
- ⁴⁵ Lehrstuhl für Experimentelle Physik IV, Technische Universität Dortmund, Dortmund, Germany
- ⁴⁶ Institut für Kern- und Teilchenphysik, Technische Universität Dresden, Dresden, Germany
- ⁴⁷ Department of Physics, Duke University, Durham NC, United States of America
- ⁴⁸ SUPA - School of Physics and Astronomy, University of Edinburgh, Edinburgh, United Kingdom
- ⁴⁹ INFN Laboratori Nazionali di Frascati, Frascati, Italy
- ⁵⁰ Fakultät für Mathematik und Physik, Albert-Ludwigs-Universität, Freiburg, Germany
- ⁵¹ Departement de Physique Nucleaire et Corpusculaire, Université de Genève, Geneva, Switzerland
- ⁵² ^(a) INFN Sezione di Genova; ^(b) Dipartimento di Fisica, Università di Genova, Genova, Italy
- ⁵³ ^(a) E. Andronikashvili Institute of Physics, Iv. Javakhishvili Tbilisi State University, Tbilisi; ^(b) High Energy Physics Institute, Tbilisi State University, Tbilisi, Georgia
- ⁵⁴ II Physikalisches Institut, Justus-Liebig-Universität Giessen, Giessen, Germany
- ⁵⁵ SUPA - School of Physics and Astronomy, University of Glasgow, Glasgow, United Kingdom
- ⁵⁶ II Physikalisches Institut, Georg-August-Universität, Göttingen, Germany
- ⁵⁷ Laboratoire de Physique Subatomique et de Cosmologie, Université Grenoble-Alpes, CNRS/IN2P3, Grenoble, France
- ⁵⁸ Laboratory for Particle Physics and Cosmology, Harvard University, Cambridge MA, United States of America
- ⁵⁹ Department of Modern Physics, University of Science and Technology of China, Anhui, China
- ⁶⁰ ^(a) Kirchhoff-Institut für Physik, Ruprecht-Karls-Universität Heidelberg, Heidelberg; ^(b) Physikalisches Institut, Ruprecht-Karls-Universität Heidelberg, Heidelberg; ^(c) ZITI Institut für technische Informatik, Ruprecht-Karls-Universität Heidelberg, Mannheim, Germany
- ⁶¹ Faculty of Applied Information Science, Hiroshima Institute of Technology, Hiroshima, Japan
- ⁶² ^(a) Department of Physics, The Chinese University of Hong Kong, Shatin, N.T., Hong Kong; ^(b) Department of Physics, The University of Hong Kong, Hong Kong; ^(c) Department of Physics and Institute for Advanced Study, The Hong Kong University of Science and Technology, Clear Water Bay, Kowloon, Hong Kong, China
- ⁶³ Department of Physics, Indiana University, Bloomington IN, United States of America
- ⁶⁴ Institut für Astro- und Teilchenphysik, Leopold-Franzens-Universität, Innsbruck, Austria
- ⁶⁵ University of Iowa, Iowa City IA, United States of America
- ⁶⁶ Department of Physics and Astronomy, Iowa State University, Ames IA, United States of America
- ⁶⁷ Joint Institute for Nuclear Research, JINR Dubna, Dubna, Russia
- ⁶⁸ KEK, High Energy Accelerator Research Organization, Tsukuba, Japan
- ⁶⁹ Graduate School of Science, Kobe University, Kobe, Japan
- ⁷⁰ Faculty of Science, Kyoto University, Kyoto, Japan
- ⁷¹ Kyoto University of Education, Kyoto, Japan

- ⁷² Department of Physics, Kyushu University, Fukuoka, Japan
⁷³ Instituto de Física La Plata, Universidad Nacional de La Plata and CONICET, La Plata, Argentina
⁷⁴ Physics Department, Lancaster University, Lancaster, United Kingdom
⁷⁵ ^(a) INFN Sezione di Lecce; ^(b) Dipartimento di Matematica e Fisica, Università del Salento, Lecce, Italy
⁷⁶ Oliver Lodge Laboratory, University of Liverpool, Liverpool, United Kingdom
⁷⁷ Department of Experimental Particle Physics, Jožef Stefan Institute and Department of Physics, University of Ljubljana, Ljubljana, Slovenia
⁷⁸ School of Physics and Astronomy, Queen Mary University of London, London, United Kingdom
⁷⁹ Department of Physics, Royal Holloway University of London, Surrey, United Kingdom
⁸⁰ Department of Physics and Astronomy, University College London, London, United Kingdom
⁸¹ Louisiana Tech University, Ruston LA, United States of America
⁸² Laboratoire de Physique Nucléaire et de Hautes Energies, UPMC and Université Paris-Diderot and CNRS/IN2P3, Paris, France
⁸³ Fysiska institutionen, Lunds universitet, Lund, Sweden
⁸⁴ Departamento de Fisica Teorica C-15, Universidad Autonoma de Madrid, Madrid, Spain
⁸⁵ Institut für Physik, Universität Mainz, Mainz, Germany
⁸⁶ School of Physics and Astronomy, University of Manchester, Manchester, United Kingdom
⁸⁷ CPPM, Aix-Marseille Université and CNRS/IN2P3, Marseille, France
⁸⁸ Department of Physics, University of Massachusetts, Amherst MA, United States of America
⁸⁹ Department of Physics, McGill University, Montreal QC, Canada
⁹⁰ School of Physics, University of Melbourne, Victoria, Australia
⁹¹ Department of Physics, The University of Michigan, Ann Arbor MI, United States of America
⁹² Department of Physics and Astronomy, Michigan State University, East Lansing MI, United States of America
⁹³ ^(a) INFN Sezione di Milano; ^(b) Dipartimento di Fisica, Università di Milano, Milano, Italy
⁹⁴ B.I. Stepanov Institute of Physics, National Academy of Sciences of Belarus, Minsk, Republic of Belarus
⁹⁵ Research Institute for Nuclear Problems of Byelorussian State University, Minsk, Republic of Belarus
⁹⁶ Group of Particle Physics, University of Montreal, Montreal QC, Canada
⁹⁷ P.N. Lebedev Physical Institute of the Russian Academy of Sciences, Moscow, Russia
⁹⁸ Institute for Theoretical and Experimental Physics (ITEP), Moscow, Russia
⁹⁹ National Research Nuclear University MEPhI, Moscow, Russia
¹⁰⁰ D.V. Skobeltsyn Institute of Nuclear Physics, M.V. Lomonosov Moscow State University, Moscow, Russia
¹⁰¹ Fakultät für Physik, Ludwig-Maximilians-Universität München, München, Germany
¹⁰² Max-Planck-Institut für Physik (Werner-Heisenberg-Institut), München, Germany
¹⁰³ Nagasaki Institute of Applied Science, Nagasaki, Japan
¹⁰⁴ Graduate School of Science and Kobayashi-Maskawa Institute, Nagoya University, Nagoya, Japan
¹⁰⁵ ^(a) INFN Sezione di Napoli; ^(b) Dipartimento di Fisica, Università di Napoli, Napoli, Italy
¹⁰⁶ Department of Physics and Astronomy, University of New Mexico, Albuquerque NM, United States of America
¹⁰⁷ Institute for Mathematics, Astrophysics and Particle Physics, Radboud University Nijmegen/Nikhef, Nijmegen, Netherlands
¹⁰⁸ Nikhef National Institute for Subatomic Physics and University of Amsterdam, Amsterdam, Netherlands
¹⁰⁹ Department of Physics, Northern Illinois University, DeKalb IL, United States of America

- ¹¹⁰ Budker Institute of Nuclear Physics, SB RAS, Novosibirsk, Russia
¹¹¹ Department of Physics, New York University, New York NY, United States of America
¹¹² Ohio State University, Columbus OH, United States of America
¹¹³ Faculty of Science, Okayama University, Okayama, Japan
¹¹⁴ Homer L. Dodge Department of Physics and Astronomy, University of Oklahoma, Norman OK, United States of America
¹¹⁵ Department of Physics, Oklahoma State University, Stillwater OK, United States of America
¹¹⁶ Palacký University, RCPTM, Olomouc, Czech Republic
¹¹⁷ Center for High Energy Physics, University of Oregon, Eugene OR, United States of America
¹¹⁸ LAL, Univ. Paris-Sud, CNRS/IN2P3, Université Paris-Saclay, Orsay, France
¹¹⁹ Graduate School of Science, Osaka University, Osaka, Japan
¹²⁰ Department of Physics, University of Oslo, Oslo, Norway
¹²¹ Department of Physics, Oxford University, Oxford, United Kingdom
¹²² ^(a) INFN Sezione di Pavia; ^(b) Dipartimento di Fisica, Università di Pavia, Pavia, Italy
¹²³ Department of Physics, University of Pennsylvania, Philadelphia PA, United States of America
¹²⁴ National Research Centre "Kurchatov Institute" B.P.Konstantinov Petersburg Nuclear Physics Institute, St. Petersburg, Russia
¹²⁵ ^(a) INFN Sezione di Pisa; ^(b) Dipartimento di Fisica E. Fermi, Università di Pisa, Pisa, Italy
¹²⁶ Department of Physics and Astronomy, University of Pittsburgh, Pittsburgh PA, United States of America
¹²⁷ ^(a) Laboratório de Instrumentação e Física Experimental de Partículas - LIP, Lisboa; ^(b) Faculdade de Ciências, Universidade de Lisboa, Lisboa; ^(c) Department of Physics, University of Coimbra, Coimbra; ^(d) Centro de Física Nuclear da Universidade de Lisboa, Lisboa; ^(e) Departamento de Física, Universidade do Minho, Braga; ^(f) Departamento de Física Teórica y del Cosmos and CAFPE, Universidad de Granada, Granada (Spain); ^(g) Dep Física and CEFITEC of Faculdade de Ciencias e Tecnologia, Universidade Nova de Lisboa, Caparica, Portugal
¹²⁸ Institute of Physics, Academy of Sciences of the Czech Republic, Praha, Czech Republic
¹²⁹ Czech Technical University in Prague, Praha, Czech Republic
¹³⁰ Faculty of Mathematics and Physics, Charles University in Prague, Praha, Czech Republic
¹³¹ State Research Center Institute for High Energy Physics (Protvino), NRC KI, Russia
¹³² Particle Physics Department, Rutherford Appleton Laboratory, Didcot, United Kingdom
¹³³ ^(a) INFN Sezione di Roma; ^(b) Dipartimento di Fisica, Sapienza Università di Roma, Roma, Italy
¹³⁴ ^(a) INFN Sezione di Roma Tor Vergata; ^(b) Dipartimento di Fisica, Università di Roma Tor Vergata, Roma, Italy
¹³⁵ ^(a) INFN Sezione di Roma Tre; ^(b) Dipartimento di Matematica e Fisica, Università Roma Tre, Roma, Italy
¹³⁶ ^(a) Faculté des Sciences Ain Chock, Réseau Universitaire de Physique des Hautes Energies - Université Hassan II, Casablanca; ^(b) Centre National de l'Energie des Sciences Techniques Nucléaires, Rabat; ^(c) Faculté des Sciences Semlalia, Université Cadi Ayyad, LPHEA-Marrakech; ^(d) Faculté des Sciences, Université Mohamed Premier and LPTPM, Oujda; ^(e) Faculté des sciences, Université Mohammed V, Rabat, Morocco
¹³⁷ DSM/IRFU (Institut de Recherches sur les Lois Fondamentales de l'Univers), CEA Saclay (Commissariat à l'Energie Atomique et aux Energies Alternatives), Gif-sur-Yvette, France
¹³⁸ Santa Cruz Institute for Particle Physics, University of California Santa Cruz, Santa Cruz CA, United States of America
¹³⁹ Department of Physics, University of Washington, Seattle WA, United States of America
¹⁴⁰ School of Physics, Shandong University, Shandong, China

- ¹⁴¹ Department of Physics and Astronomy, Key Laboratory for Particle Physics, Astrophysics and Cosmology, Ministry of Education; Shanghai Key Laboratory for Particle Physics and Cosmology (SKLPPC), Shanghai Jiao Tong University, Shanghai, China
- ¹⁴² Department of Physics and Astronomy, University of Sheffield, Sheffield, United Kingdom
- ¹⁴³ Department of Physics, Shinshu University, Nagano, Japan
- ¹⁴⁴ Fachbereich Physik, Universität Siegen, Siegen, Germany
- ¹⁴⁵ Department of Physics, Simon Fraser University, Burnaby BC, Canada
- ¹⁴⁶ SLAC National Accelerator Laboratory, Stanford CA, United States of America
- ¹⁴⁷ ^(a) Faculty of Mathematics, Physics & Informatics, Comenius University, Bratislava; ^(b) Department of Subnuclear Physics, Institute of Experimental Physics of the Slovak Academy of Sciences, Kosice, Slovak Republic
- ¹⁴⁸ ^(a) Department of Physics, University of Cape Town, Cape Town; ^(b) Department of Physics, University of Johannesburg, Johannesburg; ^(c) School of Physics, University of the Witwatersrand, Johannesburg, South Africa
- ¹⁴⁹ ^(a) Department of Physics, Stockholm University; ^(b) The Oskar Klein Centre, Stockholm, Sweden
- ¹⁵⁰ Physics Department, Royal Institute of Technology, Stockholm, Sweden
- ¹⁵¹ Departments of Physics & Astronomy and Chemistry, Stony Brook University, Stony Brook NY, United States of America
- ¹⁵² Department of Physics and Astronomy, University of Sussex, Brighton, United Kingdom
- ¹⁵³ School of Physics, University of Sydney, Sydney, Australia
- ¹⁵⁴ Institute of Physics, Academia Sinica, Taipei, Taiwan
- ¹⁵⁵ Department of Physics, Technion: Israel Institute of Technology, Haifa, Israel
- ¹⁵⁶ Raymond and Beverly Sackler School of Physics and Astronomy, Tel Aviv University, Tel Aviv, Israel
- ¹⁵⁷ Department of Physics, Aristotle University of Thessaloniki, Thessaloniki, Greece
- ¹⁵⁸ International Center for Elementary Particle Physics and Department of Physics, The University of Tokyo, Tokyo, Japan
- ¹⁵⁹ Graduate School of Science and Technology, Tokyo Metropolitan University, Tokyo, Japan
- ¹⁶⁰ Department of Physics, Tokyo Institute of Technology, Tokyo, Japan
- ¹⁶¹ Tomsk State University, Tomsk, Russia, Russia
- ¹⁶² Department of Physics, University of Toronto, Toronto ON, Canada
- ¹⁶³ ^(a) TRIUMF, Vancouver BC; ^(b) Department of Physics and Astronomy, York University, Toronto ON, Canada
- ¹⁶⁴ Faculty of Pure and Applied Sciences, and Center for Integrated Research in Fundamental Science and Engineering, University of Tsukuba, Tsukuba, Japan
- ¹⁶⁵ Department of Physics and Astronomy, Tufts University, Medford MA, United States of America
- ¹⁶⁶ Department of Physics and Astronomy, University of California Irvine, Irvine CA, United States of America
- ¹⁶⁷ ^(a) INFN Gruppo Collegato di Udine, Sezione di Trieste, Udine; ^(b) ICTP, Trieste; ^(c) Dipartimento di Chimica, Fisica e Ambiente, Università di Udine, Udine, Italy
- ¹⁶⁸ Department of Physics and Astronomy, University of Uppsala, Uppsala, Sweden
- ¹⁶⁹ Department of Physics, University of Illinois, Urbana IL, United States of America
- ¹⁷⁰ Instituto de Fisica Corpuscular (IFIC) and Departamento de Fisica Atomica, Molecular y Nuclear and Departamento de Ingeniería Electrónica and Instituto de Microelectrónica de Barcelona (IMB-CNM), University of Valencia and CSIC, Valencia, Spain
- ¹⁷¹ Department of Physics, University of British Columbia, Vancouver BC, Canada
- ¹⁷² Department of Physics and Astronomy, University of Victoria, Victoria BC, Canada

- ¹⁷³ Department of Physics, University of Warwick, Coventry, United Kingdom
¹⁷⁴ Waseda University, Tokyo, Japan
¹⁷⁵ Department of Particle Physics, The Weizmann Institute of Science, Rehovot, Israel
¹⁷⁶ Department of Physics, University of Wisconsin, Madison WI, United States of America
¹⁷⁷ Fakultät für Physik und Astronomie, Julius-Maximilians-Universität, Würzburg, Germany
¹⁷⁸ Fakultät für Mathematik und Naturwissenschaften, Fachgruppe Physik, Bergische Universität Wuppertal, Wuppertal, Germany
¹⁷⁹ Department of Physics, Yale University, New Haven CT, United States of America
¹⁸⁰ Yerevan Physics Institute, Yerevan, Armenia
¹⁸¹ Centre de Calcul de l’Institut National de Physique Nucléaire et de Physique des Particules (IN2P3), Villeurbanne, France
^a Also at Department of Physics, King’s College London, London, United Kingdom
^b Also at Institute of Physics, Azerbaijan Academy of Sciences, Baku, Azerbaijan
^c Also at Novosibirsk State University, Novosibirsk, Russia
^d Also at TRIUMF, Vancouver BC, Canada
^e Also at Department of Physics & Astronomy, University of Louisville, Louisville, KY, United States of America
^f Also at Physics Department, An-Najah National University, Nablus, Palestine
^g Also at Department of Physics, California State University, Fresno CA, United States of America
^h Also at Department of Physics, University of Fribourg, Fribourg, Switzerland
ⁱ Also at Departament de Fisica de la Universitat Autonoma de Barcelona, Barcelona, Spain
^j Also at Departamento de Fisica e Astronomia, Faculdade de Ciencias, Universidade do Porto, Portugal
^k Also at Tomsk State University, Tomsk, Russia, Russia
^l Also at Universita di Napoli Parthenope, Napoli, Italy
^m Also at Institute of Particle Physics (IPP), Canada
ⁿ Also at Horia Hulubei National Institute of Physics and Nuclear Engineering, Bucharest, Romania
^o Also at Department of Physics, St. Petersburg State Polytechnical University, St. Petersburg, Russia
^p Also at Department of Physics, The University of Michigan, Ann Arbor MI, United States of America
^q Also at Centre for High Performance Computing, CSIR Campus, Rosebank, Cape Town, South Africa
^r Also at Louisiana Tech University, Ruston LA, United States of America
^s Also at Institutio Catalana de Recerca i Estudis Avancats, ICREA, Barcelona, Spain
^t Also at Graduate School of Science, Osaka University, Osaka, Japan
^u Also at Department of Physics, National Tsing Hua University, Taiwan
^v Also at Institute for Mathematics, Astrophysics and Particle Physics, Radboud University Nijmegen/Nikhef, Nijmegen, Netherlands
^w Also at Department of Physics, The University of Texas at Austin, Austin TX, United States of America
^x Also at CERN, Geneva, Switzerland
^y Also at Georgian Technical University (GTU), Tbilisi, Georgia
^z Also at Ochadai Academic Production, Ochanomizu University, Tokyo, Japan
^{aa} Also at Manhattan College, New York NY, United States of America
^{ab} Also at Academia Sinica Grid Computing, Institute of Physics, Academia Sinica, Taipei, Taiwan
^{ac} Also at School of Physics, Shandong University, Shandong, China
^{ad} Also at Departamento de Fisica Teorica y del Cosmos and CAFPE, Universidad de Granada, Granada (Spain), Portugal
^{ae} Also at Department of Physics, California State University, Sacramento CA, United States of America
^{af} Also at Moscow Institute of Physics and Technology State University, Dolgoprudny, Russia

ag Also at Departement de Physique Nucleaire et Corpusculaire, Université de Genève, Geneva, Switzerland

ah Also at Eotvos Lorand University, Budapest, Hungary

ai Also at Departments of Physics & Astronomy and Chemistry, Stony Brook University, Stony Brook NY, United States of America

aj Also at International School for Advanced Studies (SISSA), Trieste, Italy

ak Also at Department of Physics and Astronomy, University of South Carolina, Columbia SC, United States of America

al Also at Institut de Física d'Altes Energies (IFAE), The Barcelona Institute of Science and Technology, Barcelona, Spain

am Also at School of Physics, Sun Yat-sen University, Guangzhou, China

an Also at Institute for Nuclear Research and Nuclear Energy (INRNE) of the Bulgarian Academy of Sciences, Sofia, Bulgaria

ao Also at Faculty of Physics, M.V.Lomonosov Moscow State University, Moscow, Russia

ap Also at Institute of Physics, Academia Sinica, Taipei, Taiwan

aq Also at National Research Nuclear University MEPhI, Moscow, Russia

ar Also at Department of Physics, Stanford University, Stanford CA, United States of America

as Also at Institute for Particle and Nuclear Physics, Wigner Research Centre for Physics, Budapest, Hungary

at Also at Flensburg University of Applied Sciences, Flensburg, Germany

au Also at CPPM, Aix-Marseille Université and CNRS/IN2P3, Marseille, France

av Also at University of Malaya, Department of Physics, Kuala Lumpur, Malaysia

aw Also at LAL, Univ. Paris-Sud, CNRS/IN2P3, Université Paris-Saclay, Orsay, France

* Deceased